

The University of Southern Mississippi
The Aquila Digital Community

Dissertations

Spring 5-2009

Influence of Functional Components on the Film Formation of Colloidal Dispersions

Kevin Lee Rhudy
University of Southern Mississippi

Follow this and additional works at: <https://aquila.usm.edu/dissertations>



Part of the [Materials Chemistry Commons](#), and the [Polymer Chemistry Commons](#)

Recommended Citation

Rhudy, Kevin Lee, "Influence of Functional Components on the Film Formation of Colloidal Dispersions" (2009). *Dissertations*. 1041.

<https://aquila.usm.edu/dissertations/1041>

This Dissertation is brought to you for free and open access by The Aquila Digital Community. It has been accepted for inclusion in Dissertations by an authorized administrator of The Aquila Digital Community. For more information, please contact Joshua.Cromwell@usm.edu.

The University of Southern Mississippi

**INFLUENCE OF FUNCTIONAL COMPONENTS ON THE FILM FORMATION OF
COLLOIDAL DISPERSIONS**

by

Kevin Lee Rhudy

Abstract of a Dissertation
Submitted to the Graduate Studies Office
of The University of Southern Mississippi
in Partial Fulfillment of the Requirements
for the Degree of Doctor of Philosophy

May 2009

COPYRIGHT BY

KEVIN LEE RHUDY

2009

The University of Southern Mississippi

INFLUENCE OF FUNCTIONAL COMPONENTS ON THE FILM FORMATION OF
COLLOIDAL DISPERSIONS

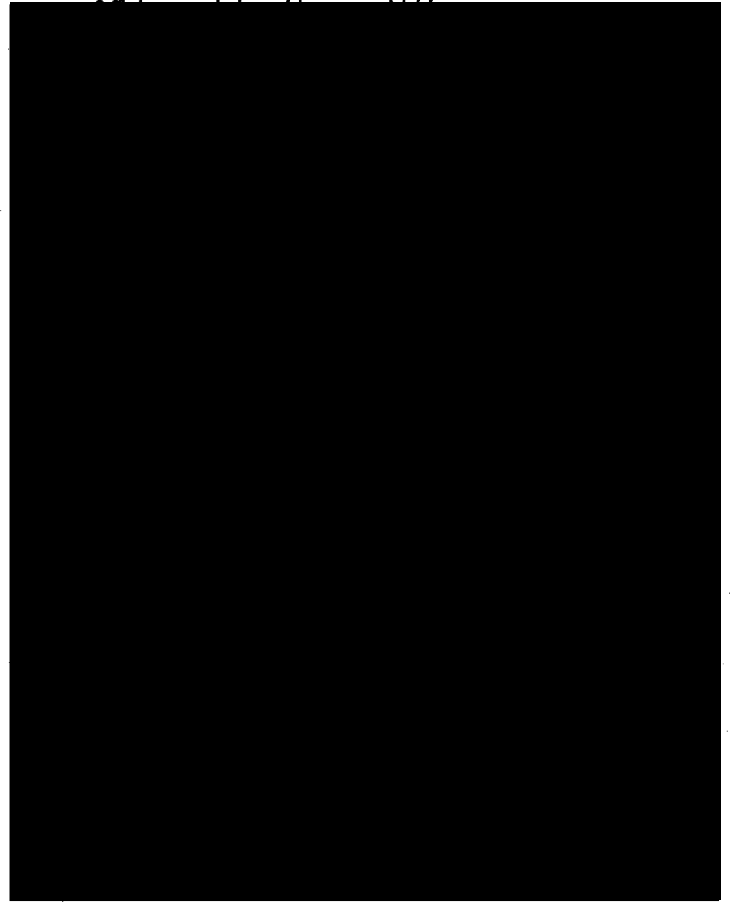
by

Kevin Lee Rhudy

A Dissertation

Submitted to the Graduate Studies Office
of The University of Southern Mississippi
in Partial Fulfillment of the Requirements
for the Degree of Doctor of Philosophy

Approved:  



May 2009

ABSTRACT

INFLUENCE OF FUNCTIONAL COMPONENTS ON THE FILM FORMATION OF COLLOIDAL DISPERSIONS

by Kevin Lee Rhudy

May 2009

A number of colloidal dispersions were synthesized to advance knowledge and gain understanding regarding interactions between individual components and for elucidation of complex processes governing their film formation. These studies show that for methyl methacrylate/n-butyl acrylate (MMA/nBA) colloidal dispersions, the presence of functional components significantly affects film formation. The incorporation of polyvinyl alcohol (PVOH) into pMMA/nBA colloidal dispersions creates competing environments between the copolymer particle surfaces, aqueous phases, and dispersing agents which results in migration with self-induced stratification occurring during coalescence. pMMA/nBA/PVOH films stratify to form sodium dodecyl sulfate (SDS) rich film-air (F-A) interfaces, and the $-\text{SO}_3^-$ moieties exhibit preferential parallel orientation with respect to the surface. At the same time, the bulk of the film is dominated by intramolecular hydrogen bonding between the PVOH phase and the copolymer matrix. This behavior is attributed to significant interactions between PVOH and pMMA/nBA resulting in limited mobility of PVOH. Also, colloidal dispersions of poly(methyl methacrylate/n-butyl acrylate) in the presence of methylene bisacrylamide (MBA), n-(hydroxyl methyl)-acrylamide (HAM), and methacrylic acid (MA) crosslinkers have significant influence on the mobility of individual components and their stratification during and after coalescence. Utilizing thermomechanical and

spectroscopic analytical tools, these studies show that physical and/or chemical crosslinking, which is a function of temperature, significantly alters interactions among the film components. While the presence of physical crosslinks significantly affects the mechanical strength of polymer networks at lower temperatures while chemical crosslinks are effective at elevated temperatures. Furthermore, the degree of crosslinking also influences stratification of selected components.

These studies also examine the role of nano-SiO₂ particles during colloidal synthesis of poly(methyl methacrylate/n-butyl acrylate) (pMMA/nBA) and their effect on the polydispersity index (PDI). Due to the presence of defects on the surface of SiO₂ nanoparticles, these entities are capable of controlling the propagation of free radicals. In contrast to previous assessments that SiO₂ nanoparticles serve as a loci of polymerization, SiO₂ nanoparticles adsorb on the exterior of surfactant micelles where they couple with carbon based propagating radicals in the oil phase and the hydroxyl radicals produced in the aqueous phase. The control of carbon based radicals as well as the trapping of highly reactive hydroxyl radicals is shown to lower the PDI of pMMA/nBA from 15 to 93%, depending upon the initiator as well as reaction conditions.

Finally, the creation of bioactive surfaces has garnered much interest due to potential applications in the medical industry. Many well-known methods used for the creation of bioactive surfaces utilize post modification techniques. With this in mind, we focused on the creation of bioactive surfaces with stimuli-responsive character without the need for further modification. These studies explored the concept of controlling inter/intramolecular interactions of multicomponent systems during the film formation process to create tailor-made surfaces of colloidal films. By utilizing the ionization of

aspartic acid (Asp) by controlling the pH of poly-(methyl methacrylate/n-butyl acrylate) (pMMA/nBA) colloidal dispersions, bioactive surfaces could not only be created but also controlled. At acidic pHs, a surfactant rich layer could be observed at the film-air interface, while at basic pHs bioactive Asp islands were observed.

ACKNOWLEDGEMENTS

I would like to express my appreciation for my dissertation director, Dr. Marek Urban, who provided me with direction and encouragement necessary to facilitate my development as a polymer scientist. Through his guidance and leadership, he empowered me with the ability to generate new ideas and expand my creative capacity. I would also like to thank him for acquiring the funding necessary for me to pursue my graduate degree in Polymer Science and Engineering, but most importantly, for his friendship and the level of intelligence I feel I have gained while under his advisement.

I would also like to thank my graduate committee members Dr. Charles Hoyle, Dr. William Jarrett, Dr. Robert Lochhead, and Dr. Shelby Thames for their advice and support through the duration of my graduate career.

Special appreciation goes to the Urban Research Group of the Department of Polymer Science at The University of Southern Mississippi (USM) for their continuous and unlimited support. Financially, this work was supported by the National Science Foundation.

TABLE OF CONTENTS

ABSTRACT	ii
ACKNOWLEDGEMENTS	v
LIST OF TABLES AND SCHEMES	viii
LIST OF ILLUSTRATIONS	ix
INTRODUCTION	1
CHAPTER	
I. COLLOIDAL DISPERSIONS AND FORMATION OF POLYMERIC FILMS	5
Synthetic Efforts	
Film Formation	
Functional Components	
References	
II. STRATIFIED FILMS OBTAINED FROM POLY-(METHYL METHACRYLATE/N-BUTYL ACRYLATE) COLLOIDAL DISPERSIONS CONTAINING POLYVINYL ALCOHOL	33
Introduction	
Experimental	
Results and Discussion	
Conclusions	
References	
III. COMPETITIVE STRATIFICATION BY CROSSLINKS IN POLY- (METHYL METHACRYLATE/N-BUTYL ACRYLATE) COLLOIDAL FILMS	51
Introduction	
Experimental	
Results and Discussion	
Conclusions	
References	

IV.	NANO-SILICA MEDIATED FREE RADICAL POLYMERIZATION; CONTROL OF PDI	69
	Introduction	
	Experimental	
	Results and Discussion	
	Conclusions	
	References	
V.	PH-CONTROLLED STRATIFICATION OF AMINO ACID IN COLLOIDAL FILMS	89
	Introduction	
	Experimental	
	Results and Discussion	
	Conclusions	
	References	
VI.	CONCLUSIONS	104

LIST OF TABLES AND SCHEMES

Table

1.	Compositions of colloidal dispersion based on final latex weight	35
2.	Dichroic ratios ($R = I_{TE}/I_{TM}$) of selected IR bands	40
3.	Compositions of colloidal dispersion based on final latex weight	92
4.	Experimental and calculated IR bands obtained from ATR FT-IR measurements and ab initio calculations using model shown in Figure 4 at pH=10	99

Scheme

1.	Incorporation of methylene bisacrylamide, methacrylic acid, and n-(hydroxymethyl)-acrylamide into methyl methacrylate and n-butyl acrylate polymerization	55
----	---	----

LIST OF ILLUSTRATIONS

Figure

1.	Schematic diagram illustrating the principles of the emulsion polymerization process	6
2.	Schematic illustration of the film formation process of colloidal particles	9
3.	Schematic diagram of possible surfactant stratification mechanisms during film formation	11
4.	Schematic diagram illustrating the ATR-FTIR process	13
5.	Schematic diagram of IRIRI set up	14
6.	Schematic diagram illustrating a photoacoustic cell and signal generation	14
7.	Schematic illustration of stimuli-responsive behaviors of surface stabilizing entities during film formation of colloidal particles	16
8.	ATR-FTIR spectra recorded from the F-A interface: (A) pMMA/nBA/PVOH, (B) pMMA/nBA, (C) SDS reference spectrum, and (D) PVOH reference spectrum	38
9.	Polarized ATR-FTIR spectra recorded from the F-A interface: (A) TM-pMMA/nBA/PVOH, (A') TE-pMMA/nBA/PVOH, (B) TM-pMMA/nBA, (B') TE-pMMA/nBA, (C) SDS reference spectrum, and (D) PVOH reference spectrum	39
10.	ATR-FTIR spectra of pMMA/nBA/PVOH films recorded from the F-A interface: (A) 0.46 μm , (B) 0.83 μm , (C) 1.42 μm , (D) 1.94 μm from the F-A interface and (E) SDS reference spectrum, and (F) PVOH reference spectrum	41
11.	Plot of volume concentration of PVOH versus film thickness	42
12.	PA-FTIR spectra of pMMA/nBA/PVOH films recorded from the F-A interface: (A) 25.2 μm , (B) 17.8 μm , (C) 8.9 μm , (D) 6.3 μm from the F-A interface and (E) SDS reference spectrum, and (F) PVOH reference spectrum	43
13.	Schematic representation of interactions during film formation: (A) In solution, (B) During coalescence, and (C) fully coalesced film	44

14.	2D PA-FTIR spectra of pMMA/nBA/PVOH at 50 Hz modulation frequency	45
15.	IRIR images recorded from the film cross-section of pMMA/nBA/PVOH	46
16.	Schematic representation of the overall film formation process when MMA and nBA are copolymerized in the presence of PVOH	47
17A.	Tan δ plotted as a function of temperature (T) for: A - pMMA/nBA/MBA; B - pMMA/nBA/MA; C - pMMA/nBA/HAM, and the D - pMMA/nBA standard	57
17B.	Storage moduli (E') plotted as a function of temperature for A - pMMA/nBA/MBA; B - pMMA/nBA/MA; C - pMMA/nBA/HAM, and D - pMMA/nBA	58
18.	Relative crosslinking density (X_i ; %) ratioed against pMMA/nBA standard plotted as a function of temperature: A - pMMA/nBA/MBA, B - pMMA/nBA/MA, and C - pMMA/nA/HAM	59
19.	Plot of volume concentration of SDS as a function of depth from the F-A interface	61
20.	2D PA-FTIR spectra of A - pMMA/nBA/MBA, B - pMMA/nBA/MA, C - pMMA/nBA/HAM, and D - pMMA/nBA at 50 Hz modulation frequency	62
21.	Schematic representations of interactions during film formation: A - in solution, B - during coalescence, and C - fully coalesced film	64
22.	PA FT-IR spectra of A - pMMA/nBA/MBA; B - pMMA/nBA/MA; C - pMMA/nBA/HAM; and D - pMMA/nBA recorded at 5.6, 8.9, and 12.6 μ m from the F-A interface	65
23.	Comparison of PDI values for pMMA/nBA with and without nano-SiO ₂ polymerized utilizing KPS and AIBN as initiators under semi-continuous and batch conditions	75
24.	Particle size measurements of aliquots taken every 15 minutes during polymerization reaction of MMA/nBA in the presence of 15 w/w% nano-SiO ₂ initiated by KPS under semi-continuous and batch conditions (A'/A''') and initiated by AIBN under semi-continuous and batch conditions (B'/B''')	76

25.	TEM micrographs of A – pMMA/nBA colloidal particles and B – pMMA/nBA colloidal particle with nano-SiO ₂ incorporated during polymerization	77
26.	¹³ C NMR of A- pMMA/nBA, B- pMMA/nBA with 15 w/w% nano-SiO ₂ , and C- pMMA/nBA with 15 w/w% nano-SiO ₂ quenched after 30 minutes reaction time	78
27.	A- representative Si ²⁹ spectrum showing the Q3 and Q4 resonances, B- Q3 and Q4 entities within the SiO ₂ lattice, and C- plot comparing the Q4/Q3 ratio for pMMA/nBA reactions with nano-SiO ₂ with different initiators	80
28.	Rearrangement of strained nano-SiO ₂ rings resulting in Si and O radicals responsible for the entrapment of OH radicals and control of propagating carbon based radicals	81
29.	Schematic representation of silica encapsulated micelle illustrating the mechanism for control and entrapment of radicals	82
30.	Proposed mechanism of nano-SiO ₂ mediated polymerization	83
31.	pH dependent structures of aspartic acid	91
32.	ATR-FTIR spectra recorded from the F-A interface of pMMA/nBA/Asp at pH =: 3 (Trace A), 7 (Trace B), 10 (Trace C), (D) pMMA/nBA reference spectrum, (E) Calculated IR spectrum of 1:1 combination of pMMA/nBA and Asp, (F) Asp reference spectrum, and (F) SDS reference spectrum	94
33.	A- IRIR images recorded from the F-A interface of pMMA/nBA/Asp colloidal films coalesced at pH = 3, 7, and 10, B – Generated IR spectra obtained from selected IRIR images	96
34.	Top view and side view of polymer-aspartic acids at pH 3, 7, and 10	97
35.	Proposed mechanism of pH dependant stratification of SDS and Asp during the film formation of pMMA/nBA/Asp	101

INTRODUCTION

This dissertation is concerned with the development of multi-component colloidal dispersions from aqueous emulsion polymerization for which their film formation in the presence of functional components will be studied. The goal is to advance limited knowledge pertaining to the influence of interactions of individual components in the presence of internal and external stimuli. Furthermore, by understanding the interactions of individual components tailor-made surfaces can be achieved.

Chapter I provides background information along with an overview of relevant literature. Various synthetic approaches for the production of colloidal particles by emulsion polymerization processes are reviewed along with the discussion of classical and more recent models governing film formation processes from multi-component colloidal dispersions. This Chapter also outlines existing studies focusing on functional components utilized in both emulsion polymerizations as well as their utilization in other polymeric systems.

Poly-(vinyl alcohol) (PVOH) exhibits unique solubility properties such as being not water insoluble below 80° C, upon heating above 80°C and cooling, remains water soluble. Another interesting property pointed out by McCarthy et al. is that PVOH may modify hydrophobic surfaces by irreversible adsorption from an aqueous phase onto a hydrophobic surface, thus changing the surface characteristics from hydrophobic to hydrophilic.^{8,9} While these attributes were examined on polymeric films, our interests in colloidal dispersions, Chapter II focuses on how the presence of PVOH will affect colloidal particles in solutions as well as during and after coalescence. For instance, PVOH has been used to stabilize colloidal latex particles against flocculation in an

aqueous media by entropy-driven adsorption on the particle surface displacing pre-adsorbed surfactants.¹⁰ Previous studies also indicated that the viscosity of PVOH solutions is mainly affected by the molecular weight and polymer concentrations.¹¹⁻¹⁵ In view of these considerations we synthesized pMMA/nBA colloidal particles in the presence of PVOH and examined the role of PVOH on colloidal dispersions and distribution of individual components and their mobility during coalescence. The ability of PVOH to interact with water and colloidal particles facilitates slower evaporation rates which may also alter organization of individual components during coalescence, thus providing an opportunity for controlled self-stratification and consequently useful surface/interfacial properties.

The utilization of crosslinks for the enhancement of physical properties is well documented, and the primary role of crosslinkers was to enhance mechanical strength as well as network permeability.^{12,13} However, depending upon the nature of the crosslinking mechanism, physio-chemical properties upon coalescence will also be altered. The main focus of Chapter III is to examine the effect of chemical, physical, and the combination of both types of crosslinkers on coalescence of poly-(methyl methacrylate/n-butyl acrylate) (pMMA/nBA) colloidal dispersions. Methacrylic acid (MA) was incorporated to introduce physical crosslinks, whereas methylene bisacrylamide (MBA) was chosen due to its ability to form chemical crosslinks. To combine the influence of physical and chemical crosslinks, n-methylol acrylamide (HAM) was copolymerized with methyl methacrylate (MMA) and n-butyl acrylate (nBA), and such colloidal dispersions were allowed to coalesce to form uniform films.

Chapter IV examines the role of nano-SiO₂ particles during colloidal synthesis of poly(methyl methacrylate/n-butyl acrylate) (pMMA/nBA) and their effect on polydispersity index (PDI). Recently, it was recognized that when polymerization is conducted in the presence of SiO₂, the rate of polymerization rate constants for monomers with similar reactivities were altered. This behavior was thought to be attributed to the adsorption of sulfate radicals on SiO₂ nanoparticles.^{26,27} However further insights regarding the mechanism of radical influence as well as the influence of the silica nanoparticles on the particle coalescence were not addressed. With the concept of controlled radical polymerizations in an aqueous environment as well as the influence of SiO₂ particles on polymerization rate constants in mind, these studies focus on the insitu effect of nano SiO₂ on free radical emulsion polymerization of (meth)acrylate monomers with a particular focus on the propagation and radical entrapment during the synthesis, thus affecting the polydispersity index (PDI) of produced macromolecules.

The concept of creating bioactive surfaces by controlling the interactions of individual components is discussed in Chapter V. The creation of bioactive surfaces has garnered much interest due to potential applications in the medical industry. Many well-known methods used for the creation of bioactive surfaces utilize post modification techniques. With this in mind, we focused on creating bioactive surfaces without the need for further modification. The studies explored the concept of controlling inter/intramolecular interactions of multicomponent systems during the film formation process to create tailor-made surfaces of colloidal films. By utilizing the ionization of aspartic acid (Asp) by controlling pH of poly-(methyl methacrylate/n-butyl acrylate) (pMMA/nBA) colloidal dispersions, bioactive surfaces could not only be created but also

controlled. At acidic pH's, a surfactant rich layer could be observed at the film-air interface while at basic pH's bioactive Asp islands were observed.

CHAPTER I

COLLOIDAL DISPERSIONS AND FORMATION OF POLYMERIC FILMS

Synthetic Efforts

Colloidal dispersions represent one of the most challenging polymeric systems because of the complexities involved not only in their water dispersive characteristics, but also the resulting particle morphologies. While the latter determines film properties during and after colloidal particle coalescence, the former effect solutions characteristics, and thus synthetic efforts of making colloidal particles. One of the most intriguing features of these polymeric systems is their synthesis which, although studied for many years, still presents a number of challenges and opportunities. While challenges arise from the fact that very often identical synthetic procedures will lead to different products, opportunities come from the ability to vary monomers utilized in synthesis, thus providing the possibility to create novel particle morphologies with unique film properties.

Colloidal dispersions are polymeric systems in which finely dispersed particles are placed within a continuous medium in a manner that prevents them coming into contact with their neighbors. The primary synthetic methods utilized for generating colloidal dispersions are suspension or emulsion polymerization processes. While emulsion polymerization is the main focus of this work, it is important to outline the differences between the two techniques. Suspension polymerization occurs when monomer is suspended as a non-continuous phase in a continuous aqueous medium. Organic soluble initiators facilitate polymerization by diffusion into the monomer droplets. Surfactants can be added as stabilizing agents, however their concentration

levels are too low to form micellar structures. Polymeric particles produced from suspension polymerization have sizes ranging from 50-500 μm . Without proper agitation, the suspended particles only remain in the continuous phase on the order of seconds to minutes.

Colloidal dispersions can also be synthesized using emulsion polymerization techniques. Although similar to suspension polymerization, emulsion polymerization produces colloidal dispersions typically having smaller sizes and increased stability within the continuous phase. As shown in Figure 1, emulsion polymerization proceeds through a free-radical polymerization process whereby monomers (oil-phase) are polymerized in the presence of surfactant molecules suspended in an aqueous medium.

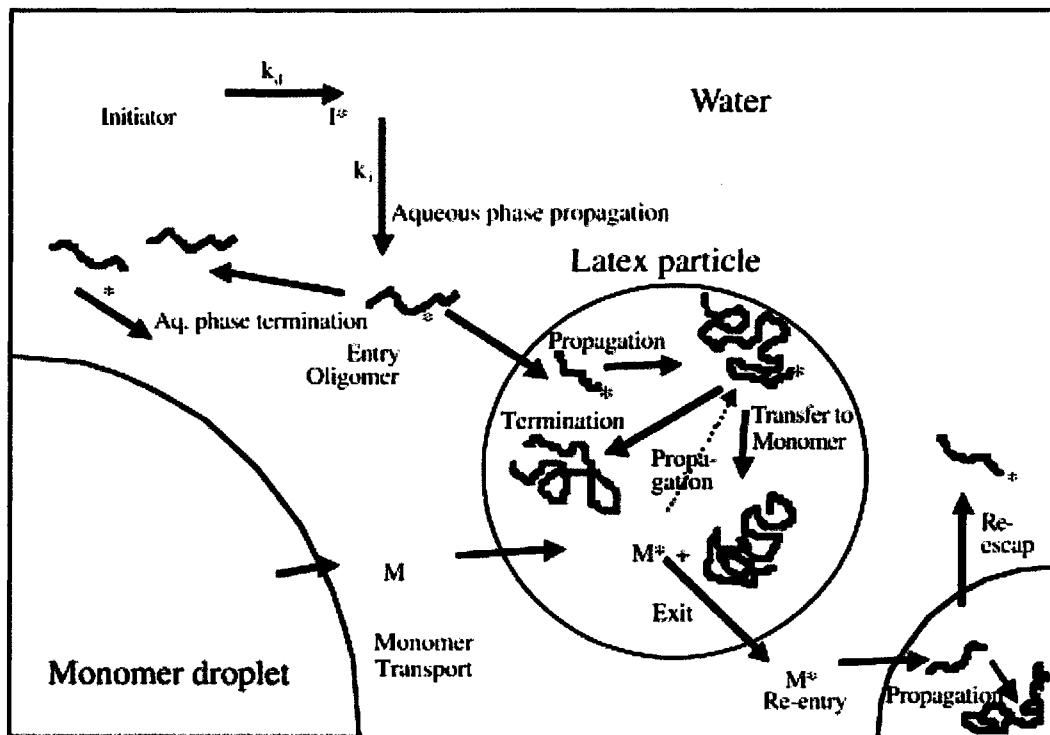


Figure 1: Schematic diagram illustrating the principles of the emulsion polymerization process.

The mechanism of polymer particle formation proceeds by two simultaneous processes. The first step is micellar nucleation which takes place by the entry of radicals (primary or oligomeric) from the aqueous phase into the micelles, followed homogenous nucleation, which occurs when solution polymerized oligomeric radicals become insoluble and are ultimately stabilized by free surfactant. When the concentration of surfactant molecules surpasses the critical micelle concentration (CMC), liquid-crystalline micellar structures are formed serving as polymerization loci for monomer molecules that have diffused through the continuous phase from the larger monomer droplets. At the same time, a water-soluble initiator (cleaved either thermally or photo-chemically) initiates polymerization in the hydrophobic core of the micelle. As monomer diffuses from the droplets and polymerize within micelles, surfactant molecules may be adsorbed from other micelles, solution, or monomer droplets.¹⁻³ Upon exhaustion of the monomer droplets, the reaction ceases thus forming solid colloidal particles dispersed in the aqueous phase.

Emulsion polymerization reactions are typically conducted by batch, semi-continuous, or continuous processes. In a batch polymerization, water, initiator, surfactant, and monomer are incorporated into the reactor at the same time, and the cleavage of the initiator beginning the polymerization process. Although used commercially, this process provides little control over particle nucleation and particle growth, and therefore, limits reproducibility. For that reason, semi-continuous processes have been developed to provide better control over reaction conditions. During this process, one or more of the ingredients are added into the reactor over an extended period of time, while monomer is added neat or as a semi-stable pre-emulsion formed during

continuous agitation of water, surfactant, and monomer. In order to increase particle nucleation reproducibility, a small percentage of the pre-emulsion, often referred to as a seed, is used to initially induce polymerization followed by the controlled addition of the remainder of the pre-emulsion. This approach offers significantly greater control over particle size and distribution. Continuous emulsion polymerization is often utilized industrially which consists of a continual feed of components into a stirred reactor, or series of reactors in which colloidal product is removed from the reactors at the same rate new components are added. This process facilitates high production rates as well as reproducibility of the resulting colloidal dispersions.²

Colloidal particles in aqueous environments are traditionally spherical in shape. However, emulsion polymerization technologies have advanced such that an enormous variety of structured particles, with a growing number of applications, may be obtained.^{4,5} Today, composite particle morphologies include core-shell, interpenetrating, champignon, salami, and hollow particles, etc.⁴ Nevertheless, these particles still remain spherical in nature. These varying spherical particle types are often prepared via a two-step emulsion polymerization. During the first step, monodisperse particles are synthesized utilizing a semi-continuous process under controlled reaction conditions. The second step utilizes starve fed conditions in order to hinder monomer accumulation in the main reactor, and as a consequence, the nucleation of new particles. The particles produced in the first step serve as polymerization sites for the second step. The resulting particle morphologies ultimately result from differences in polymerization rates and/or interfacial energies between the monomers. However, particles with tailored physical and chemical properties can be prepared through sequential monomer addition or by

using different dispersing agents. For example, the creation of fluorine-containing colloidal dispersions with non-spherical particle morphology has been achieved by utilizing non-traditional surfactants, such as phospholipids, under starve-fed conditions. By utilizing phospholipids, the fluorine-containing content of the copolymer was able to reach never before observed values of 15%.^{6,7}

Film Formation

Although colloidal dispersions have been widely studied, there is limited knowledge pertaining to their film formation. It has been proposed that the film forming process can be broken down into the following steps⁸ shown in Figure 2: 1) water evaporates bringing the particles in close proximity to one another; 2) as the water continues to evaporate, the particles become deformed; and 3) the polymer chains fuse together to form a continuous, mechanically stable film.

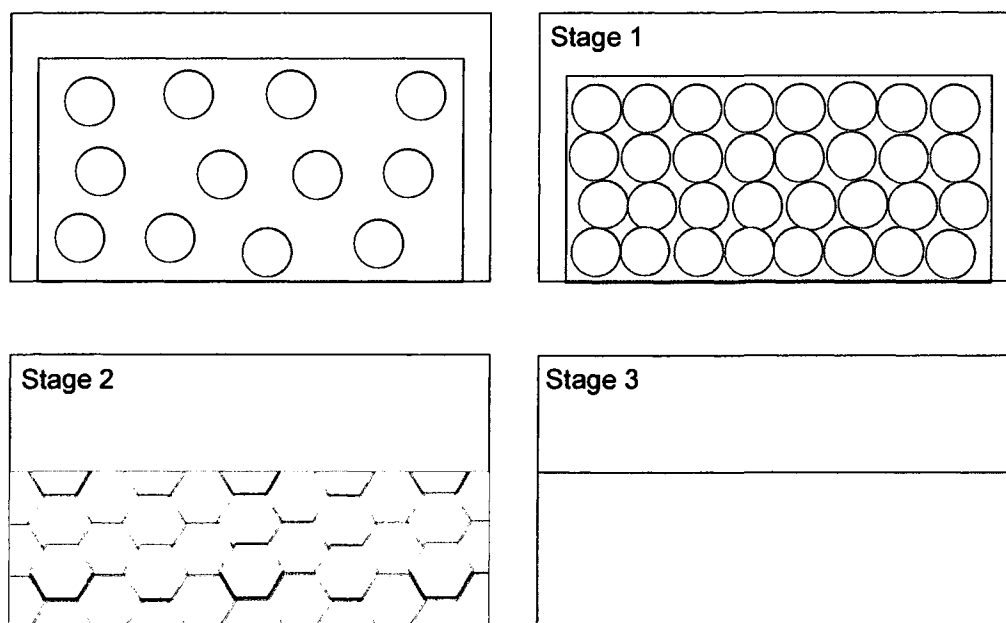


Figure 2: Schematic illustration of the film formation process of colloidal particles.

While the process illustrated in Figure 2 appears to describe the phenomenon of film formation, there are numerous theories that account for various states of film formation. For example, it was proposed that the latex particles dry before losing their original shape with particle deformation a direct result of the particle-air interfacial tension.⁹ This theory, however, ignores viscoelastic characteristics of macromolecules.¹⁰ Brown¹¹ proposed a theory based on the fact that there are forces promoting and resisting the deformation of the particles and their magnitude will determine the actual particle deformation. The wet sintering theory¹² utilizes the concept of a pressure gradient across the particles, similar to the capillary approach. Here, the presence of a thin layer of water around the particles initiates particle deformation which leads to coalescence. In contrast, Sheetz¹³ suggested that particle coalescence results from stresses induced at the particle interfaces which are due to the evaporation of water from the colloidal film. Routh and co-workers¹⁴ recently summarized these models and proposed approaches that use these classical models for specific situations. Although these models have scholastic and historical values offering insight into the coalescence process, as a whole, numerous factors that significantly affect film formation processes are omitted.

Recent advances in various spectroscopic techniques such as atomic force microscopy (AFM), small angle neutron scattering (SANS), non-radiative energy transfer (NRET), and free-fracture transmission electron microscopy (TEM) have provided further understanding of processes governing film formation. For example, AFM was first utilized in 1992 by Goh and Wang to monitor the surface of a coalescing film. They found that the surface flattens during coalescence due to polymer rearrangement or diffusion between adjacent particles.^{15,16} The use of SANS and NRET was also utilized

to explore the concept of rearrangements resulting from polymer chain diffusion across particle-particle interfacial boundaries through the labeling of polymer particles.¹⁷⁻²⁰

TEM studies involving the free fracture of particles have shown that during the second stage of coalescence, colloidal films are mechanically weak due to the fact that fracturing of the film occurs predominately at the particle-particle interface and not as a cohesive fracture.²¹⁻²³ While these models and spectroscopic techniques have contributed to the advancement in film formation processes of colloidal dispersions, none of these models take into consideration particle morphology, minimum film formation temperature (MFFT), glass transition temperature (T_g). Also omitted is the role of low molecular weight species such as surfactants, crosslinking agents, or cosolvents during the processes governing film formation. Figure 3 shows a schematic of the possible location of surfactant molecules during particle collision and deformation.

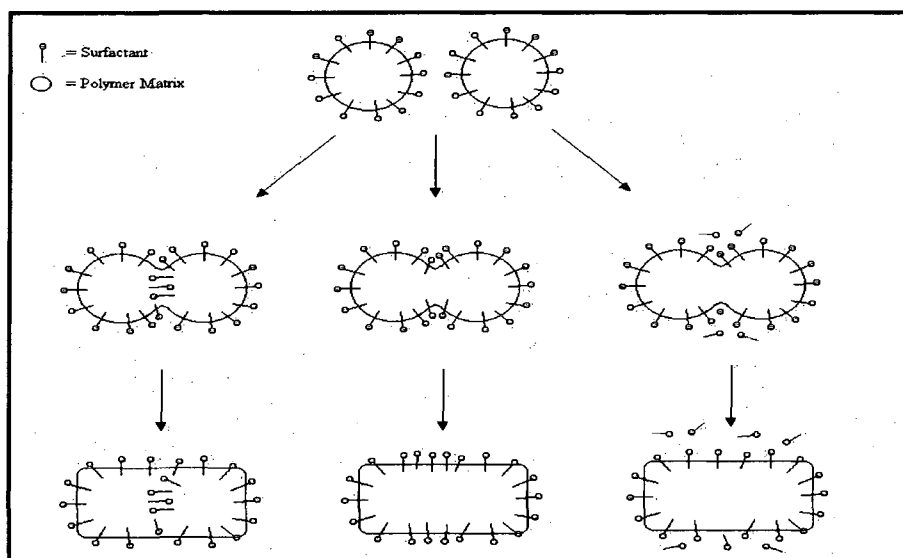


Figure 3: Schematic diagram of possible surfactant stratification mechanisms during film formation.

As shown in Figure 3-1, surfactant molecules may become trapped at the interface or as it is shown in Figure 3-2, some surfactant may be displaced from the interface but under these circumstances surfactants will congregate at the particle interstices. Finally, in Figure 3-3 surfactant molecules may be displaced from the particle surface, and under these conditions, significant migration may occur. Also, the spectroscopic techniques previously mentioned suggest changes in surface energies and interactions. However, these methods are not capable of producing molecular level chemical information or the location of individual components within colloidal films.

To gain mechanistic and chemical information concerning film formation processes, recent studies have utilized attenuated total reflectance infrared spectroscopy (ATR FTIR), photoacoustic infrared spectroscopy (PA FTIR), and internal reflection infrared imaging (IRIRI) to gain molecular level information of the X, Y, and Z planes of colloidal films. Due to the need for information from the interior of the film, attenuated total reflectance infrared spectroscopy (ATR FTIR) can be utilized to monitor film formation at various depths.^{24,25} One drawback to this technique deals with the fact that light passes through media that have different refractive indices. If the light does travel through areas of changing refractive indices, distorted data may be obtained due to changes in band intensities as well as wavenumber shifts which can be corrected by the use of developed algorithm.²⁶ This approach shown in Figure 4 allows one to analyze the film-air (F-A) and film-substrate (F-S) interfaces at shallow depths ranging from 0-3 μm , thereby assessing the degree of stratification of individual components found within colloidal dispersions.

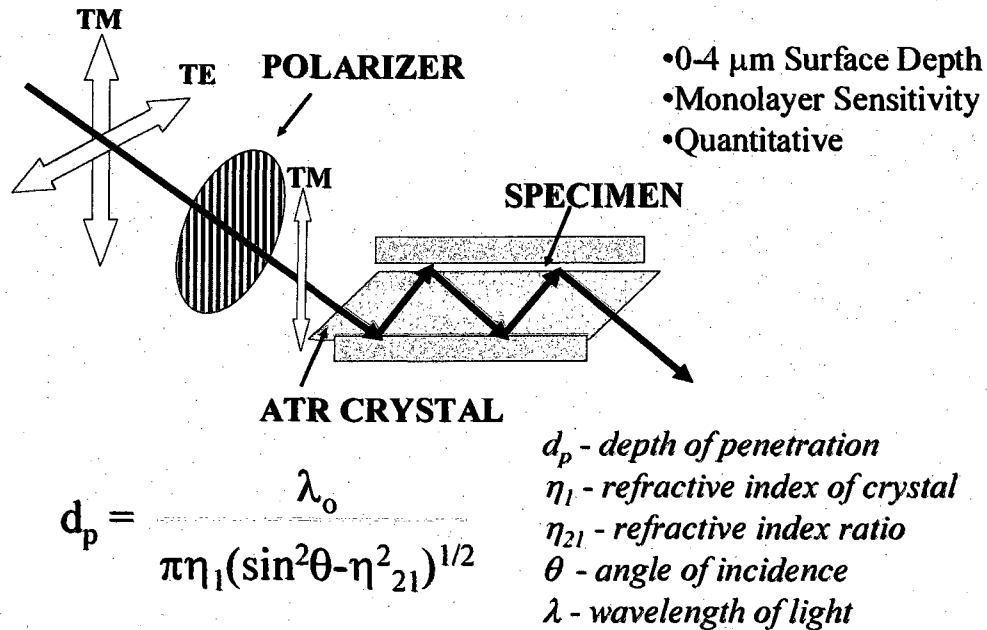


Figure 4: Schematic diagram illustrating the ATR-FTIR process.

To gain molecular level understanding of surface characteristics in the X-Y plane, infrared internal reflectance imaging (IRIRI) can be utilized to monitor surfactant distribution and the distribution of macromolecules in core-shell or blended particles.²⁷ Here chemical images are acquired by attaching a Ge crystal to the surface and using FTIR spectrometer Stingray imaging system to obtain chemical information from areas of the order of 1 micron. A schematic diagram shown in Figure 5 shows the methodology that overcomes standard IR detection limits, which are typically in the 6-10 micron range.

- Unique Surface/Interfacial Characterization Tool for Polymers
- 1 micron/pixel Spatial Resolution
- Complementary to Optical Microscopy, AFM, ESEM, ATR-FTIR, Photoacoustic FTIR.

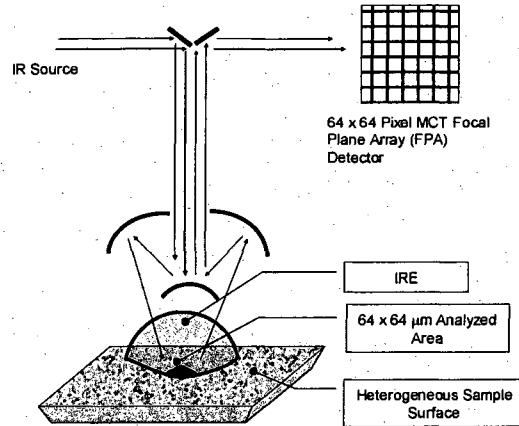


Figure 5: Schematic diagram of IRIRI set up.

Photoacoustic spectroscopy (PAS) is a unique sampling technique, because it does not require that the sample be transmitting, has low sensitivity to surface conditions, and can probe a range of selectable sampling depths from several micrometers to more than 100 μm . As illustrated in Figure 6, PAS directly measures infrared (IR) absorption by sensing absorption-induced heating of the sample within an experimentally controllable sampling depth below the sample's surface.

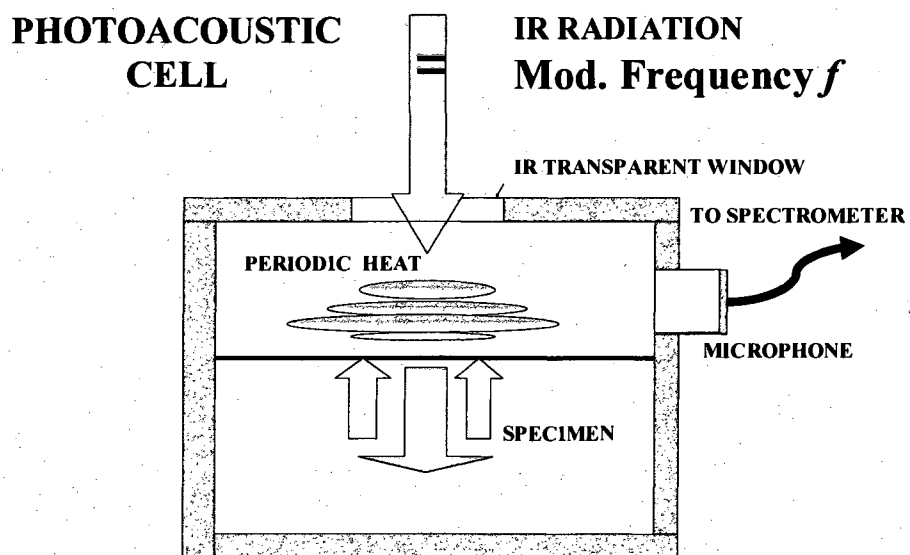


Figure 6: Schematic diagram illustrating a photoacoustic cell and signal generation.

Heat deposited within this depth transfers to the surrounding gas at the sample surface, producing a thermally expansion-driven pressurization in the gas (i.e the PAS signal) detected by a microphone. The phase of the PAS signal corresponds to the time delay associated with heat transfer within the sample. PAS signal generation is initiated when an oscillating FT-IR beam is absorbed by the sample, resulting in the absorption-induced heating in the sample and oscillation of the sample temperature. The temperature oscillations occurring in each light-absorbing layer within the sample launch propagating temperature waves called thermal-waves, which decay strongly as they propagate through the sample. It is this thermal-wave decay process that defines the layer thickness, or sampling depth, from which spectral information is obtained in an FT-IR PAS analysis. The sampling depth can be increased by decreasing, via FT-IR computer control, the IR beam modulation frequency imposed by the interferometer. The lower modulation frequency allows a longer time for thermal-waves to propagate from deeper within the sample into the gas. As the sampling depth increases, the saturation of strong bands in PAS spectra increases just as it does in absorption spectra measured by transmission as sample thickness increases.

As indicated above, the presence of low molecular weight species can play an important role in film formation, but their contribution is often neglected during coalescence. Figure 7 illustrates the complexity of colloidal dispersions, since they possess a number of different film formation avenues depending on the components utilized and the film forming environment.

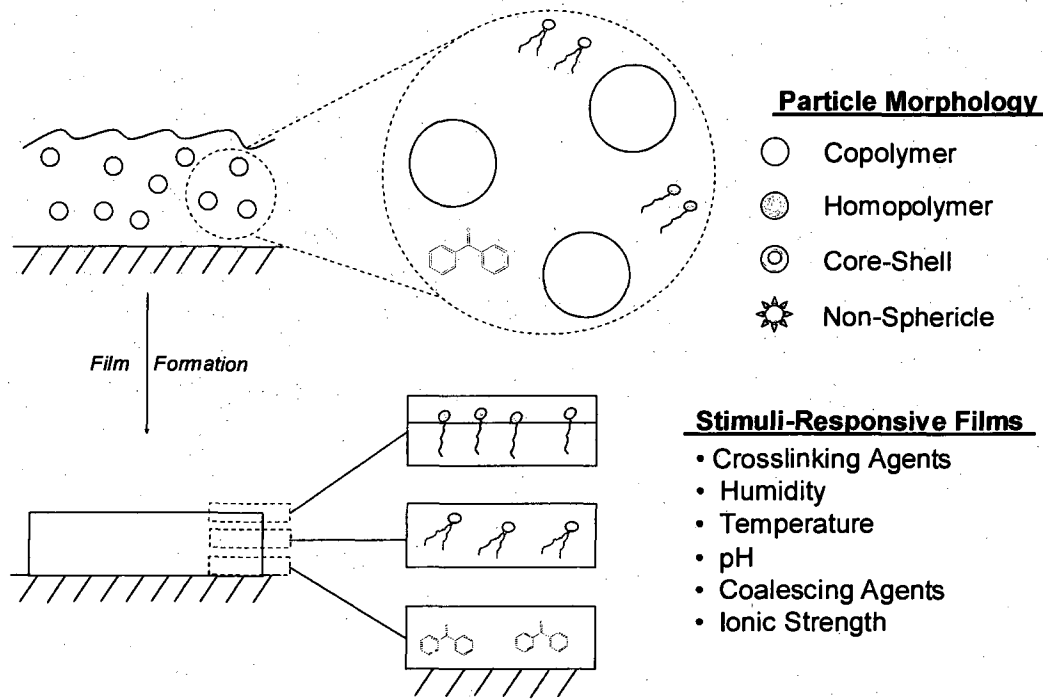


Figure 7: Schematic illustration of stimuli-responsive behaviors of surface stabilizing entities during film formation of colloidal particles.

Numerous studies²⁸⁻³⁸ have shown that upon coalescence, the distribution of surfactant molecules in colloidal films are greatly effected by such stimuli as particle morphology, temperature, pH, and even the nature of the substrate. In each case, stratification of low molecular weight species was attributed to external or internal stimuli. For example, under ambient coalescence conditions, sodium dioctyl sulfocuccinate (SDOSS) in polystyrene/poly-(n-butyl acrylate) colloidal blends was not observed at the film-air (F-A) interface. However, upon annealing the films at 90 and 120°C, SDOSS was released from the interior of the film with subsequent migration to the F-A interface.³⁶

When considering low molecular weight species included into emulsion polymerizations, surfactant molecules are the most common. Two traditional stabilizing

agents that have been of interest for years concerning both their solution characteristics and also their distribution within colloid films are sodium dodecyl sulfate (SDS) and SDOSS.^{34,37-41} Their distribution after film formation has been shown to be effected in the presence of alternate copolymer compositions as well as external stimuli. For example, the migration of SDOSS to the F-A or film substrate (F-S) interface can be controlled in the presence of ethyl acrylate/methacrylic acid (EA/MAA) colloidal particles,⁴² and that the F-S concentration of SDOSS in EA/MAA is directly related to the surface tension of the substrate utilized during coalescence. When polytetrafluoroethylene (PTFE) was utilized, SDOSS migrated to the F-A and F-S interfaces. However, when the substrate was changed to glass, the concentration of SDOSS at the F-S decreased. Also, numerous studies⁴²⁻⁵¹ have shown that SDS displays similar responses to SDOSS in regards to its nature when exposed to external and internal stimuli. For example, the lowering of pH by the inclusion of acrylic acid (AA) and methacrylic acid (MA) to polystyrene and p-(methyl methacrylate/ethyl hexyl acrylate), respectively, resulted in not only migration of SDS to the F-A interface but also specific orientation of the SDS hydrophobic tails exhibit distinct responsiveness dependent on the coalescing polymer matrix.^{42,43} In similar studies,²⁴ using SDS to stabilize p-MMA/nBA/AA colloidal particles, localized ionic clusters (LICs) were detected between SDS and AA moieties. However, utilizing propylene glycol as a co-solvent stimulus, LICs were disrupted, thus mobilizing SDS which stratified near the F-A interface.

Functional Components

While it has been previously mentioned that the main components of colloidal dispersions are water, monomer(s), initiator, and surfactant, additional components are often added to alter solution properties as well as aid in the film formation process.

Water-soluble polymers are frequently utilized to stabilize colloidal latex particles against flocculation in aqueous media thus acting to increase the shelf stability.⁵² One example of such a water soluble polymer is polyvinyl alcohol (PVOH). For instance, PVOH has been used to stabilize colloidal latex particles against flocculation in an aqueous media by entropy-driven adsorption on the particle surface displacing pre-adsorbed surfactants⁵².

PVOH also has excellent film forming, emulsifying, and adhesive properties, and because it is only soluble in a few solvents, it has high solvent resistance. Because of these unique properties, recent research of PVOH has focused on other areas of research such as the insulating and magnetic properties of PVOH.^{53,54} Also, in the area of fuel cell applications, PVOH is being investigated as alternative fuel cell membranes.⁵⁵⁻⁵⁷

Although these are just a few of the applications of PVOH, it is most commonly recognized as a rheological modifier. Previous studies indicated that the viscosity of PVOH solutions is directly affected by the molecular weight and polymer concentrations.^{52,58-62} Another interesting property pointed out by McCarthy et al. is that PVOH is able to modify hydrophobic surfaces by irreversible adsorption from an aqueous phase onto a hydrophobic surface, thus changing the surface characteristics from hydrophobic to hydrophilic.⁶³⁻⁶⁵ Because colloidal dispersions are made up of hydrophobic and hydrophilic portions, this gives rise to new areas of research since PVOH can adsorb to the hydrophobic/hydrophilic interface of the polymeric micelles.

There is also great research opportunity regarding the role PVOH during the film formation processes of colloidal dispersions, because of viscosity changes of PVOH of colloidal dispersions. However, the role of PVOH during the film formation and its interaction with individual components is currently not known.

Another functional component of particular interest is the influence of chemical stimuli such as crosslinking agents on the mobility of surfactant molecules in colloidal films. It is well known that the presence of crosslinkable moieties can reinforce a polymer network, whereby the mobility of species that are not chemically bound within the polymer matrix is altered.^{66,67} As a consequence, the resulting surface morphology and orientation of low molecular weight species may be affected. A number of studies have focused on the role of physical crosslinks in blended systems and their effect on the glass transition temperature as well as their influence on the miscibility of these systems.⁶⁸⁻⁷² Also, studies pertaining to crosslinked colloidal systems have shown that the amount of crosslinks and their effect on the mechanical properties can be controlled by the blend composition, the use of a chain transfer agents, and the ability to control the interdiffusion properties of crosslinking agents.⁷³⁻⁷⁵ However, depending upon the nature of the crosslinking mechanism, coalescence will be altered. Recent studies of styrene/ethyl hexyl acrylate/methacrylic acid (Sty/EHA/MAA) colloidal films²⁴ have shown that incorporation adipic dihydrazide (ADDH) and diacetone acrylamide) as covalently bound crosslinking agents inhibits the coalescence of Sty/EHA/MAA particles giving rise to a decrease in the surface concentration of SDS. However, while diffusion of species to the F-A interface occurs through an intricate path manifested by the crosslink network, other external stimuli can elicit alternate surface responsiveness. For

example, in response to elevated temperatures, the same specimen exhibited enhanced stratification of SDS at the F-A interface. While it is evident that the inclusion of crosslinking agents within colloidal systems does alter the film formation process, there is further need to investigate the role of different types of crosslinks, whether physical, chemical, or a combination of both, on the film formation process.

Another functional component are inorganic particles, and in particular nanoparticles. Inorganic particles are included into polymer matrices for a specific purpose, usually to enhance physical properties of the polymer. The particle properties change as their size approaches the nanoscale and as the percentage of atoms at the material's surface becomes significant. For bulk materials larger than one micrometer in diameter, the percentage of atoms at the surface is minuscule relative to the total number of atoms of the material. Interesting and sometimes unexpected properties of nanoparticles are due to the increased particle surface area. Moreover, nanoparticles can impart additional properties to various day to day products. For example, the presence of titanium dioxide nanoparticles into coatings applications induce a self-cleaning effect.⁷⁶⁻
⁸⁰Nano zinc oxide particles have superior UV blocking properties compared to its bulk substitute.⁸¹⁻⁸³ Clay nanoparticles, when incorporated into polymer matrices reinforces plastics, as verified by a higher glass transition temperature and other mechanical properties.⁸⁴⁻⁸⁸ While it is evident that nanoparticles can impart favorable properties, it is not clear how the increased surface area alters the molecular level interactions between the polymer and inorganic phase. Numerous studies dealing with the incorporation of silicon dioxide (SiO₂) and other particles into polymer matrices have been conducted over the past several decades.^{67,89-94} These efforts were primarily directed toward

enhancement of overall polymer composite properties through particle surface modifications,^{95,96} or the use of nanoparticles as seeds during emulsion polymerization.⁹⁷ It was only recently recognized that when polymerization is conducted in the presence of SiO₂, the polymerization rate constants for monomers with similar reactivities was altered. This behavior was attributed to the adsorption of sulfate radicals on SiO₂ nanoparticles.^{98,99} However, these studies do not provide further insights regarding the mechanism of radical influence as well as the influence of the silica nanoparticles on polymer particle coalescence. Although SiO₂ has been studied within colloidal systems, there are no studies that would correlate the film formation with the inclusion of SiO₂ macroparticles much less nano sized ones. Therefore, there are numerous opportunities to study the influence of nano-SiO₂ on the influence of not only the film formation processes of colloidal dispersions but also the influence of SiO₂ particles on propagating/degradative radicals.

Although recent trends in materials research have focused on polymeric systems with bioactive surfaces, primarily driven by the desire to create bioactive supports in surgery, orthopedics, and tissue engineering, limited fundamental knowledge regarding biocompatibility as well as control of interfaces has prevented many applications. For example, although titanium plates and materials have been utilized within the body for many years, recent research has focused on utilizing bioactive components to increase surface bioactivity.¹⁰⁰ Furthermore, the availability of a recombinant silica-synthesizing enzyme, silicatein, provides new opportunities for the synthesis of silica containing surfaces that do not damage proteins when applied to substrates such as glass.¹⁰¹ Along the same lines, mica and poly-(dimethylsiloxane) (PDMS) can be rendered bioactive by

the self-assembly of hydrophobin II, giving the surface sufficient hydrophilicity for protein immobilization.⁹⁰ One strategy for the modification of surfaces is by plasma techniques, which show promise in creating surfaces with covalently attached species to form bioactive and antimicrobial surfaces. For example, expanded poly-(tetrafluoroethylene) (ePTFE) was modified by the covalent attachment of the antibiotics ampicillin and penicillin, which inhibited microbial growth on the surface.^{90,102-104,105} Amoxicillin and polyethylene glycol were attached to PDMS in a similar manner.

While the above examples illustrate new pathways for the creation of bioactive surfaces using surface techniques, there is a need to develop bioactive surfaces using stratification approaches. Colloidal dispersions show great promise for creating bioactive surfaces through the specific utilization of bioactive components and control of the film formation process. For example, pMMA/nBA colloidal dispersion stabilized by n-dodecyl B-D-maltoside (DDM) form surfaces capable of recognizing lectin.¹⁰⁶ Upon particle coalesce under specific environmental conditions, DDM is released to the film-air (F-A) interface providing sites for interaction with lectin. Furthermore, stimuli-responsive systems are sensitive to a number of external and internal stimuli such as mechanical deformation, light, electrical/magnetic fields, temperature, pH, and ionic strength are other examples.¹⁰⁷ In addition, the mobility of individual components during the film formation process of colloidal dispersions stabilized by a combination of bioactive surfactants and traditional dispersing agents can be controlled by altering the ionic strength and coalescing temperature of these systems.^{108,109}

Amino acids are the principal building blocks of proteins and enzymes and are incorporated into proteins by transfer RNA, thus their utilization in film formation may

result in a variety of recognition processes. This is because during and after protein or enzyme assembly, amino acids dictate the spatial and biochemical properties. One amino acid with potential applications in waterborne systems is aspartic acid (Asp). Asp is important in the metabolic process during construction of other amino acids in the citric acid cycle because such species as asparagines, arginine, lysine, methionine, threonine, isoleucine, and several nucleotides can be synthesized. It is also important in the functioning of RNA, DNA, as well as the production of immunoglobulin and antibody synthesis. It is conceivable that the inclusion of aspartic acid could create a self-stratifying stimuli-responsive system resulting in colloidal films with bioactive surface(s). Previous studies^{24,35,110} have shown that the inclusion of components capable of intramolecular hydrogen bonding can create competing interactions capable of releasing individual components to the film-air interface. With this in mind, it is believed by controlling the ionic character by pH and diminishing hydrogen bonding capabilities of aspartic acid, aspartic acid will gain added mobility to stratify to the surface(s) of the colloidal film.

References

- (1) Flory, P. *Principles of Polymer Chemistry*; Cornell University Press: Ithaca, 1953.
- (2) Lovell, P. A.; El-Aasser, M. S., Eds. *Emulsion Polymerization and Emulsion Polymers*; John Wiley and Sons: New York, 1998.
- (3) Provder, T.; Winnick, M. A.; Urban, M. W., Eds. *Film Formation in Waterborne Coatings*; American Chemical Society: Washington D.C., 1996; Vol. ACS Symp. Ser. 648.
- (4) Duda, Y.; Vazquez, F. *Langmuir* **2005**, *21*, 1096-1102.
- (5) Tiarks, F.; Landfester, K.; Antonietti, M. *Langmuir* **2001**, *17*, 908-918.
- (6) Misra, A.; Jarrett, W. L.; Urban, M. W. *Macromolecules (Washington, DC, United States)* **2007**, *40*, 6190-6198.
- (7) Singh, A.; Dreher, W. R.; Urban, M. W. *Langmuir* **2006**, *22*, 524-527.
- (8) Lovell, P. A.; El-Aasser, M. S. *Emulsion Polymerization and Emulsion Polymers*; John Wiley & Sons: New York.
- (9) Dillon, R. E. *J. Coll. Sci.* **1951**, *6*, 108.
- (10) Doubler, F.; Holl, Y. In *ACS Symposium Series*, 1996; p 223.
- (11) Kashiwagi, T.; Inaba, A.; Brown, J. E.; Hatada, K.; Kitayama, T.; Masuda, E. *Macromolecules* **1986**, *19*, 2160-2168.
- (12) Vanderhoff, P. A.; Tarkowski, J. W.; Jenkins, M. C.; Bradford, E. B. *J. Macromol. Chem.* **1966**, *1*, 131.
- (13) Sheetz, S. *J. Appl. Polym. Sci.* **1965**, *9*, 3759.
- (14) Routh, A. F.; Russel, W. B. *Langmuir* **1999**, *15*, 7762-7773.

- (15) Goh, M. C.; Juhue, D.; Leung, O. M.; Wang, Y.; Winnik, M. A. *Langmuir* **1993**, *9*, 1319-1322.
- (16) Juhue, D.; Lang, J. *Langmuir* **1993**, *9*, 792-796.
- (17) Hahn, K.; Ley, G.; Schuller, H.; Oberthur, R. *Colloid and Polymer Science* **1986**, *264*, 1092-1096.
- (18) Linne, M. A.; Klein, A.; Miller, G. A.; Sperling, L. H.; Wignall, G. D. *Journal of Macromolecular Science, Physics* **1988**, *B27*, 217-231.
- (19) Yoo, J. N.; Sperling, L. H.; Glinka, C. J.; Klein, A. *Macromolecules* **1990**, *23*, 3962-3967.
- (20) Zhao, C. L.; Wang, Y.; Hruska, Z.; Winnik, M. A. *Macromolecules* **1990**, *23*, 4082-4087.
- (21) LoNostro, P.; Choi, S.-M.; Ku, C.-Y.; Chen, S.-H. *Journal of Physical Chemistry B* **1999**, *103*, 5347-5352.
- (22) Roulstone, B. J.; Wilkinson, M. C.; Hearn, J.; Wilson, A. J. *Polymer International* **1991**, *24*, 87-94.
- (23) Wang, Y.; Kats, A.; Juhue, D.; Winnik, M. A.; Shivers, R. R.; Dinsdale, C. J. *Langmuir* **1992**, *8*, 1435-1442.
- (24) Dreher, W. R.; Zhang, P.; Urban, M. W.; Porzio, R. S.; Zhao, C.-L. *Macromolecules* **2003**, *36*, 1228-1234.
- (25) Urban, M. *Attenuated Total Reflectance Spectroscopy of Polymers: Theory and Practice*; ACS: Washington D.C., 1996.
- (26) Urban, M. *Encyclopedia of Analytical Chemistry*; John Wiley & Sons: New York, 2000.

- (27) Otts, D. B.; Zhang, P.; Urban, M. W. *Langmuir* **2002**, *18*, 6473-6477.
- (28) Aydogan, N.; Abbott, N. L. *Langmuir* **2001**, *17*, 5703-5706.
- (29) Holl, Y. *Macromolecular Symposia* **2000**, *151*, 473-478.
- (30) Lam, S.; Hellgren, A. C.; Sjoberg, M.; Holmberg, K.; Schoonbrood, H. A. S.; Unzue, M. J.; Asua, J. M.; Tauer, K.; Sherrington, D. C.; Goni, A. M. *Journal of Applied Polymer Science* **1997**, *66*, 187-198.
- (31) Mallegol, J.; Gorce, J. P.; Dupont, O.; Jeynes, C.; McDonald, P. J.; Keddie, J. L. *Langmuir* **2002**, *18*, 4478-4487.
- (32) Zhao, C. L.; Dobler, F.; Pith, T.; Holl, Y.; Lambla, M. *Journal of Colloid and Interface Science* **1989**, *128*, 437-449.
- (33) Zhao, C. L.; Holl, Y.; Pith, T.; Lambla, M. *Colloid and Polymer Science* **1987**, *265*, 823-829.
- (34) Zhao, Y.; Urban, M. W. *Macromolecules* **2000**, *33*, 2184-2191.
- (35) Zhao, Y.; Urban, M. W. *Macromolecules* **2000**, *33*, 8426-8434.
- (36) Zhao, Y.; Urban, M. W. *Macromolecules* **2000**, *33*, 7573-7581.
- (37) Zhao, Y.; Urban, M. W. *Langmuir* **2000**, *16*, 9439-9447.
- (38) Zhao, Y.; Urban, M. W. *Langmuir* **2001**, *17*, 6961-6967.
- (39) Evanson, K. W.; Thorstenson, T. A.; Urban, M. W. *Journal of Applied Polymer Science* **1991**, *42*, 2297-2307.
- (40) Evanson, K. W.; Urban, M. W. *Journal of Applied Polymer Science* **1991**, *42*, 2287-2296.
- (41) Evanson, K. W.; Urban, M. W. *Journal of Applied Polymer Science* **1991**, *42*, 2309-2320.

- (42) Urban, M. W.; Koenig, J. L. *Applied Spectroscopy* **1987**, *41*, 1028-1032.
- (43) Amalvy, J. I.; Soria, D. B. *Progress in Organic Coatings* **1996**, *28*, 279-283.
- (44) Khanal, A.; Li, Y.; Takisawa, N.; Kawasaki, N.; Oishi, Y.; Nakashima, K. *Langmuir* **2004**, *20*, 4809-4812.
- (45) Lauten, R. A.; Kjoniksen, A.-L.; Nystroem, B. *Langmuir* **2001**, *17*, 924-930.
- (46) Lee, J.; Moroi, Y. *Langmuir* **2004**, *20*, 4376-4379.
- (47) Meszaros, R.; Thompson, L.; Bos, M.; Varga, I.; Gilanyi, T. *Langmuir* **2003**, *19*, 609-615.
- (48) Smith, L. A.; Hammond, R. B.; Roberts, K. J.; Machin, D.; McLeod, G. *Journal of Molecular Structure* **2000**, *554*, 173-182.
- (49) Sperline, R. P. *Langmuir* **1997**, *13*, 3715-3726.
- (50) Wei, H.; Shen, Q.; Zhao, Y.; Wang, D.; Xu, D. *Journal of Crystal Growth* **2004**, *260*, 511-516.
- (51) Xu, Z.; Ducker, W.; Israelachvili, J. *Langmuir* **1996**, *12*, 2263-2270.
- (52) Backfolk, K.; Lagerge, S.; Rosenholm, J. B.; Eklund, D. *Colloid Polym. Sci.* **2002**, *280*, 701-709.
- (53) Marini, M.; Pilati, F.; Saccani, A.; Toselli, M. *Polymer Degradation and Stability* **2008**, *93*, 1170-1175.
- (54) Yang, E.; Qin, X.; Wang, S. *Materials Letters* **2008**, *62*, 3555-3557.
- (55) Gu, S.; He, G.; Wu, X.; Guo, Y.; Liu, H.; Peng, L.; Xiao, G. *Journal of Membrane Science* **2008**, *312*, 48-58.
- (56) Xiong, Y.; Fang, J.; Zeng, Q. H.; Liu, Q. L. *Journal of Membrane Science* **2008**, *311*, 319-325.

- (57) Yang, C.; Guan, Y.; Xing, J.; Shan, G.; Liu, H. *Journal of Polymer Science, Part A: Polymer Chemistry* **2007**, *46*, 203-210.
- (58) Briscoe, B.; Luckham, P.; Zhu, S. *Polymer* **2000**, *41*, 3851-3860.
- (59) Kim, S. S.; Seo, I. S.; Yeum, J. H.; Ji, B. C.; Kim, J. H.; Kwak, J. W.; Yoon, W. S.; Noh, S. K.; Lyoo, W. S. *J. Appl. Polym. Sci.* **2004**, *92*, 1426-1431.
- (60) Lyoo, W. S.; Lee, S. J.; Kim, J. H.; Noh, S. K.; Ji, B. C.; Kim, B. C. *J. Appl. Polym. Sci.* **2004**, *93*, 41-46.
- (61) Ricciardi, R.; Gaillet, C.; Ducouret, G.; Lafuma, F.; Laupretre, F. *Polymer* **2003**, *44*, 3375-3380.
- (62) Song, S. I.; Kim, B. C. *Polymer* **2004**, *45*, 2381-2386.
- (63) Kozlov, M.; McCarthy, T. J. *Langmuir* **2004**, *20*, 9170-9176.
- (64) Kozlov, M.; McCarthy, T. J. *Polymer Preprints (American Chemical Society, Division of Polymer Chemistry)* **2004**, *45*, 259.
- (65) Kozlov, M.; Quarmyne, M.; Chen, W.; McCarthy, T. J. *Macromolecules* **2003**, *36*, 6054-6059.
- (66) Ferry, J. D. *Viscoelastic Properties of Polymers*, 2nd ed.; John Wiley and Sons, Inc.: New York, 1970.
- (67) Lequieu, W.; Du Prez, F. E. *Polymer* **2004**, *45*, 749-757.
- (68) Kuo, S. W.; Chang, F. C. *Macromolecules* **2001**, *34*, 5224-5228.
- (69) Kwei, T. K.; Pearce, E. M.; Pennacchia, J. R.; Charton, M. *Macromolecules* **1987**, *20*, 1174-1176.
- (70) Li, D.; Brisson, J. *Polymer* **1998**, *39*, 793-800.

- (71) Pedrosa, P.; Pomposo, J. A.; Calahorra, E.; Cortazar, M. *Macromolecules* **1994**, *27*, 102-109.
- (72) Prinos, J.; Panayiotou, C. *Polymer* **1995**, *36*, 1223-1227.
- (73) Boyars, B.; Daniels, E. S.; Storer, R.; Klein, A. *Journal of Applied Polymer Science* **2007**, *104*, 3774-3779.
- (74) Krishnan, S.; Klein, A.; El-Aasser, M. S.; Sudol, E. D. *Macromolecules* **2003**, *36*, 3511-3518.
- (75) Mazuel, F.; Bui, C.; Charleux, B.; Cabet-Deliry, E.; Winnik, M. A. *Macromolecules* **2004**, *37*, 6141-6152.
- (76) Bettenbuehl, J.; Proft, B. *Tenside, Surfactants, Detergents* **2007**, *44*, 360-365.
- (77) Chung, C.-J.; Lin, H.-I.; Tsou, H.-K.; Shi, Z.-Y.; He, J.-L. *Journal of Biomedical Materials Research, Part B: Applied Biomaterials* **2008**, *85B*, 220-224.
- (78) Madaeni, S. S.; Ghaemi, N. *Journal of Membrane Science* **2007**, *303*, 221-233.
- (79) Evans, P.; Pemble, M. E.; Sheel, D. W.; Yates, H. M. *Journal of Photochemistry and Photobiology, A: Chemistry* **2007**, *189*, 387-397.
- (80) Zhang, X.; Fujishima, A.; Jin, M.; Emeline, A. V.; Murakami, T. *Journal of Physical Chemistry B* **2006**, *110*, 25142-25148.
- (81) Ammala, A.; Hill, A. J.; Meakin, P.; Pas, S. J.; Turney, T. W. *Journal of Nanoparticle Research* **2002**, *4*, 167-174.
- (82) Guedri, L.; Ben Amor, S.; Gardette, J. L.; Jacquet, M.; Rivaton, A. *Polymer Degradation and Stability* **2005**, *88*, 199-205.

- (83) Moustaghfir, A.; Tomasella, E.; Jacquet, M.; Rivaton, A.; Mailhot, B.; Gardette, J. L.; Beche, E. *Thin Solid Films* **2006**, *515*, 662-665.
- (84) Abdurrahmanoglu, S.; Can, V.; Okay, O. *Journal of Applied Polymer Science* **2008**, *109*, 3714-3724.
- (85) El-Mabrouk, K.; Vaudreuil, S.; Zegloul, A.; Bousmina, M. *Journal of Nanoscience and Nanotechnology* **2008**, *8*, 1895-1900.
- (86) Kelarakis, A.; Giannelis, E. P.; Yoon, K. *Polymer* **2007**, *48*, 7567-7572.
- (87) Lin, J.-C. *Composites, Part B: Engineering* **2006**, *38B*, 79-85.
- (88) Yalcin, B.; Ergungor, Z.; Konishi, Y.; Cakmak, M.; Batur, C. *Polymer* **2008**, *49*, 1635-1650.
- (89) Baxter, S. M.; Sperry, P. R.; Fu, Z. *Langmuir* **1997**, *13*, 3948-3952.
- (90) Qin, M.; Wang, L.-K.; Feng, X.-Z.; Yang, Y.-L.; Wang, R.; Wang, C.; Yu, L.; Shao, B.; Qiao, M.-Q. *Langmuir* **2007**, *23*, 4465-4471.
- (91) Hergeth, W. D.; Steinau, U. J.; Bittrich, H. J.; Simon, G.; Schmutzler, K. *Polymer* **1989**, *30*, 254-258.
- (92) Tian, C.; Mao, B.; Wang, E.; Kang, Z.; Song, Y.; Wang, C.; Li, S. *J. Phys. Chem. C* **2007**, *111*, 3651-3657.
- (93) Van Durme, K.; Van Mele, B.; Loos, W.; Du Prez, F. E. *Polymer* **2005**, *46*, 9851-9862.
- (94) Yu, Y.-Y.; Chen, C.-Y.; Chen, W.-C. *Polymer* **2002**, *44*, 593-601.
- (95) Sugimoto, H.; Daimatsu, K.; Nakanishi, E.; Ogasawara, Y.; Yasumura, T.; Inomata, K. *Polymer* **2006**, *47*, 3754-3759.

- (96) Wang, Y.; Li, Y.; Zhang, R.; Huang, L.; He, W. *Polymer Composites* **2006**, *27*, 282-288.
- (97) Luna-Xavier, J.-L.; Guyot, A.; Bourgeat-Lami, E. *J. Coll. Int. Sci.* **2002**, *250*, 82-92.
- (98) Caregnato, P.; Carrillo Le Roux, G.; Martire, D. O.; Gonzalez, M. C. *Langmuir* **2005**, *21*, 8001-8009.
- (99) Caregnato, P.; Mora, V. C.; Le Roux, G. C.; Martire, D. O.; Gonzalez, M. C. *J. Phys. Chem. B* **2003**, *107*, 6131-6138.
- (100) Arvidsson, A.; Franke-Stenport, V.; Andersson, M.; Kjellin, P.; Sul, Y.-T.; Wennerberg, A. *Journal of Materials Science: Materials in Medicine* **2007**, *18*, 1945-1954.
- (101) Schroeder, H. C.; Boreiko, O.; Krasko, A.; Reiber, A.; Schwertner, H.; Mueller, W. E. G. *Journal of Biomedical Materials Research, Part B: Applied Biomaterials* **2005**, *75B*, 387-392.
- (102) Aumsuwan, N.; Danyus, R. C.; Heinhorst, S.; Urban, M. W. *Biomacromolecules* **2008**, *9*, 1712-1718.
- (103) Aumsuwan, N.; Heinhorst, S.; Urban, M. W. *Biomacromolecules* **2007**, *8*, 3525-3530.
- (104) Aumsuwan, N.; Heinhorst, S.; Urban, M. W. *Biomacromolecules* **2007**, *8*, 713-718.
- (105) Bae, W.-S.; Urban, M. W. *Langmuir* **2006**, *22*, 10277-10283.
- (106) Bae, W.-S.; Urban, M. W. *Biomacromolecules* **2006**, *7*, 1156-1161.

- (107) Winnik, F. M.; Whitten, D. G.; Urban, M. W.; Lopez, G. *Langmuir* **2007**, *23*, 1-2.
- (108) Lestage, D. J.; Urban, M. W. *Langmuir* **2005**, *21*, 6753-6761.
- (109) Lestage, D. J.; Urban, M. W. *Responsive Polymer Materials* **2006**, 168-183.
- (110) Rhudy, K. L.; Su, S.; Howell, H. R.; Urban, M. W. *Langmuir* **2008**, *24*, 1808-1813.

CHAPTER II

STRATIFIED FILMS OBTAINED FROM POLY-(METHYL METHACRYLATE/N-BUTYL ACRYLATE) COLLOIDAL DISPERSIONS CONTAINING POLYVINYL ALCOHOL

Introduction

Over the past decade considerable advances in synthesis and analysis have facilitated further understanding how colloidal dispersions, particularly after coalescence, may exhibit desirable or undesirable surface and interfacial properties.^{1,2} Considering that minute chemical changes in particle morphology and/or polymer structural compositions significantly effect film formation, the question concerning self organization and interactions between individual components and the driving forces responsible for these processes, and consequently film properties, is important. Recent studies^{3,4} indicated that not just commonly accepted polymer attributes, such as the chemical composition of a polymer backbone, molecular weight, or glass transition temperature (T_g), play a significant role on coalescence. There are a number of other factors requiring consideration. For example, colloidal dispersions prepared from copolymers and blends of the same monomers will exhibit quite different behavior in the presence of different stabilizing agents or pH variations.⁵⁻⁷ Furthermore, minute chemical or compositional drifts significantly influence numerous physical properties. For example, known as viscosity modifier of polymeric solutions, poly-(vinyl alcohol) (PVOH) exhibits unique solubility properties: being not water insoluble below 80° C, upon heating above 80°C and cooling, remains water soluble. Another interesting property pointed out by McCarthy et al. is that PVOH modifies hydrophobic surfaces by

irreversible adsorption from an aqueous phase onto a hydrophobic surface, thus changing the surface characteristics from hydrophobic to hydrophilic.^{8,9}

While these attributes were examined on polymeric films, our interests in colloidal dispersions focus on how the presence of PVOH will affect colloidal particles in solutions as well as during and after coalescence. For instance, PVOH has been used to stabilize colloidal latex particles against flocculation in an aqueous media by entropy-driven adsorption on the particle surface displacing pre-adsorbed surfactants.¹⁰ Previous studies also indicated that the viscosity of PVOH solutions is mainly affected by the molecular weight and polymer concentrations.¹¹⁻¹⁵ In view of these considerations, we synthesized pMMA/nBA colloidal particles in the presence of PVOH and examined the role of PVOH on colloidal dispersions and distribution of individual components and their mobility during coalescence. The ability of PVOH to interact with water and colloidal particles facilitates slower evaporation rates, which may also alter organization of individual components during coalescence, thus providing an opportunity for controlled self-stratification and consequently useful surface/interfacial properties.

Experimental

Methyl methacrylate (MMA), n-butyl acrylate (nBA), potassium persulfate (KPS), sodium dodecyl sulfate (SDS), and poly-(vinyl alcohol) (PVOH) having a molecular weight of 89,000 g/mol were purchased from Aldrich Chemical Co. PVOH and deionized water (DI) were added to a 1 L reaction kettle equipped with a reflux condenser at 75°C in N₂ atmosphere under continuous agitation (300 rpm) using a Caframo BDC3030 digital stirrer. The PVOH was allowed to solubilize in DI-water for 30 min, followed by feeding a solution of MMA, nBA, SDS and DI-water were fed using

monomer-starved conditions using a semi-continuous polymerization process.¹⁶ Particle size measurements were obtained using a Microtrac UPA 250, and Table I lists the resulting particle sizes and concentration levels of individual components.

Colloidal Dispersion Composition		
	MMA/nBA	MMA/nBA
Particle Size (nm)	104	108
DDI (w/w%)	77.5	77.1
MMA (w/w)%	11.3	11.1
nBA (w/w)%	10.4	10.4
KPS (w/w)%	0.2	0.2
SDS (w/w)%	0.6	0.6
PVOH (w/w)%	-----	0.5

Table 1: Particle size and compositions of colloidal dispersion based on final latex weight.

Such prepared colloidal dispersions were cast on a polyvinylchloride (PVC) substrate and allowed to coalesce at 50% relative humidity (RH) for 3 days at 24 °C for the MMA/nBA system. For MMA/nBA/PVOH dispersions the films were allowed to coalesce for an additional 4 days. The resulting films formed approximately 400 μm thick films.

Polarized and non-polarized (ZnSe polarizer) attenuated total reflectance Fourier transform infrared (ATR FT-IR) spectra were collected using a Bio-Rad FTS-6000 FT-IR single-beam spectrometer set at a 4 cm^{-1} resolution A 45° face angle Ge crystal with

50×20×3 mm dimensions and a 45° face angle KRS-5 crystal with 50×20×3 dimensions were used. This configuration allows the analysis of the film-air (F-A) interface at approximately 0.46 μm and 1.94 μm from the F-A interface, and the use of a ZnSe polarizer facilitates orientation studies by utilizing TE (transverse electric) and TM (transverse magnetic) modes.

Determination of PVOH's extinction coefficient was accomplished by preparing standard solutions with known concentrations of PVOH in dimethyl sulfoxide (DMSO) (3.1, 1.6, 0.7, and 0.4×10⁻⁷ mol/L) followed by transmission FT-IR measurements recorded as a function of concentration. A liquid transmission cell with 0.1 mm path length was utilized. A plot of band intensity versus concentration was used to determine the extinction coefficient of PVOH which was 7.9 L/(mol cm).

IR images were obtained using internal reflection IR imaging (IRIRI) with a Ge internal reflection element. This system consists of a Bio-Rad FTS 6000 spectrometer, a UMA 500 microscope, ImagerIR focal plane array detector, and a semispherical Ge crystal which facilitates a spatial resolution of about 1 μm.¹⁷ IRIRI images were collected using the following spectral acquisition parameters: undersampling ratio = 4, step scan speed = 2.5 Hz, number of spectrometer steps = 1777, number of images per step = 64, and spectral resolution = 8 cm⁻¹. In a typical experiment, a spectral data acquisition time was approximately 15 min. Image processing was performed using ENVI (The Environmental for Visualizing Images, Research Systems Inc.) version 3.5.

Photoacoustic FT-IR spectra were obtained using a Bio-Rad FTS 7000 spectrometer. A phase modulation step-scan mode was used to analyze the MMA/nBA/PVOH film. Interferograms were collected at 8 cm⁻¹ resolution using 800,

400, 100, and 50 Hz modulation frequencies, and a MTEC model 300 photoacoustic detector was used to acquire all spectra with He as the carrier gas. Two dimensional photoacoustic spectra were obtained using in-phase and quadrature photoacoustic spectra collected at 8 cm^{-1} resolution using 800, 400, 100, and 50 Hz modulation frequencies and later analyzed using Bio-Rad Win-IR Pro 3.4 computer program.

Results and Discussion

The presence of PVOH during MMA/nBA colloidal synthesis provides an opportunity to develop films with unique characteristics. The first observation is the increased particle size by about 10 nm as well as enhanced viscosity from 0.0013 to 0.005 Pa.s. Such colloidal dispersions were allowed to coalesce to form films, and their F-A interfacial features were analyzed spectroscopically. As shown in Figure 8, Traces A and B, illustrate ATR-FTIR spectra recorded for the coalesced MMA/nBA and MMA/nBA/PVOH films, respectively. For reference, Traces C and D represent SDS and PVOH spectra. As seen in Trace A, the 1096 cm^{-1} band due to OH groups of PVOH in the MMA/nBA copolymer matrix is present, indicating the presence of PVOH near the F-A interface.

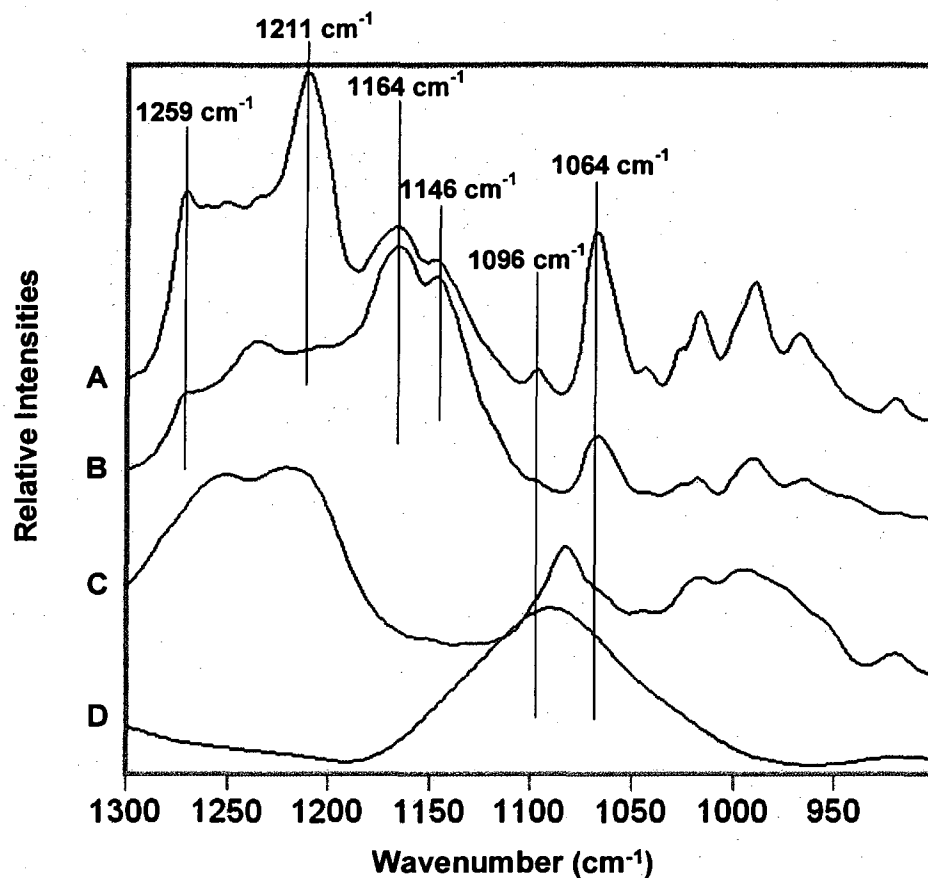


Figure 8: ATR-FTIR spectra recorded from the F-A interface: (A) pMMA/nBA/PVOH, (B) pMMA/nBA, (C) SDS reference spectrum, and (D) PVOH reference spectrum.

Comparison of the band intensities in Traces A and B also shows the increase of the 1064 cm^{-1} band due to S-O stretching vibrations, while the 1164 cm^{-1} and 1146 cm^{-1} bands attributed to MMA and nBA of the copolymer matrix are diminished. When PVOH is present in the system, the 1215 cm^{-1} band splits into two bands at 1211 and 1259 cm^{-1} , which are attributed to $\text{SO}_3^-\text{Na}^+/\text{H}_2\text{O}$ and $\text{SO}_3^-\text{Na}^+/\text{-COO-}$ interactions.^{3,6} These bands indicate that the addition of PVOH enhances the concentration levels of SDS at the F-A interface.

Postponing temporarily the origin of the migration and PVOH/SDS interactions, ATR-FTIR analysis using TE and TM polarizations was utilized. Figure 9, Traces A/A'

and B/B' show ATR FT-IR spectra recorded from the F-A interfaces of MMA/nBA/PVOH and MMA/nBA films, respectively.

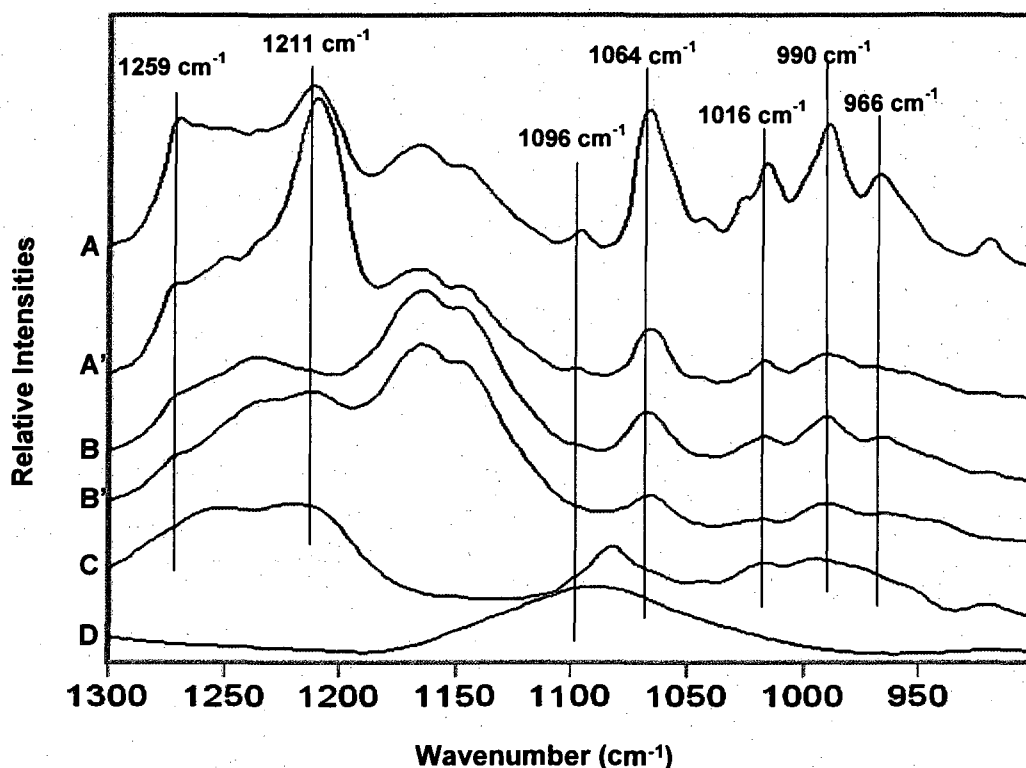


Figure 9: Polarized ATR-FTIR spectra recorded from the F-A interface: (A) TM-pMMA/nBA/PVOH, (A') TE-pMMA/nBA/PVOH, (B) TM-pMMA/nBA, (B') TE-pMMA/nBA, (C) SDS reference spectrum, and (D) PVOH reference spectrum.

Comparison of Traces A and A' indicates the increase of the 1096 cm^{-1} band due to O-H bending vibrations in TE polarization, thus indicating that the O-H segments of PVOH are preferentially parallel to the F-A interface. Enhanced band intensities of the 1064, 1016, 990, and 966 cm^{-1} bands due to $\text{SO}_3^- \text{Na}^+$ hydrophilic ends of SDS also indicate preferential parallel orientation of these species at the F-A interface. However, a comparison of the TE and TM spectra of pMMA/nBA (Traces B and B') reveals no intensity changes, consisted for a random orientation of SDS at the F-A interface. The

spectra recorded using TE and TM polarizations were utilized to determine dichroic ratio (R) values listed in Table 2.

Dichroic Ratios (R) of Selected IR bands					
Sample	1096 cm ⁻¹	1064 cm ⁻¹	1016 cm ⁻¹	990 cm ⁻¹	966 cm ⁻¹
MMA/nBA/PVOH	10.0	4.8	4.9	10.9	26.4
MMA/nBA	N/A	0.25	0.12	0.74	0.58

Table 2: Dichroic ratios ($R = I_{TE}/I_{TM}$) of selected IR bands.

When $R < 1.0$, molecular segments are preferentially aligned perpendicular to the film interface, whereas for $R > 1.0$, parallel orientation is present. For the pMMA/nBA/PVOH films, the R values of the selected IR bands attributed to PVOH and SDS are > 1 , thus indicating that SO_3Na^+ groups exhibit preferential parallel orientation near the F-A interface. For pMMA/nBA films, $0 < R < 1$, implying random orientation of the SDS functional groups near the F-A interface.

Previous studies^{3,6} showed that interactions between hydrophilic SO_3Na^+ groups of SDS and H_2O and/or COOH lead to preferential parallel orientation of SO_3Na^+ species. Such interactions are also observed near the F-A interface of pMMA/nBA/PVOH films, but for pMMA/nBA films the SO_3Na^+ heads are randomly orientated. Thus, the question is why does the addition of PVOH in the synthesis of colloidal dispersions affect the orientation of SO_3Na^+ species near the F-A interface? For pMMA/nBA films, the SO_3Na^+ species interact with H_2O and $-\text{COO}-$ groups via formation of localized ionic clusters (LICs),¹⁸ but when PVOH is present, terminal OH groups create an opportunity to compete for hydrogen bonding with the carbonyls of the matrix and with $\text{SO}_3\text{Na}^+/-\text{COO}-$ and $-\text{COO}/\text{OH}$ species. If $-\text{COO}/\text{OH}$ interactions are more favorable, the SO_3Na^+ species exhibit higher propensity for interactions with H_2O and during coalescence are driven to the F-A interface.

With these considerations in mind, let us further consider distribution of SDS and PVOH near the F-A interface. Figure 10, Traces A-D, represent a series of ATR-FTIR spectra recorded from the F-A interface of MMA/nBA/PVOH at 0.46, 0.83, 1.42, and 1.94 μm depths from the F-A interface, respectively. Again, Traces E and F represent the reference spectra of SDS and PVOH, respectively.

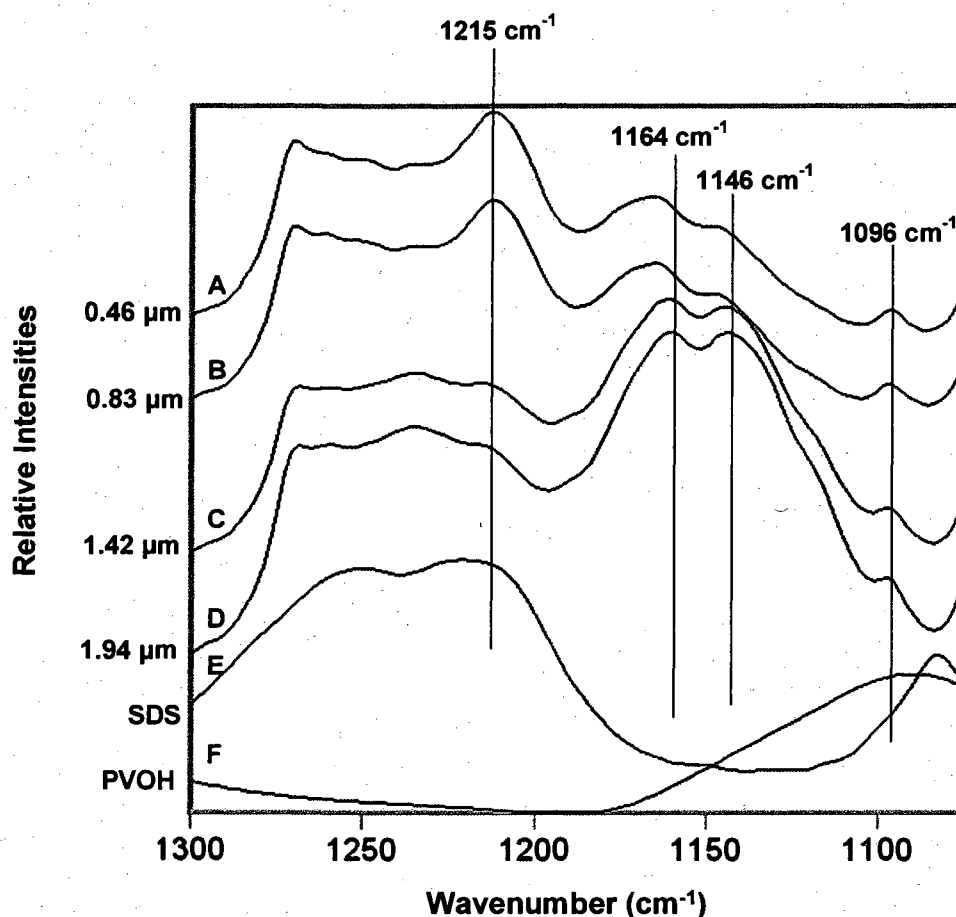


Figure 10: ATR-FTIR spectra of pMMA/nBA/PVOH films recorded from the F-A interface: (A) 0.46 μm , (B) 0.83 μm , (C) 1.42 μm , (D) 1.94 μm from the F-A interface and (E) SDS reference spectrum, and (F) PVOH reference spectrum.

Analysis of the 1096 cm^{-1} O-H band due to PVOH as well as the 1164 cm^{-1} and 1146 cm^{-1} bands of the copolymer matrix clearly indicate that going further away from the F-A interface PVOH concentrations and the copolymer matrix increase, whereas the SDS

content decreases. As shown in the Experimental Section, ATR FT-IR measurements allow us to quantitatively determine PVOH content as a function of depth near the F-A interface.¹⁹⁻²² As shown in Figure 11, going further away from the F-A interface, the PVOH concentration increases.

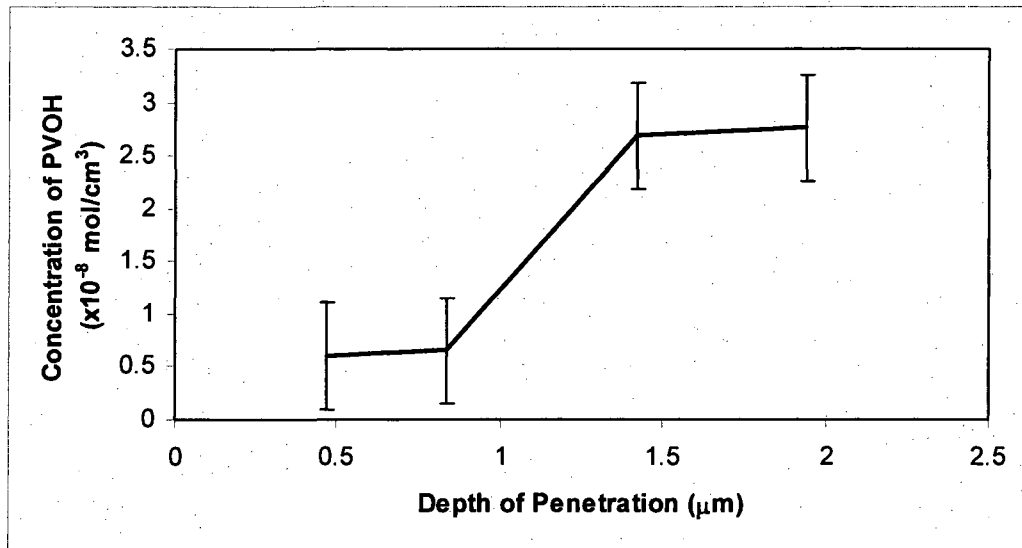


Figure 11: Plot of volume concentration of PVOH versus film thickness.

The next question is how far from the interfacial regions PVOH and SDS are competing for interacting with coalesced colloidal particles. In order to obtain information further away from the F-A interface, step-scan PA FT-IR spectroscopy was employed. Figure 12, Traces A-D represents PA FT-IR spectra recorded from the F-A interface of MMA/nBA/PVOH films from depths ranging from 6.3 to 25.2 μm .^{23,24} To follow the distribution of PVOH, the 3340 cm^{-1} O-H stretching band was utilized.

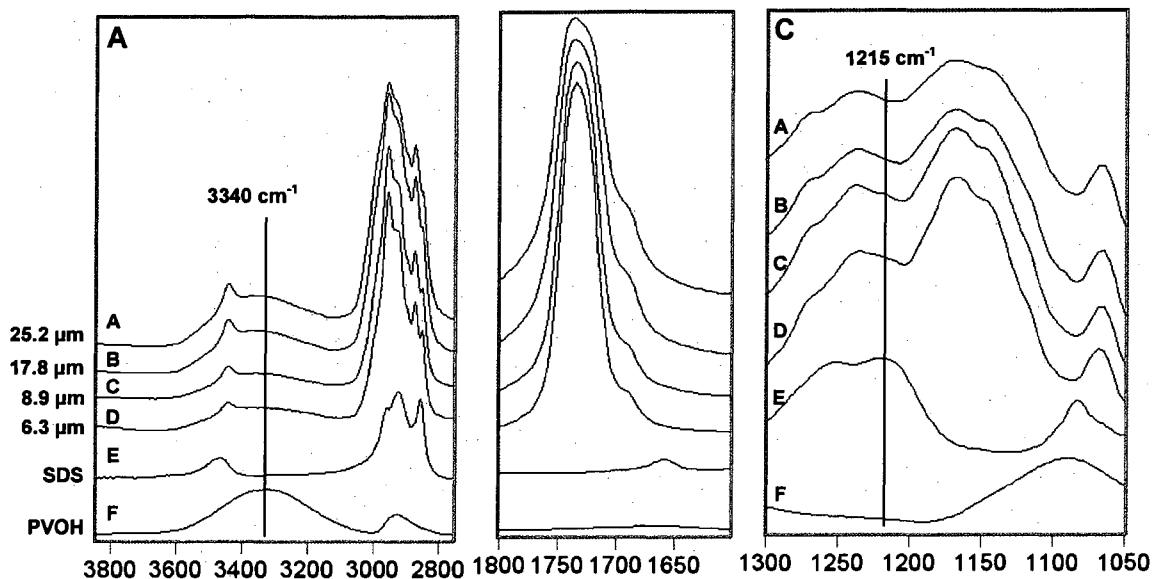


Figure 12: PA-FTIR spectra of pMMA/nBA/PVOH films recorded from the F-A interface: (A) 25.2 μm , (B) 17.8 μm , (C) 8.9 μm , (D) 6.3 μm from the F-A interface and (E) SDS reference spectrum, and (F) PVOH reference spectrum.

As seen, further away from the F-A interface the intensity of the O-H stretching band increases. In contrast, as shown in Figure 5C, further from the F-A interface, the 1215 cm^{-1} band attributed to the S-O stretching vibrations of SDS decreases. In addition, the presence of a shoulder on the C=O stretching band at 1690 cm^{-1} is detected, which is attributed to intramolecular hydrogen bonding of hydroxyl and carbonyl groups.²⁵ Analysis of these data shows that free OH and H-bonded PVOH content increases in the bulk of the film.

In view of the above data, it appears that during the film formation of pMMA/nBA/PVOH the following interactions occur: SO_3Na^+ head groups of SDS form hydrogen bonding with H_2O and $-\text{COO}-$ groups of the copolymer matrix, but the presence of PVOH in pMMA/nBA creates a competing environment with the OH groups

of PVOH and carbonyl groups of the matrix. These interactions are depicted in Figure 13 which control the degree of stratification of individual components.

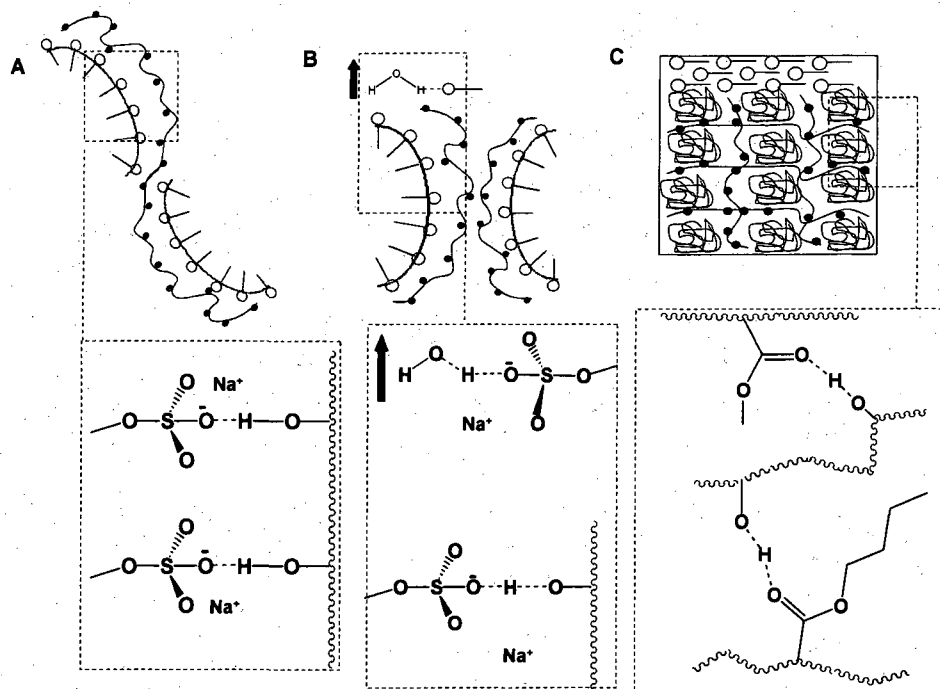


Figure 13: Schematic representation of interactions during film formation: (A) In solution, (B) During coalescence, and (C) fully coalesced film.

As seen in Figure 13A, in an aqueous phase, OH groups of PVOH form hydrogen bonds with the $\text{SO}_3^- \text{Na}^+$ entities stabilizing particles by sharing the proton from the hydroxyl group. As water begins to leave dispersed particles, the particles come to closer contact with each other (Figure 13B), and $\text{SO}_3^- \text{Na}^+ - \text{H}_2\text{O}$ interactions drive SDS molecules to the F-A interface (Figure 13C), where the SDS rich F-A interface is formed. However, a fraction of PVOH remains trapped by the hydrogen bonding with the $-\text{COO}-$ groups of the pMMA/nBA copolymer matrix, thus forming self-stratified films.

As previously indicated, PA-FTIR spectroscopy can be utilized to analyze chemical species at various depths from the F-A interface. However, often intramolecular interactions of the probed chemical species cannot be detected directly.

For that reason, 2D PA-FTIR²⁶ was utilized whereby using both in-phase and in-quadrature spectra, two dimensional representations may reveal further interactions of individual components. Figure 14 represents a 2D-PA-FTIR experiment, where the O-H and C=O stretching regions were monitored for MMA/nBA/PVOH films.

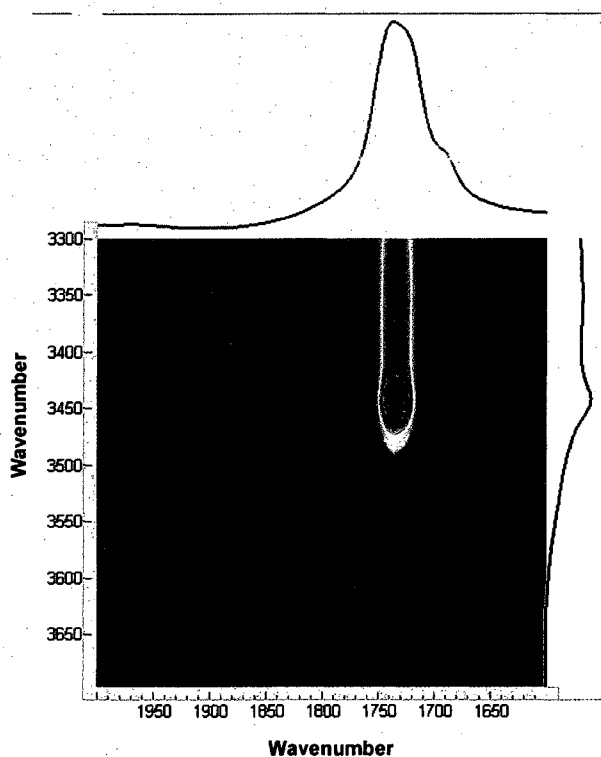


Figure 14: 2D PA-FTIR spectra of pMMA/nBA/PVOH at 50 Hz modulation frequency.

The cross-peak correlates a modulation frequency change of the carbonyl vibrations due to its close proximity to O-H functional group of PVOH indicating a through space interaction. Thus, the 2D PA FT-IR measurements validate the presence of the shoulder detected at 1690 cm^{-1} which results from intramolecular interactions between PVOH and the C=O groups of the copolymer matrix.

Further evidence for stratification illustrated in Figures 15, A, B, and C, which represent IR images of the bands at 1215, 1146 and 1096 cm^{-1} vibrations recorded from the cross-section of the MMA/nBA/PVOH films. As we recall, these bands are due to the S-O and C-O stretching vibrations in SDS and nBA, respectively, and O-H bending modes in PVOH. Analysis of the images shown in Figure 15 indicates that the cross-section of the pMMA/nBA films containing PVOH supports ATR-FTIR and PA-FTIR data and also show that SDS is located near the F-A interface. At the same time PVOH is localized in the interior of the film. While Figures 15A, B, and C provide a spatial distribution of different entities, Figure 15 D represents IR spectra recorded from the regions labeled 1, 2, and 3 in Figures 15 A, B, and C.

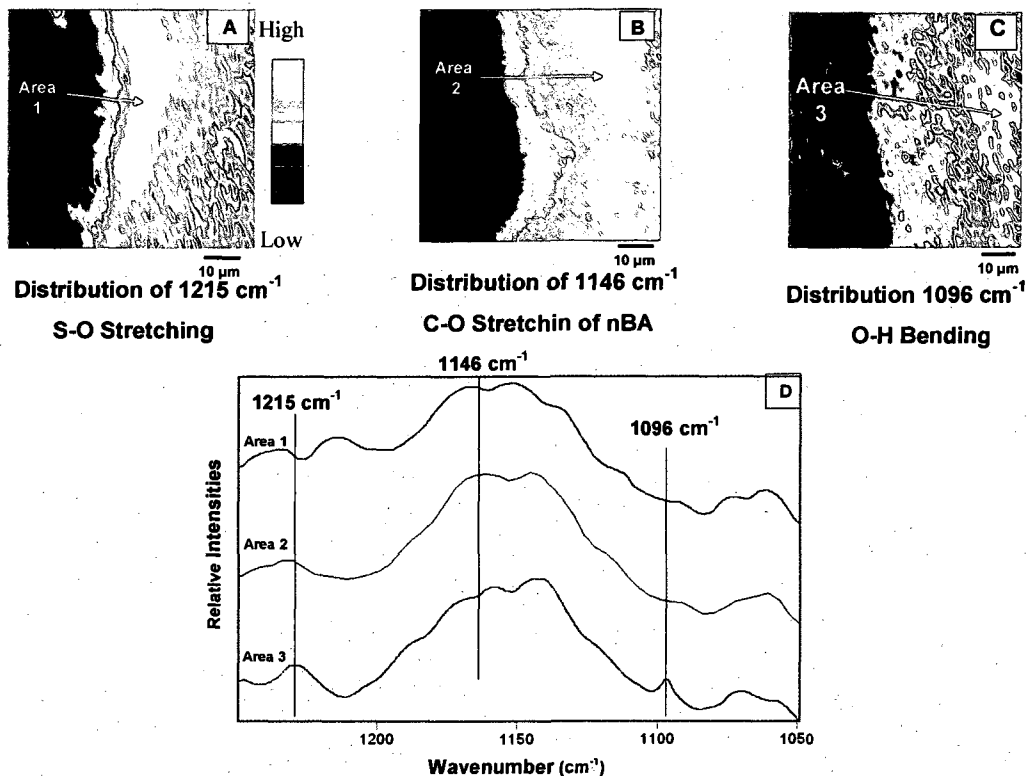


Figure 15: IRIR images recorded from the film cross-section of pMMA/nBA/PVOH

As seen, IR spectra recorded from area 1 indicate the presence of the 1215 cm^{-1} S-O stretching vibration due to SDS. In contrast, area 3 shows no presence of this band, but the presence of the 1096 cm^{-1} O-H bending modes due to PVOH is detected. The spectra recorded from Area 2 shows the presence of the 1146 cm^{-1} band attributed to nBA. It should be noted that the highest concentration levels of PVOH are observed in the same distance from the F-A interface as for copolymer matrix which results from the H-bonding between PVOH and the C=O groups of the matrix.

The above data allows us to propose the model for stratification processes during coalescence which is depicted in Figure 16.

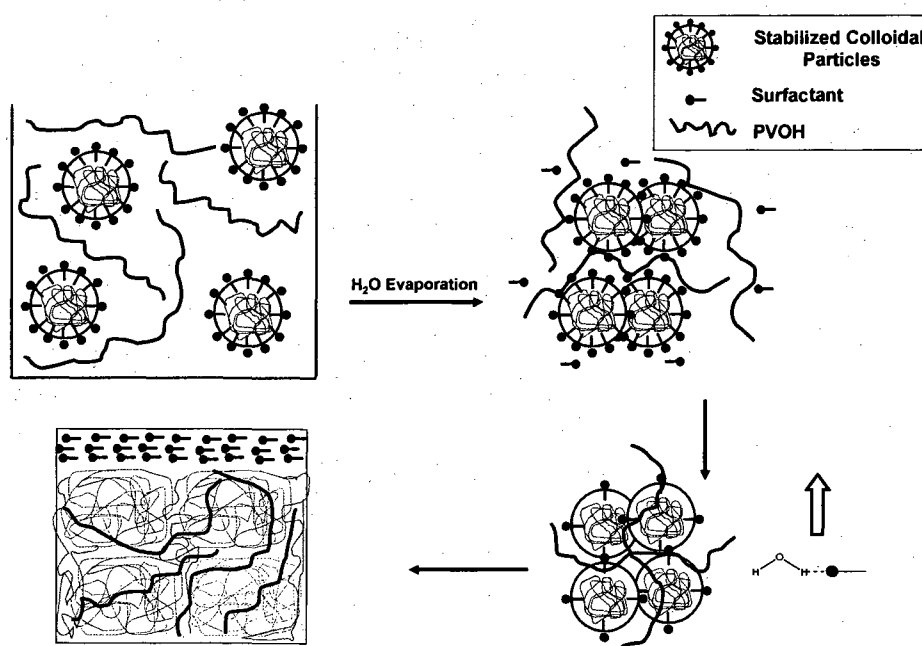


Figure 16: Schematic representation of the overall film formation process when MMA and nBA are copolymerized in the presence of PVOH.

Due to the fact that PVOH is soluble in an aqueous phase and polymerization process is conducted in the presence of PVOH, hydroxyl groups of PVOH interact with the polar head groups of SDS. Once the evaporation of an aqueous phase begins, surfactant-

stabilized colloidal particles are brought in close proximity during which surfactant molecules are displaced from the surface as a result of competing interactions between pMMA/nBA and PVOH. As a consequence, self-stratification of surfactant molecules occur near the F-A interface, and PVOH occupies the space left behind as a result of hydrogen bonding with the copolymer matrix. Upon completion of this process, there is a surfactant rich layer near the F-A interface whereas PVOH remains in the bulk of the copolymer matrix.

Conclusions

These studies show that during coalescence of pMMA/nBA particles stabilized by SDS, the presence of PVOH causes the displacement of SDS and its stratification near the F-A interface. At the same time, PVOH remains in the bulk of the film. This behavior is attributed to competing interactions between C=O groups of the polymer matrix, SO_3Na^+ polar groups of SDS, and OH of PVOH. As a consequence, stratification of these compounds can be controlled by changing their concentration levels as well as film formation conditions.

References

- (1) Urban, M. W. *Film Formation*; American Chemical Society: Washington D.C., 2002.
- (2) Lovell, P. A. *Emulsion Polymerization and Emulsion Polymers*; John Wiley and Sons: New York, 1997.
- (3) Zhao, Y.; Urban, M. W. *Langmuir* **2001**, *17*, 6961-6967.
- (4) Zhao, Y.; Urban, M. W. *Macromolecules* **2000**, *33*, 2184-2191.
- (5) Lestage, D. J.; Schleis, D. J.; Urban, M. W. *Langmuir* **2004**, *20*, 7027-7035.
- (6) Dreher, W. R.; Zhang, P.; Urban, M. W.; Porzio, R. S.; Zhao, C.-L. *Macromolecules* **2003**, *36*, 1228-1234.
- (7) Dreher, W. R.; Jarrett, W. L.; Urban, M. W. *Macromolecules* **2005**, *38*, 2205-2212.
- (8) Kozlov, M.; Quarmyne, M.; Chen, W.; McCarthy, T. J. *Macromolecules* **2003**, *36*, 6054-6059.
- (9) Kozlov, M.; McCarthy, T. J. *Langmuir* **2004**, *20*, 9170-9176.
- (10) Backfolk, K.; Lagerge, S.; Rosenholm, J. B.; Eklund, D. *Colloid Polym. Sci.* **2002**, *280*, 701-709.
- (11) Song, S. I.; Kim, B. C. *Polymer* **2004**, *45*, 2381-2386.
- (12) Ricciardi, R.; Gaillet, C.; Ducouret, G.; Lafuma, F.; Laupretre, F. *Polymer* **2003**, *44*, 3375-3380.
- (13) Lyoo, W. S.; Lee, S. J.; Kim, J. H.; Noh, S. K.; Ji, B. C.; Kim, B. C. *J. Appl. Polym. Sci.* **2004**, *93*, 41-46.

- (14) Kim, S. S.; Seo, I. S.; Yeum, J. H.; Ji, B. C.; Kim, J. H.; Kwak, J. W.; Yoon, W. S.; Noh, S. K.; Lyoo, W. S. *J. Appl. Polym. Sci.* **2004**, *92*, 1426-1431.
- (15) Briscoe, B.; Luckham, P.; Zhu, S. *Polymer* **2000**, *41*, 3851-3860.
- (16) Gerrens, H. *Polymer Preprints (American Chemical Society, Division of Polymer Chemistry)* **1966**, *7*, 699-706.
- (17) Otts, D. B.; Zhang, P.; Urban, M. W. *Langmuir* **2002**, *18*, 6473-6477.
- (18) Lestage, D. J.; Urban, M. W. *Langmuir* **2005**, *21*, 2150-2157.
- (19) Zhao, Y.; Urban, M. W. *Langmuir* **1999**, *15*, 3538-3544.
- (20) Urban, M. W. *Attenuated Total Reflectance Spectroscopy of Polymers Theory and Practice*; American Chemical Society: Washington DC, 1996.
- (21) Kim, H.; Urban, M. W. *Langmuir* **1996**, *12*, 1051-1055.
- (22) Bae, W.-S.; Urban, M. W. *Langmuir* **2004**, *20*, 8372-8378.
- (23) Zhang, P.; Urban, M. W. *Langmuir* **2004**, *20*, 10691-10699.
- (24) Rosencwaig, A. *Photoacoustics and Photoacoustic Spectroscopy*; John Wiley and Sons: New York, 1980.
- (25) Colthup, N. *The Handbook of Infrared and Raman Characteristic Frequencies of Organic Molecules*; Academic Press: San Diego, 1991.
- (26) Jiang, E. Y.; McCarthy, W. J.; Drapcho, D. L.; Crocombe, R. A. *Applied Spectroscopy* **1997**, *51*, 1736-1740.

CHAPTER III

COMPETITIVE STRATIFICATION INFLUENCED BY CROSSLINKS IN POLY-(METHYL METHACRYLATE/N-BUTYL ACRYLATE) COLLOIDAL FILMS

Introduction

The introduction of crosslinks complicates the process of colloidal particle coalescence and film formation.^{1,2} For example, utilizing covalent crosslinks requires that the kinetics of coalescence and crosslinking be controlled in order to provide adequate conditions for film formation. In contrast, the use of ionic or hydrogen bonding crosslinks facilitates leeway during coalescence, since they typically lead to reversible bonding of polymer matrix components controllable by colloidal solution properties such as pH and ionic strength. A number of studies have focused on the role of physical crosslinks in blended systems and their effect on the glass transition temperature as well as their influence on the miscibility of these systems.³⁻⁸ Recent studies pertaining to crosslinked colloidal systems have shown that the amount of crosslinks and their effect on physio-chemical properties can be controlled by the blend composition, the use of a chain transfer agents, and the ability to control the interdiffusion properties of crosslinking agents.⁹⁻¹¹

The utilization of crosslinks for the enhancement of physical properties is well documented, and the primary role of crosslinkers is to enhance mechanical strength as well as network permeability.^{12,13} However, depending upon the nature of the crosslinking mechanism, different crosslinkers will exhibit different attributes, and often molecular level processes responsible for the property changes are not well understood. To further understand the molecular processes of colloidal dispersions, we utilized chemical and physical crosslinkers as well as the combination in the precise synthesis of

pMMA/nBA colloidal dispersions. Methacrylic acid (MA) was incorporated to introduce physical crosslinks, whereas methylene bisacrylamide (MBA) was chosen due to its ability to form chemical crosslinks. A combination of physical and chemical crosslinks was obtained using n-methylol acrylamide (HAM). These colloidal dispersions were coalesced, and the effectiveness of different types of crosslinker on molecular level interactions at different temperatures examined. The ultimate goal of this study is to elucidate the effect of crosslinkers on stratification near the film-air (F-A) interfaces.

Experimental

Methyl methacrylate (MMA), n-butyl acrylate (nBA), potassium persulfate (KPS), sodium dodecyl sulfate (SDS), n-(hydroxymethyl)-acrylamide (HAM), methacrylic acid (MA), and n,n'-methylene bisacrylamide (MBA) were purchased from Aldrich Chemical Co. Deionized water (DI) was added to a 1 L reaction kettle equipped with a reflux condenser at 75°C in N₂ atmosphere under continuous agitation (300 rpm) using a Caframo BDC3030 digital stirrer. The formation of the pre-emulsion was as follows: 1) For the pMMA/nBA/MBA system, MBA and SDS were allowed to dissolve in DI water for 30 mins, followed by addition of MMA and nBA to SDS/MBA/DI water solution and allowed to form micelles for 30 additional minutes; 2) For the pMMA/nBA/MA system, MMA, nBA, and MA were allowed to solubilize for 30 minutes. The MMA/nBA/MA solution was then added to a SDS/DI water solution to form micelles for 30 mins; 3) For the pMMA/nBA/HAM system, MMA, nBA, and HAM were allowed to solubilize for 30 mins. The MMA/nBA/HAM solution was then added to a SDS/DI water solution to form micelles for 30 mins. The pre-emulsions consisting of monomers, surfactant, and DI-water were fed using monomer-starved conditions using a semi-continuous

polymerization process. To facilitate the crosslinking reaction of pMMA/nBA/HAM, 1.0 mL of sulfuric acid was added to the kettle after polymerization was complete to acid catalyze the crosslinking reaction. Particle size measurements were obtained using a Microtrac UPA 250. Such prepared colloidal dispersions were cast in a Teflon mold having wells with a depth of 3 mm and allowed to coalesce at 50% relative humidity (RH) for 3 days at 24 °C. The resulting films had an approximate thickness of 1mm.

Attenuated total reflectance Fourier transform infrared (ATR FT-IR) spectra were collected using a Bio-Rad FTS-6000 FT-IR single-beam spectrometer set at a 4 cm^{-1} resolution. A 45° face angle Ge crystal with $50\times 20\times 3$ mm dimensions and a 45° face angle KRS-5 crystal with $50\times 20\times 3$ mm dimensions were used. This configuration permits both quantitative and qualitative analysis of the film-air (F-A) interface at approximately $0.46\ \mu\text{m}$ and $1.94\ \mu\text{m}$ from the F-A interface.

Dynamic mechanical analysis (DMA) data was obtained using a TA Instruments DMA Q800 in tensile mode with an amplitude of 2 Hz. The samples were analyzed through a temperature range of -10 to 200°C while utilizing a temperature ramp of $2^\circ\text{C}/\text{min}$. Data was processed using TA Universal Analysis software and Microsoft Excel and crosslink density calculations were performed using a previously reported method.¹⁴

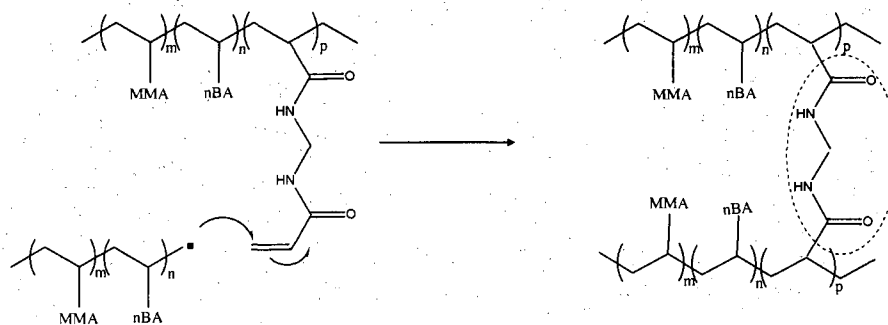
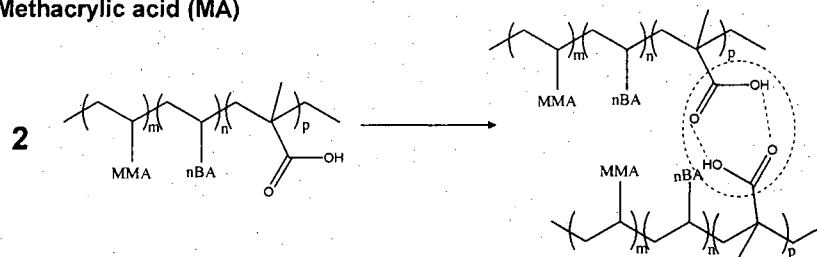
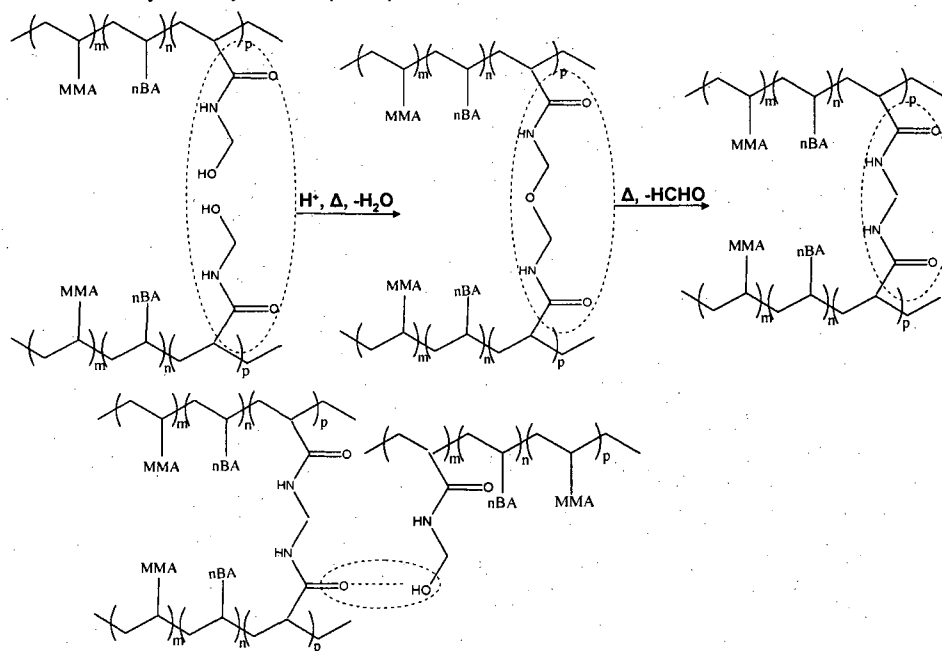
IR images were obtained using internal reflection IR imaging (IRIRI) with a Ge internal reflection element. This system consist of a Bio-Rad FTS 6000 spectrometer, a UMA 500 microscope, and ImagIR focal plane array detector, and a semispherical Ge crystal which facilitates a spatial resolution of about $1\ \mu\text{m}$.¹⁵ IRIRI images were collected using the following spectral acquisition parameters: undersampling ratio = 4, step scan speed = 2.5 Hz, number of spectrometer steps = 1777, number of images per step = 64,

and spectral resolution = 8 cm^{-1} . In a typical experiment, a spectral data acquisition time was approximately 17 min. Image processing was performed using ENVI (The Environmental for Visualizing Images, Research Systems Inc.) version 3.5

Photoacoustic FT-IR spectra were obtained using a Bio-Rad FTS 7000 spectrometer using a phase modulation step-scan mode. Interferograms were collected at 8 cm^{-1} resolution using 1000, 400, and 200 Hz modulation frequencies, and a MTEC model 300 photoacoustic detector was used to acquire all spectra with He as the carrier gas.

Results and Discussion

To set the stage and address the effect of physio-chemical crosslinking upon coalescence of colloidal particles, Schemes 1, A, B, and C illustrates the possible crosslinking scenarios for the crosslinkers implemented.

A: Methylene bisacrylamide (MBA)**B: Methacrylic acid (MA)****C: n-methylol acrylamide (HAM)**

Scheme 1: Incorporation of methylene bisacrylamide, methacrylic acid, and n-(hydroxymethyl)-acrylamide into methyl methacrylate and n-butyl acrylate polymerization.

As illustrated in Scheme 1, A, when MBA is incorporated into pMMA/nBA backbone in such a way that the MBA C=C is preserved for further reactions, the presence of free radicals will facilitate chemical crosslinks during particle coalescence. However, when MBA is replaced by MA, shown in Scheme 1, B, it is anticipated that H-bonding between the network acid protons will participate in physical crosslinks. In contrast, Scheme 1, C, upon incorporation of HAM into pMMA/nBA system, the neighboring HAM molecules under acidic conditions and elevated temperatures will result in condensation reactions and an ether intermediate, which upon further reactions and loss of formaldehyde will result in crosslinked networks. Due to the nature of the crosslinking reaction it is also anticipated that not all HAM molecules will chemically crosslink, leaving hydroxyl terminated side chains capable of further H-bonding.

To set the stage, we prepared precisely controlled colloidal dispersions following reactions depicted in Scheme 1 which after coalescence formed films and analyzed their dynamic mechanical properties as a function of temperature in the context of molecular level processes responsible for these properties. Figure 17-A-, Traces A, B, and C, illustrate $\tan \delta$ curves plotted as a function of temperature for pMMA/nBA/MBA, pMMA/nBA/MA, and pMMA/nBA/HAM, respectively. For reference, the $\tan \delta$ curve for pMMA/nBA is shown in Figure 17, D.

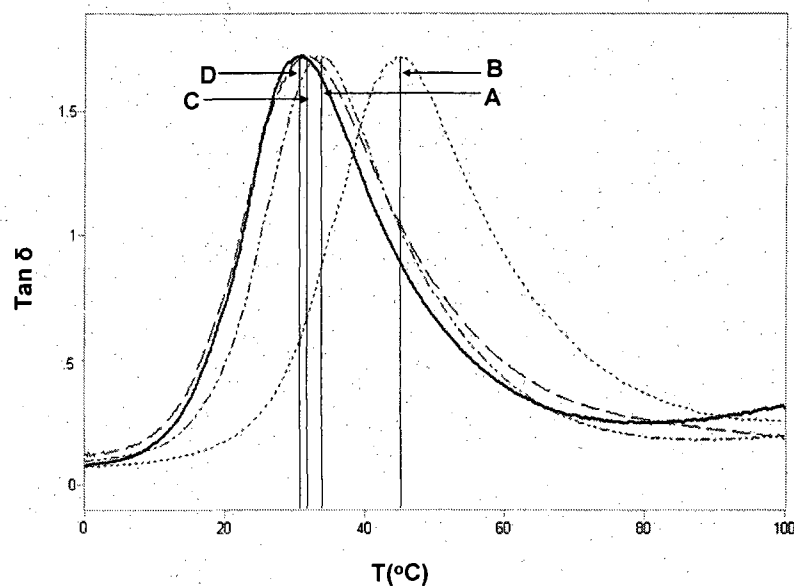


Figure 17A: $\tan \delta$ plotted as a function of temperature (T) for: A - pMMA/nBA/MBA; B - pMMA/nBA/MA; C - pMMA/nBA/HAM, and the D - pMMA/nBA standard.

These data show that the max $\tan \delta$, which corresponds to the glass transition temperature (T_g), increases from 28°C for pMMA/nBA (D) to 30°C for pMMA/nBA/HAM (C), 33°C for pMMA/nBA/MBA (A), and 42°C (B) for pMMA/nBA/MA. These systematic T_g changes indicate reduced segmental mobility of the polymer network components induced by physical and chemical crosslink density changes, and each crosslinker reduces the free volume to a different degree. Figure 17B illustrates storage moduli ($\log E'$) for the same specimens measured as a function of temperature.

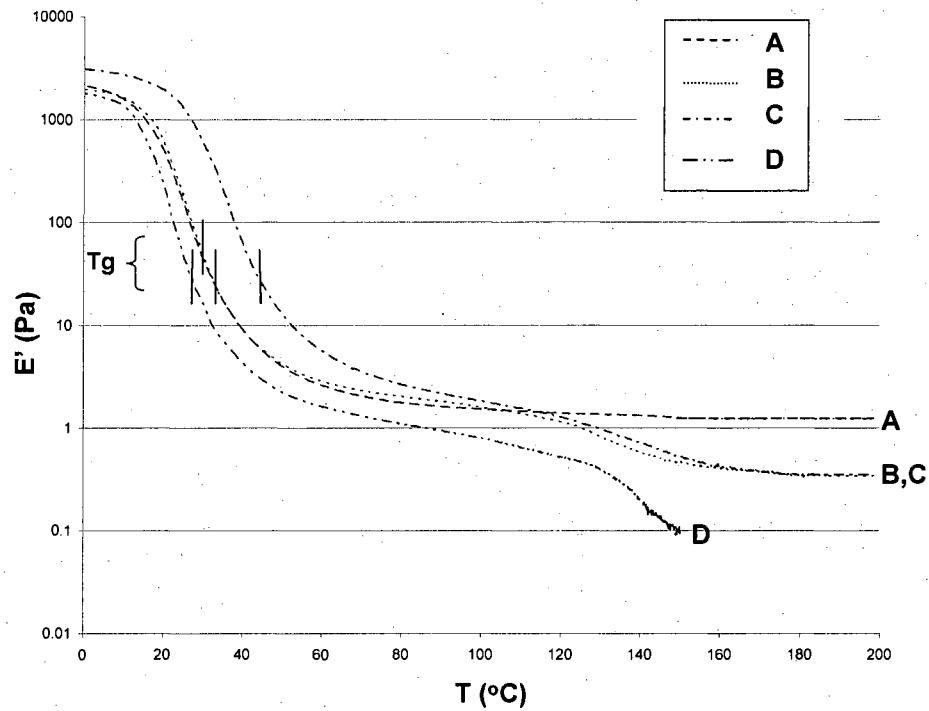


Figure 17B: Storage moduli (E') plotted as a function of temperature for A - pMMA/nBA/MBA; B - pMMA/nBA/MA; C - pMMA/nBA/HAM, and D - pMMA/nBA.

As seen, the rubbery plateau region of pMMA/nBA drops off at 150°C, while for the other networks level off, and each crosslinker contributes to the overall storage modulus, with pMMA/nBA/MA exhibiting the highest storage modulus throughout the rubbery plateau region (80-120°C), which diminishes for other networks in the following order: pMMA/nBA/MBA > pMMA/nBA/HAM > pMMA/nBA (control).

In an effort to elucidate the contribution of each crosslinker with respect to the uncrosslinked pMMA/nBA network, the relative crosslink density, X_i , for each network was calculated over a temperature range and ratioed against the pMMA/nBA control. This approach allows us to minimize the contribution of physical chain entanglements of the pMMA/nBA portion of each network and determine how chemical and physical

crosslinks affect the network integrity. Figure 18 illustrates the X_i values for pMMA/nBA/MBA (Trace A), pMMA/nBA/MA (Trace B), and pMMA/nBA/HAM (Trace C) plotted as a function of temperature.

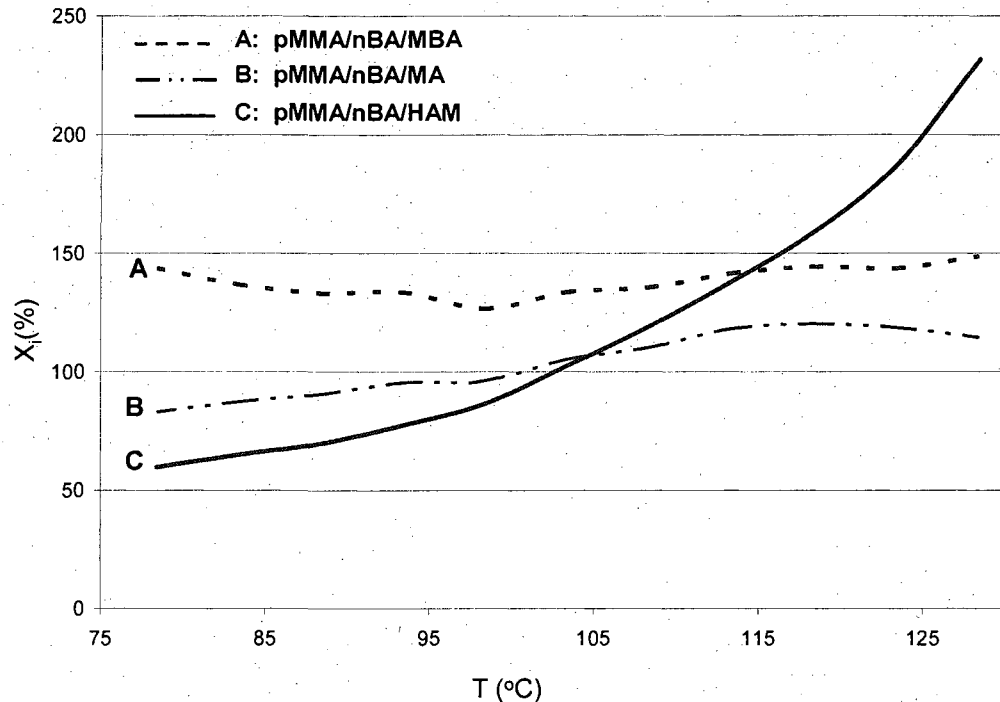


Figure 18: Relative crosslinking density (X_i %) ratioed against pMMA/nBA standard plotted as a function of temperature: A – pMMA/nBA/MBA B – pMMA/nBA/MA C – pMMA/nBA/HAM.

As seen, Trace A remains unchanged, thus indicating stability of chemical crosslinks in pMMA/nBA/MBA in this temperature range. However, when MBA is replaced with MA (Scheme 1, B) in pMMA/nBA/MA, the X_i values slightly increase and, at approximately 115° C, begin to diminish. This observation compared to the data obtained for pMMA/nBA/MBA indicates that the overall crosslink density is diminished, but H-bonding maintains the network integrity via H-bonding, which expectedly decreased

above 120°C. In contrast to pMMA/nBA/MA, the presence of HAM in pMMA/nBA/HAM significantly increases the X_i values of the rubbery plateau region, which is attributed to the presence of not only physical crosslinks, but also chemical crosslinks. As illustrated in Scheme 1, C, one would anticipate chemical crosslinks are responsible for enhanced crosslink density at elevated temperatures, and the analysis of Trace C illustrates that at the onset of the rubbery plateau, the X_i values are the lowest, but as the temperature increases, they significantly increase. This is attributed to the presence of physical crosslinks at lower temperatures and as the chemical reactions progress at elevated temperatures, the X_i values increase.

These data clearly indicate that the presence of chemical and physical crosslinks significantly affects crosslink density, but numerous studies¹⁶⁻²² showed that the distribution of individual components, and particularly their stratification, dictate many surface and interfacial properties of polymeric films. In order to determine distribution of crosslinkers as well as crosslink density along with other components of the network across the film thickness, we utilized ATR and PA-FTIR spectroscopy. As shown in the Experimental Section, ATR FT-IR measurements allow us to quantitatively determine SDS content as a function of depth near the F-A interface in the range of 0-2 μm .²³⁻²⁵ As shown in Figure 19, going further away from the F-A interface, SDS concentration increases, as illustrated in Traces A and D representing pMMA/nBA/MBA and pMMA/nBA, respectively. At the same time, for pMMA/nBA/MA and pMMA/nBA/HAM (Traces B and C) the opposite trend is observed, where the concentration of SDS decreases with the increasing film thickness.

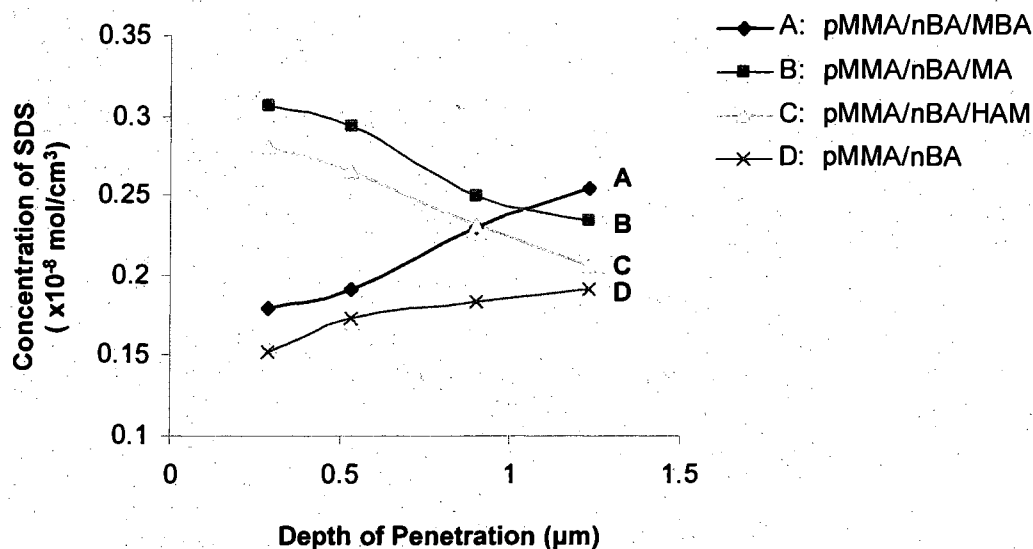


Figure 19: Plot of volume concentration of SDS as a function of depth from the F-A interface.

Surface depth profiling is also possible with PA-FTIR spectroscopy but at significantly greater depths from the F-A interface.^{26,27} Furthermore, in order to enhance the ability to detect subtle intramolecular interactions, 2D PA-FTIR²⁸ can be utilized, whereby using both in-phase and in-quadrature spectra, 2D representations will reveal further interactions of individual components further away from the interface. Figure 20 illustrates the results of 2D-PA-FTIR experiments, where the O-H and C=O stretching regions were measured in pMMA/nBA/MBA, pMMA/nBA/MA, pMMA/nBA/HAM, and pMMA/nBA copolymers.

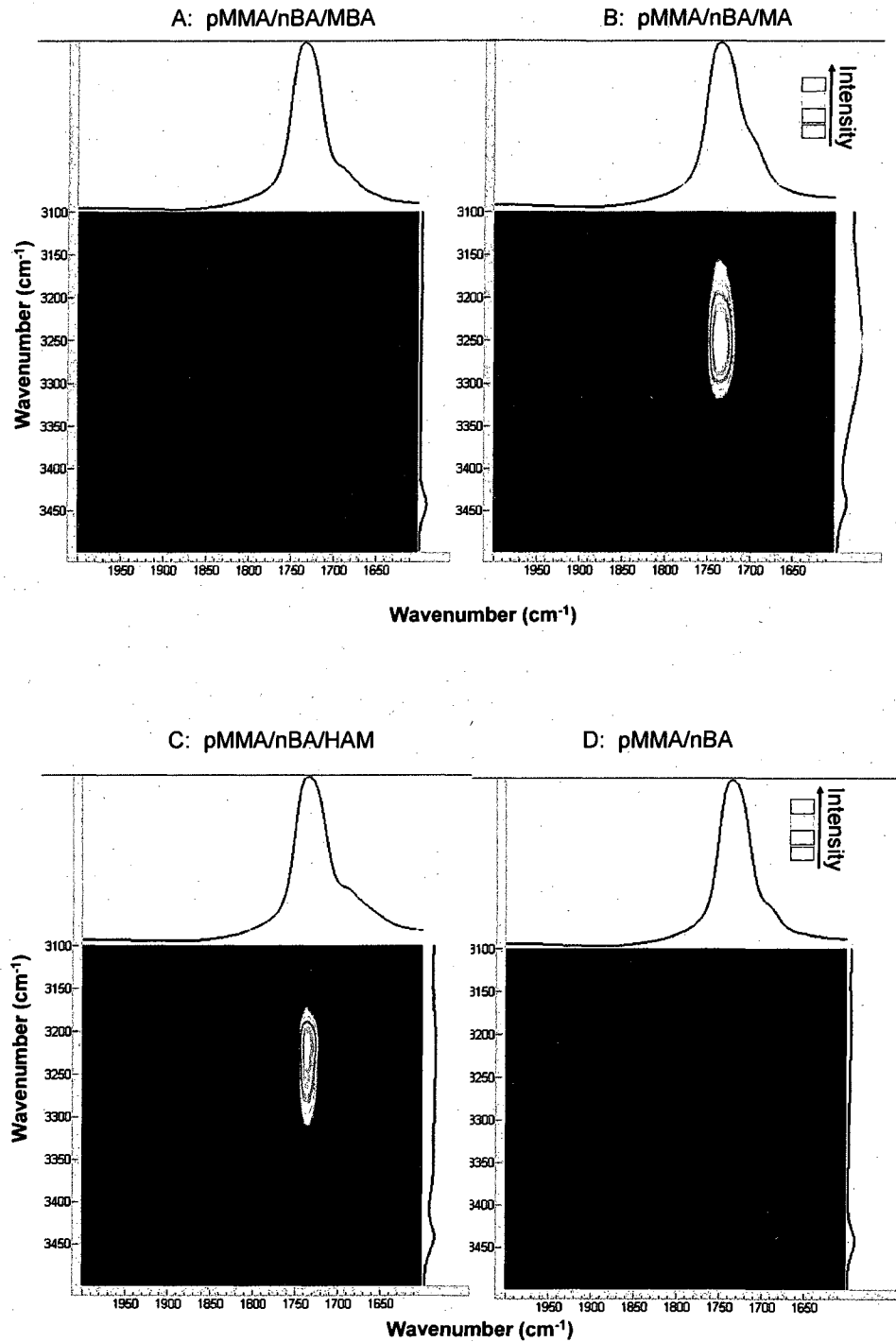


Figure 20: 2D PA-FTIR spectra of A - pMMA/nBA/MBA, B – pMMA/nBA/MA, C – pMMA/nBA/HAM, and D – pMMA/nBA at 50 Hz modulation frequency.

The cross-peak observed for pMMA/nBA/MA and pMMA/nBA/HAM films correlates a modulation frequency change of the carbonyl vibrations due to its close proximity to O-H functional group found on the side chains of both MA and HAM indicating a through space interaction. On the other hand, a cross-peak is not observed for the pMMA/nBA/MBA and pMMA/nBA copolymers which was expected due to the absence of hydroxyl groups in these systems. Thus, the 2D PA FT-IR measurements indicate the presence of hydrogen bonds between C=O groups of the copolymer matrix and OH groups found on the side chains of MA and HAM, which are responsible for reversible crosslinking.

In view of the above data, the following interactions pMMA/nBA and pMMA/nBa/MBA copolymers are detected: SO_3Na^+ head groups of SDS form hydrogen bonding with H_2O and ionic interactions with C=O groups of the copolymer matrix, but the presence of hydroxyl terminated side chains in pMMA/nBA/MA and pMMA/nBA/HAM creates a competing environment with the OH groups of MA and HAM and carbonyl groups of the copolymer matrix. These interactions are depicted in Figure 21 which illustrates the degree of stratification of individual components.

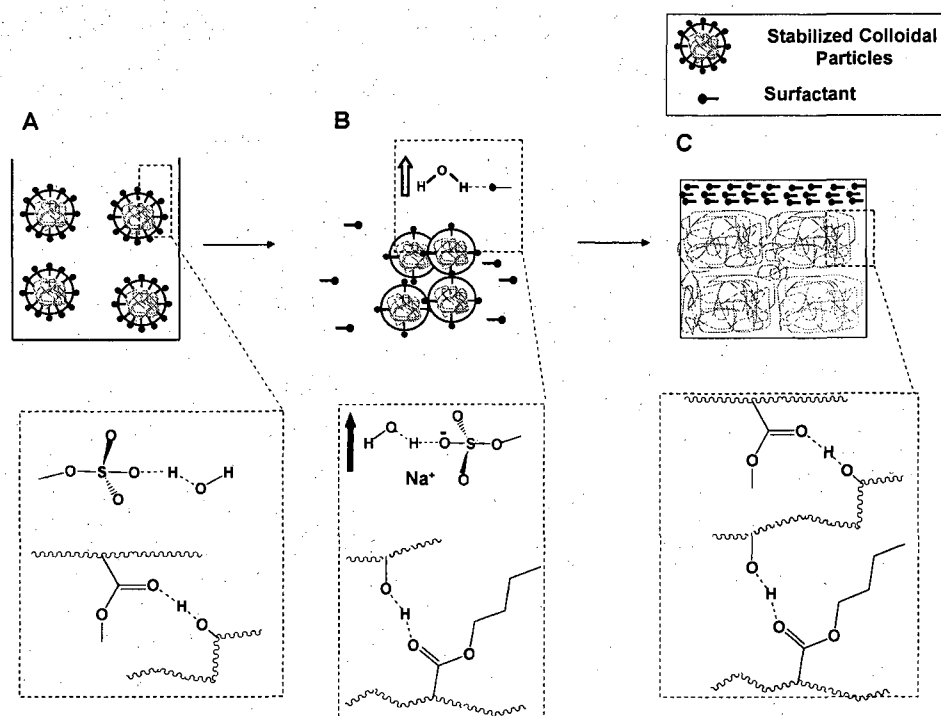


Figure 21: Schematic representations of interactions during film formation: A – in solution, B – during coalescence, and C – fully coalesced film.

Starting with an aqueous phase (Figure 21,A), OH groups of pMMA/nBA/MA and pMMA/nBA/HAM form hydrogen bonds with carbonyl groups of neighboring polymer chains, while the polar $\text{SO}_3^- \text{Na}^+$ heads of SDS are present in the aqueous phase interacting with H_2O molecules. As water begins to evaporate, the particles come to closer contact with each other (Figure 21,B), and $\text{SO}_3^- \text{Na}^+ - \text{H}_2\text{O}$ interactions drive SDS molecules to the F-A interface (Figure 21,C), where the SDS rich F-A interface is formed. The lack of stratification observed for pMMA/nBA and pMMA/nBA/MBA systems (Figure 19) is likely from the absence of the hydrogen bonds allowing for the formation of ionic interactions between SDS and the polymer matrix, thus “anchoring” surfactant in the bulk of the film, and not allowing the evaporation of water to drive surfactant to the F-A interface.

Since MA and HAM are crosslinkers with hydroxyl functionalities, it is of interest to determine the location of this functional group. To determine spatial distribution, we utilized PA FT-IR Spectroscopy. Figure 22 A, B, C, and D illustrate PA-FTIR spectra of pMMA/nBA/MBA, pMMA/nBA/MA, and pMMA/nBA/HAM crosslinked films as well as the pMMA/nBA reference.

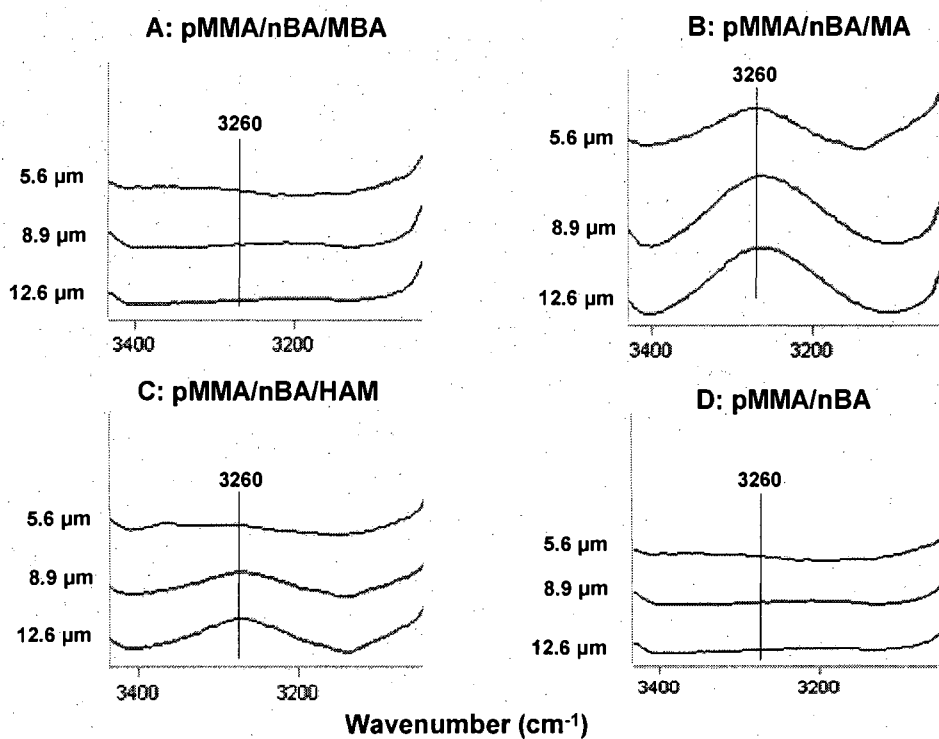


Figure 22: PA FT-IR spectra of A - pMMA/nBA/MBA; B - pMMA/nBA/MA; C - pMMA/nBA/HAM; and D - pMMA/nBA recorded at 5.6, 8.9, and 12.6 μm from the F-A interface.

As anticipated, pMMA/nBA/MBA and pMMA/nBA (Figure 22, A and B) do not show IR activity in the O-H stretching region due to the absence of hydroxyl groups. In contrast, pMMA/nBA/MA and pMMA/nBA/HAM (Figure 22, B and C) exhibit intensity changes as a function of depth from the F-A interface. As seen, the O-H stretching vibrations at 3260 cm^{-1} due to the hydroxyl group of the crosslinkers increases as the

depth from the F-A interface increases. These data further support the concept of physical crosslinking being important at lower temperatures. With the DMA illustrated in Figure 17B in mind, the rubbery plateau region at 80-120°C shows an order of strength of pMMA/nBA/HAM > pMMA/nBA/MA > pMMA/nBA/MBA > pMMA/nBA while above temperatures of 120°C chemical crosslinks prevail and the order shifts to pMMA/nBA/MBA > pMMA/nBA/HAM > pMMA/nBA/MA > pMMA/nBA. It is evident that the choice of crosslinking agent is not a trivial one and influences not only the mobility of individual components during the film formation process, but also the strength of the final colloidal film.

Conclusions

These studies show that when pMMA/nBA colloidal dispersions are crosslinked with chemical crosslinks there is an increase storage modulus at higher temperatures, whereas physical crosslinks are effective at lower temperatures. The overall strength of film is not only dictated by the type of crosslink formed but also the distribution of individual components. Physical crosslinks facilitate stratification of dispersing agents to the F-A interface which results from lack of ionic interactions between the polar head groups of SDS and the polymer matrix. Chemical crosslinks inhibit stratification of dispersing agents which remain in the bulk of the film and provide plasticization of the matrix. A combination of chemical and physical crosslinks permit stratification of dispersing agents to the F-A interface, thus eliminating the plasticization effect observed for chemically crosslinked networks maintaining storage modulus at higher temperatures.

References

- (1) Lovell, P. A.; El-Aasser, M. S., Eds. *Emulsion Polymerization and Emulsion Polymers*; John Wiley and Sons: New York, 1998.
- (2) Provder, T.; Winnick, M. A.; Urban, M. W., Eds. *Film Formation in Waterborne Coatings*; American Chemical Society: Washington D.C., 1996; Vol. ACS Symp. Ser. 648.
- (3) Kuo, S. W.; Chang, F. C. *Macromolecules* **2001**, *34*, 5224-5228.
- (4) Kwei, T. K.; Pearce, E. M.; Pennacchia, J. R.; Charton, M. *Macromolecules* **1987**, *20*, 1174-1176.
- (5) Li, D.; Brisson, J. *Polymer* **1998**, *39*, 793-800.
- (6) Li, D.; Brisson, J. *Polymer* **1998**, *39*, 801-810.
- (7) Pedrosa, P.; Pomposo, J. A.; Calahorra, E.; Cortazar, M. *Macromolecules* **1994**, *27*, 102-109.
- (8) Prinos, J.; Panayiotou, C. *Polymer* **1995**, *36*, 1223-1227.
- (9) Boyars, B.; Daniels, E. S.; Storer, R.; Klein, A. *Journal of Applied Polymer Science* **2007**, *104*, 3774-3779.
- (10) Krishnan, S.; Klein, A.; El-Aasser, M. S.; Sudol, E. D. *Macromolecules* **2003**, *36*, 3511-3518.
- (11) Mazuel, F.; Bui, C.; Charleux, B.; Cabet-Deliry, E.; Winnick, M. A. *Macromolecules* **2004**, *37*, 6141-6152.
- (12) Kalakkunnath, S.; Kalika, D. S.; Lin, H.; Freeman, B. D. *Macromolecules* **2005**, *38*, 9679-9687.
- (13) Lequieu, W.; Du Prez, F. E. *Polymer* **2004**, *45*, 749-757.

- (14) Ferry, J. D. *Viscoelastic Properties of Polymers*, 2nd ed.; John Wiley and Sons, Inc.: New York, 1970.
- (15) Otts, D. B.; Heidenreich, E.; Urban, M. W. *Polymer* **2005**, *46*, 8162-8168.
- (16) Dreher, W. R.; Jarrett, W. L.; Urban, M. W. *Macromolecules* **2005**, *38*, 2205-2212.
- (17) Dreher, W. R.; Urban, M. W. *Langmuir* **2004**, *20*, 10455-10463.
- (18) Dreher, W. R.; Zhang, P.; Urban, M. W.; Porzio, R. S.; Zhao, C.-L. *Macromolecules* **2003**, *36*, 1228-1234.
- (19) Lestage, D. J.; Schleis, D. J.; Urban, M. W. *Langmuir* **2004**, *20*, 7027-7035.
- (20) Lestage, D. J.; Urban, M. W. *Langmuir* **2005**, *21*, 6753-6761.
- (21) Zhao, Y.; Urban, M. W. *Macromolecules* **2000**, *33*, 2184-2191.
- (22) Zhao, Y.; Urban, M. W. *Langmuir* **2001**, *17*, 6961-6967.
- (23) Zhao, Y.; Urban, M. W. *Langmuir* **1999**, *15*, 3538-3544.
- (24) Urban, M. W. *Attenuated Total Reflectance Spectroscopy of Polymers Theory and Practice*; American Chemical Society: Washington DC, 1996.
- (25) Cho, E. C.; Kim, Y. D.; Cho, K. *Journal of Colloid and Interface Science* **2005**, *286*, 479-486.
- (26) Bae, W.-S.; Urban, M. W. *Langmuir* **2004**, *20*, 8372-8378.
- (27) Jiang, E. Y.; McCarthy, W. J.; Drapcho, D. L.; Crocombe, R. A. *Applied Spectroscopy* **1997**, *51*, 1736-1740.

CHAPTER IV

NANO-SILICA MEDIATED FREE RADICAL POLYMERIZATION; CONTROL OF
PDI

Introduction

Conventional free-radical polymerization is an important commercial process for preparing high molecular weight polymers and is found in applications involving the polymerization of many vinyl monomers under mild reaction conditions. While requiring the absence of oxygen, it is tolerant to water and is effective over a broad temperature range.¹ In addition, many monomers are easily copolymerized via a radical route, leading to an infinite number of copolymers with tailored properties dependent on the proportion of incorporated co-monomers. The main limitation of radical polymerization is the poor control over some of the key elements of macromolecular structures such as molecular weight (MW), polydispersity index (PDI), end functionality, chain architecture, and composition. Until the 1990's, well-defined polymers with precisely controlled structures were only accessible by ionic living polymerization. However, ionic living polymerization requires stringent conditions and are limited to a relatively smaller number of monomers.^{2,3} The necessity to overcome all these limitations have challenged synthetic polymer chemists to develop new methods that allow for a living free-radical polymerization process.

Living polymerization was first defined by Swarc⁴ as a chain growth process without chain breaking reactions (chain transfer and termination). Such polymerizations enable end group control as well as the synthesis of block copolymers via sequential monomer addition. However, it does not necessarily provide polymers with molecular weight control and molecular weight distribution. The term "controlled" free radical

polymerization was coined for systems that control molecular weight and distribution, but permit chain breaking reactions to continue as in conventional radical polymerization. Major growth in controlled/living polymerizations began in the 1990's by utilizing nitroxide mediated polymerization (NMP)⁵, atom transfer radical polymerization (ATRP)^{6,7}, degenerative transfer with alkyl iodides⁸, and reversible addition fragmentation transfer polymerization (RAFT).⁹ The common feature of these techniques is the existence of an equilibrium between active and dormant species, and the exchange between the active and dormant species allows for slow but simultaneous growth of all chains while keeping the concentration of radicals low enough to minimize termination. This exchange also enables quantitative initiation necessary for building polymers with special architectures and functionalities, presently accessible in classic living polymerizations. The challenge is to prepare these architectures in environmentally friendly media, water.

The major advantages of dispersing media over bulk or solution is that the polymerization is carried out in water making heat transfer highly efficient while achieving high conversions with low monomer residuals. In addition, there are no volatile organic compounds, thereby providing an opportunity for synthesizing high polymer solids in low viscosity environments.¹⁰ Controlled radical polymerizations in bulk or solution are well understood. However, in heterogeneous polymerizations, such as emulsion polymerizations, the complex kinetics are further complicated by the ever changing location of the activating species in the various environments, the rate of transportation of these species and larger dormant ones to the reaction locus, the presence of aqueous-phase reactions, the choice of surfactant, and the control of the particle size

distribution (PDI), just to name a few. Nevertheless, once the correct experimental conditions are determined, molecular weight distribution and polymer structure are controlled in emulsion systems by utilizing NMP,¹¹⁻¹³ ATRP,¹⁴⁻¹⁶ degenerative transfer to alkyl iodides,^{17,18} and RAFT.¹⁹⁻²²

Although controlled radical techniques are used with specific monomer(s) to achieve physical property enhancement, particular applications call for physical properties not obtainable by monomer selection alone, often times calling for the addition of functional components. For example, numerous studies have been conducted on the inclusion of silicon dioxide (SiO_2) and other inorganic particles into polymer matrices to enhance physical properties, especially through particle surface modifications,^{23,24} or the use of inorganic particles as seeds during emulsion polymerization.²⁵ Only recently, however, it was recognized that when polymerization is conducted in the presence of SiO_2 , the rate of polymerization rate constants for monomers with similar reactivities are altered. This behavior was thought to be attributed to the adsorption of sulfate radicals on SiO_2 nanoparticles.^{26,27} However, further insights regarding the mechanism of radical influence as well as the influence of the silica nanoparticles on the particle coalescence were not addressed. With the concept of controlled radical polymerizations in an aqueous environment as well as the influence of SiO_2 particles on polymerization rate constants in mind, these studies focus on the in-situ effect of nano- SiO_2 on free radical emulsion polymerization of methacrylate monomers with a particular emphasis on how propagation and radical entrapment during the synthesis affects the polydispersity index (PDI) of the produced macromolecules.

Experimental

Methyl methacrylate (MMA), n-butyl acrylate (nBA), potassium persulfate (KPS), 2,2'-Azobis(2-methylpropionitrile) (AIBN), t-butyl hydroperoxide, hydrogen peroxide, and sodium dodecyl sulfate (SDS) were purchased from Aldrich Chemical Co. A solution of 10 nm diameter silicon (IV) oxide (SiO) in H₂O (30% by weight) was purchased from Alfa Aesar. The nano-SiO₂ solution was added to additional DI water and allowed to stir for 15 minutes while SDS was solublized in the solution for an additional 10 minutes. In order to form the pre-emulsion, a compatibalized mixture of MMA/nBA monomers were added to the SiO/DI H₂O/SDS solution and stirred for 30 minutes. After that time, the pre-emulsion was added to a 1 L reaction kettle equipped with a reflux condenser in a 75°C water bath under a N₂ atmosphere under continuous agitation (300 rpm) using a Caframo BDC3030 digital stirrer. The reaction kettle was kept at these conditions for 30 minutes. At this point, 33mL of a 8.3x10⁻² M solution of KPS and DI H₂O was fed into the reaction kettle for 3.5 hours, followed by further reaction for additional 30 minutes and subsequent cooling to room temperature. Such prepared colloidal dispersions were cast in a silicone rubber mold and allowed to coalescence at 50% relative humidity (RH) for 3 days at 24 °C. The resulting films formed approximately 1.5mm thick films.

Attenuated total reflectance Fourier transform infrared (ATR FT-IR) spectra were collected using a Bio-Rad FTS-6000 FT-IR single-beam spectrometer set at a 4 cm⁻¹ resolution and utilizing a 45° face angle Ge crystal with 50×20×3 mm dimensions. Each spectrum represents 100 co-added scans ratioed against the same number of scans

collected using an empty ATR cell. All spectra were corrected for spectral distortions using software for the Urban-Huang algorithm.²⁸

Dynamic mechanical analysis (DMA) was performed using a TA Instruments DMA Q800 in tensile mode with an amplitude of 2 Hz. The samples were analyzed over a temperature range of -10 to 200°C using a temperature ramp of 2°C/min. Data was processed using TA Universal Analysis software and Microsoft Excel. Thermal gravimetric analysis (TGA) was obtained on a TA Instruments TGA Q50 over 20 – 600°C temperature range at a heating rate 10°C/min.

Particle size measurements were obtained using a Microtrac UPA 250. Colloidal dispersion particle morphologies were analyzed using the JEOL JEM-2100 transmission electron microscope (TEM). For TEM, colloidal dispersions were diluted at a 20:1 vol. ratio (DI H₂O: dispersion) and deposited on carbon-reinforced Formvar coated copper TEM grids and allowed to dry for 24 hours.

Gel permeation chromatography (GPC) was performed using a Waters 515 HPLC pump equipped with an evaporative light scattering detector PL-ELS1000 (Polymer Laboratories Inc.) and a crosslinked divinylbenzene mixed bed linear GPC column (Jordi FLP.). The columns were calibrated using a polystyrene standard along with a toluene flowmarker. Prior to the GPC analysis could be conducted, the SiO₂ nanoparticles were removed by dissolving the PMMA/nBA colloidal dispersions in 1mL of toluene. A 49% HF(aq) solution was added to the particle solution and allowed to stir at room temperature overnight. PMMA/nBA was recovered by precipitation into methanol and vacuum filtration through fine glass frit, yielding a white powder. The precipitated polymer was then dissolved in THF for GPC analysis.

Solid-state ^{29}Si and ^{13}C NMR spectroscopy was performed on a Varian UNITY INOVA 400 spectrometer using a Chemagnetics HXY probe. Samples were loaded into zirconia rotor sleeves, sealed with Teflon™ caps, and spun at rate of 4.0 kHz. The standard cross-polarization/magic angle spinning (CP/MAS) technique was used with high-power proton decoupling implemented during data acquisition. The acquisition parameters were as follows: The ^1H 90° pulse width was 3.5 μs , the cross-polarization contact time was 1.0 ms, the dead time delay was 6.6 μs , and the acquisition time was 45 ms. A recycle delay of 4.0 seconds between scans was utilized and 4096 - 10240 scans were accumulated for each spectra. The FIDs were zero filled to 32k points and a Gaussian filter applied prior to Fourier transformation.

Results and Discussion

As indicated in the Introduction, there is significant interest in incorporating nanoparticles into the polymerization of colloidal dispersions in order to incorporate an inorganic phase in a polymer matrix. While location of nanoparticles is one question, the influence of the particle size and location on molecular weight is another. For example, Figure 23 illustrates the results of molecular weight measurements expressed in the form of polydispersity index (PDI) for pMMA/nBA under the following polymerization conditions: both monomers were polymerized in the presence of KPS (A series) and AIBN (B series) initiators using semi-continuous process (A, A' and B, B') and batch (A'', A''' and B'', B''') polymerization.

24 provides particle size measurements of aliquots taken every 15 minutes during polymerization of MMA and nBA in the presence of 15% w/w nano-SiO₂ utilizing KPS and AIBN initiators under both semi-continuous and batch conditions.

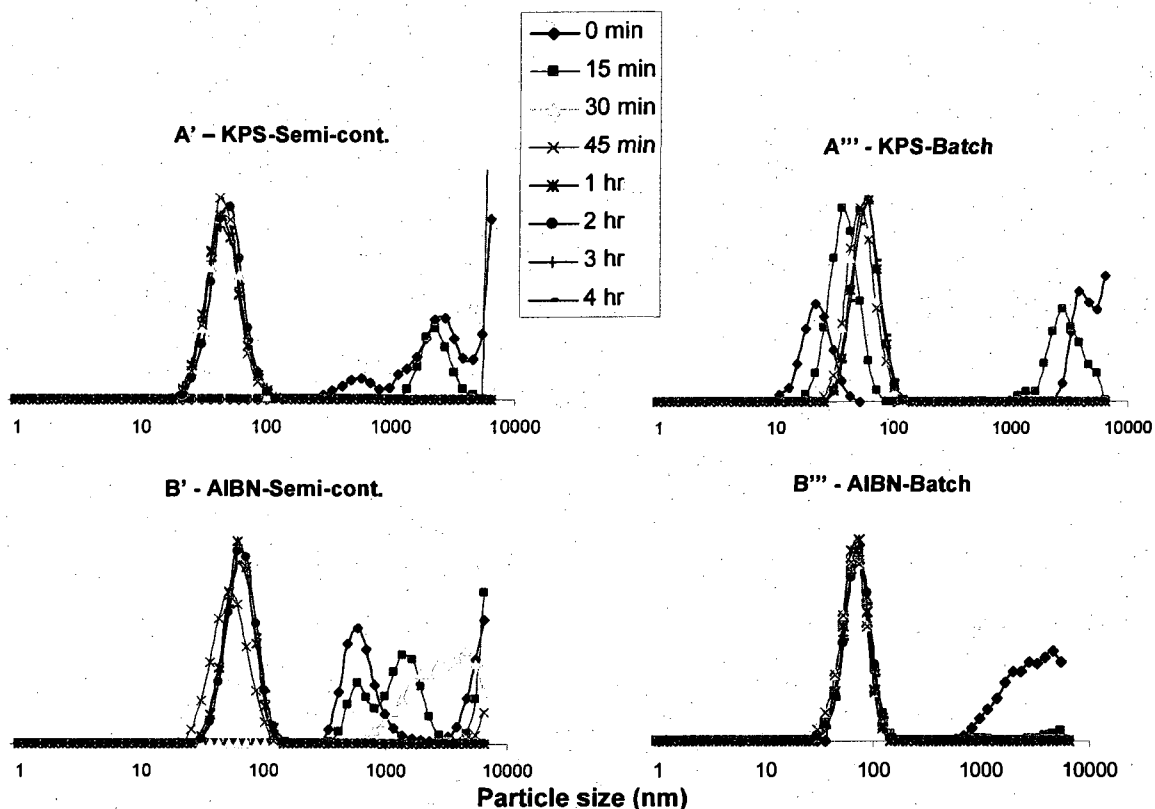


Figure 24: Particle size measurements of aliquots taken every 15 minutes during polymerization reaction of MMA/nBA in the presence of 15 w/w% nano-SiO₂ initiated by KPS under semi-continuous and batch conditions (A'/A''') and initiated by AIBN under semi-continuous and batch conditions (B'/B''').

Analysis of these data reveals that for all systems before polymerization there were two particle sizes: one attributed to monomer swollen micelles with an average particle diameter of approximately 70 nm, and one > 6000 nm, attributed to monomer droplets. After 15 minutes of the reaction, the droplets > 6000 nm decrease, and after 45 minutes,

only one particle size with an average particle size of 70 nm is detected which remains constant throughout the polymerization process. These data indicate that the particle size evolution is similar for both initiators and reaction conditions, but does not explain the influence of nano-SiO₂. Since the results of these experiments reveal no particles in the 10 nm range, the next question is the role and location of the nano-SiO₂ during polymerization. Although one could attribute this observation to the formation of SiO₂-copolymer core-shell type particles, as proposed in the previous studies,^{25,29,30} in an effort to determine these morphological features, TEM analysis shown in Figure 25 was conducted.

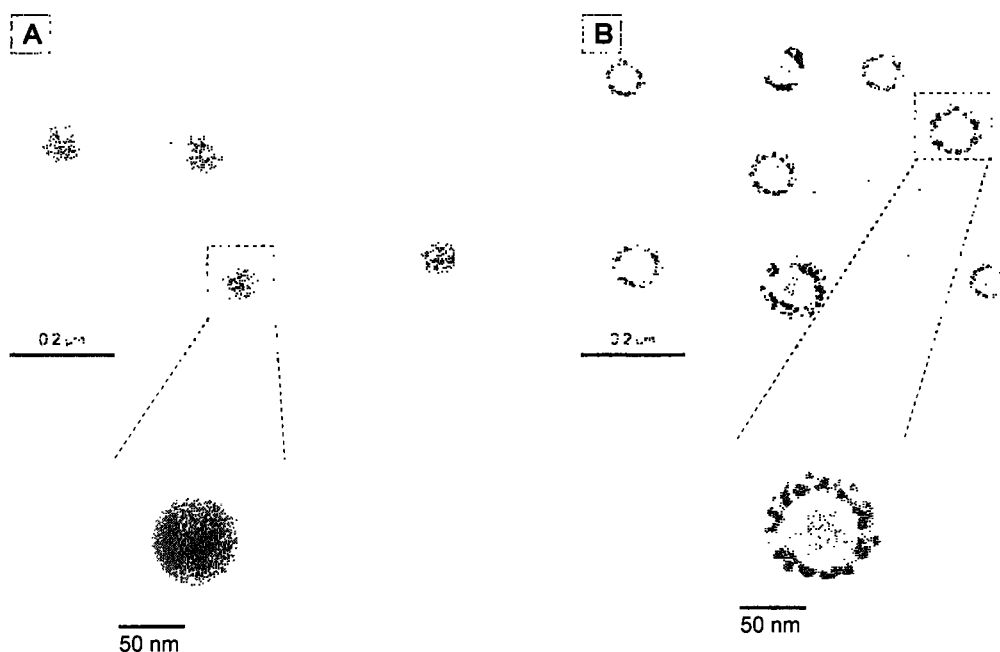


Figure 25: TEM micrographs of A – pMMA/nBA colloidal particles and B – pMMA/nBA colloidal particle with nano-SiO₂ incorporated during polymerization.

Figure 25, A shows TEM micrographs of standard pMMA/nBA colloidal particles exhibiting uniform morphology. In contrast, Figure 25, B shows the same particles

copolymerized in the presence of nano-SiO₂ particles. Here the pMMA/nBA particles are surrounded by significantly smaller nano-SiO₂ necklace attracted to the surface of pMMA/nBA. This is somewhat surprising because the zeta potential of nano-SiO₂ is approximately -30 mV and pMMA/nBA particles -60 mV, which should result in electrostatic particle repulsion. However, if there are stronger interactions present, such as covalent bonding between the particles, electrostatic interactions may be overcome.

To determine if covalent bonding between pMMA/nBA and nano-SiO₂ particles has occurred, we conducted solid state ¹³C and ²⁹Si NMR experiments were done. Figure 26 illustrates a series of ¹³C solid state NMR spectra for pMMA/nBA (Trace A) and pMMA/nBA containing nano-SiO₂ (Trace B).

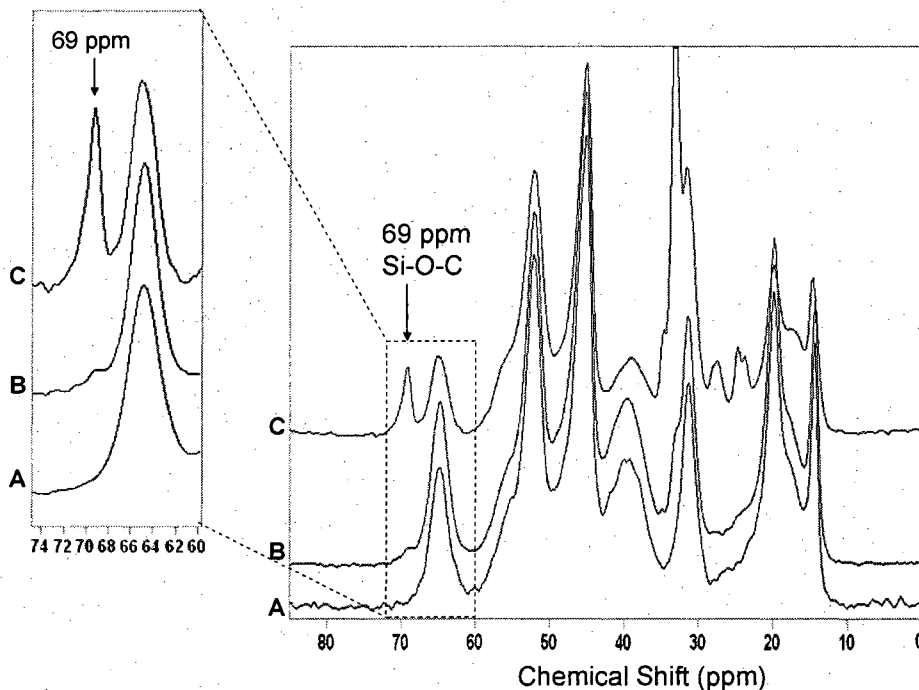


Figure 26: ¹³C NMR of A- pMMA/nBA, B- pMMA/nBA with 15 w/w% nano-SiO₂, and C- pMMA/nBA with 15 w/w% nano-SiO₂ quenched after 30 minutes reaction time.

As seen, the only spectral change detected in pMMA/nBA containing nano-SiO₂ (Trace B) spectrum is the presence of a shoulder at 69 ppm, which is attributed to Si-O-C species. In an effort to establish if indeed the 69 ppm signal results from Si-O-C covalent bonding, we quenched the reaction after 30 minutes and the resulting ¹³C NMR spectrum shown in Trace C illustrates even stronger Si-O-C signal which is attributed to high mobility low molecular weight pMMA/nBA chains connected to the nano-SiO₂ particles.

In an effort to identify the role of nano-SiO₂ in the polymerization process, we conducted several controlled experiments. Figure 27, A illustrates ²⁹Si NMR spectrum with the resonances at -112, -103, and -92 ppm due to SiO₂(OH)₂, SiO₃OH, and SiO₄, respectively. Furthermore, we prepared pMMA/nBA containing methoxy trimethylsilane coated nano-SiO₂ specimen in order to disturb the Si-O-C bonding. We ratioed Q3 and Q4 peaks due to (SiO₃)Si-OH (Q3) and (SiO₄)Si (Q4) in Figure 27, B and plotted for specimens containing pure 10 nm SiO₂, 10 nm SiO₂ with 3x KPS concentration, pMMA/nBA with SiO₂ (1x KPS concentration), pMMA/nBA with SiO₂ pretreated with methoxy trimethylsilane (1x KPS concentration), and pMMA/nBA with nano-SiO₂ initiated with AIBN.

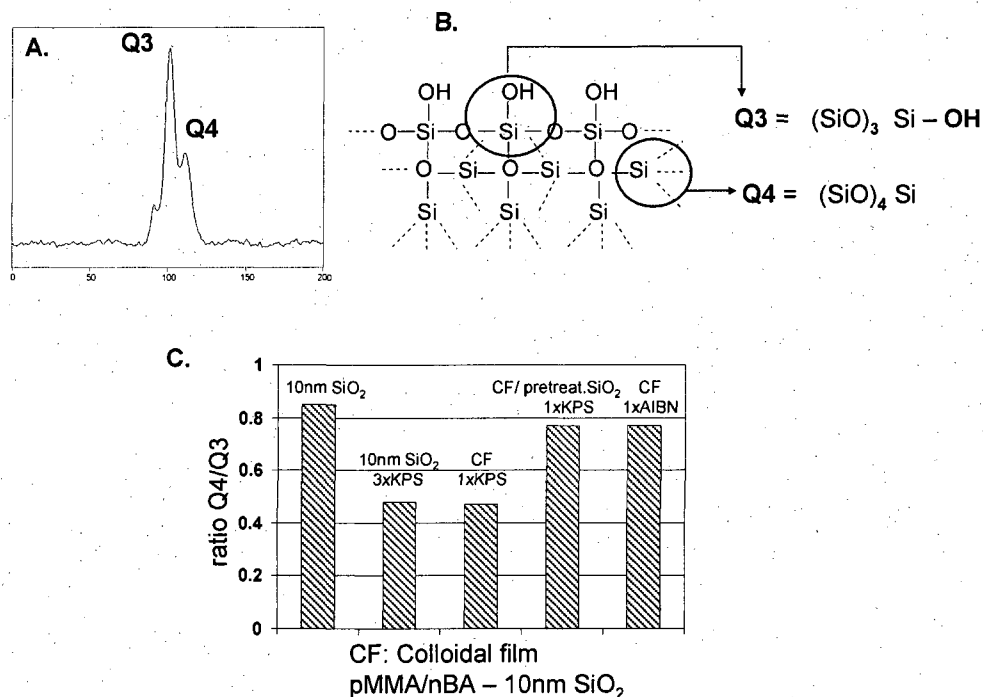


Figure 27: A- representative Si^{29} spectrum showing the Q3 and Q4 resonances, B- Q3 and Q4 entities within the SiO_2 lattice, and C- plot comparing the Q4/Q3 ratio for pMMA/nBA reactions with nano- SiO_2 with different initiators.

As seen in Figure 27, for nano- SiO_2 pretreated with methoxy trimethylsilane in the presence of AIBN initiator, the Q4/Q3 ratio is similar to that of the pure nano- SiO_2 standard. However, the ratio decreases when KPS is used as the initiator in the presence of the nano- SiO_2 , thus indicating an enrichment of Si-OH bonds. We also determined the effect AIBN and KPS initiators on the Q4/Q3 ratio. For pMMA/nBA polymerized in the presence of SiO_2 initiated by AIBN, the Q4/Q3 is 0.78 and diminishes to 0.47 for KPS. This behavior is expected and it has been previously shown that during the decomposition of KPS, OH radicals are produced as a side-reaction,^{31,32} which raises the question as to how OH radicals are being trapped on the surface of the nano- SiO_2 .

While both solid state C^{13} and Si^{29} NMR have confirmed the trapping of both carbon based and hydroxyl radicals, the origin of the oxygen and silicon radicals found

on and within the nano-SiO₂ lattice is not a surprise. Previous studies have shown that “defects” present on nano-SiO₂ originate from strained Si-O rings due to cleavage of Si-O bond which generate Si and O radicals. For example, Figure 28 illustrate an example of free radical generation from the radical precursor which is known to be the main source of radical though Si-O-O-Si peroxy bridges which rearrange are another source of Si and O radicals.³³⁻³⁹

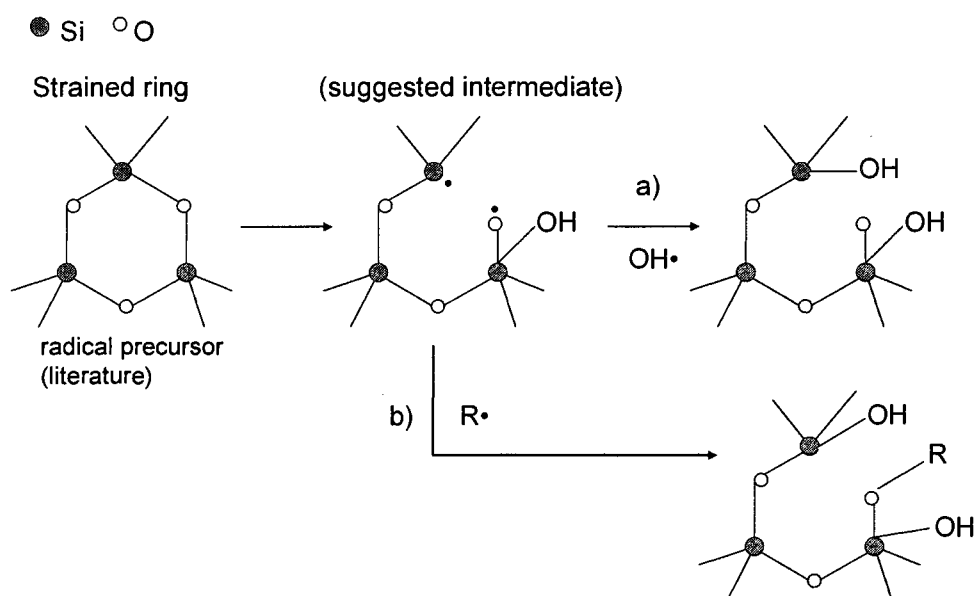


Figure 28: Rearrangement of strained nano-SiO₂ rings resulting in Si and O radicals responsible for the entrapment of OH radicals and control of propagating carbon based radicals.

Based on the above data, the proposed mechanism for radical entrapment is illustrated in Figure 29. As shown previously in Figure 25, TEM micrograph shows the formation of a silica nanoparticle “necklace” on the surface of the colloidal particle. The hydroxyl radicals generated as a side product of the decomposition of KPS initiator in the aqueous phase become trapped when a covalent bond is formed through the coupling of

hydroxyl radicals and Si radicals found on the nanoparticle. This is supported by the large differences in PDI for pMMA/nBA initiated by KPS with and without nano-SiO₂.

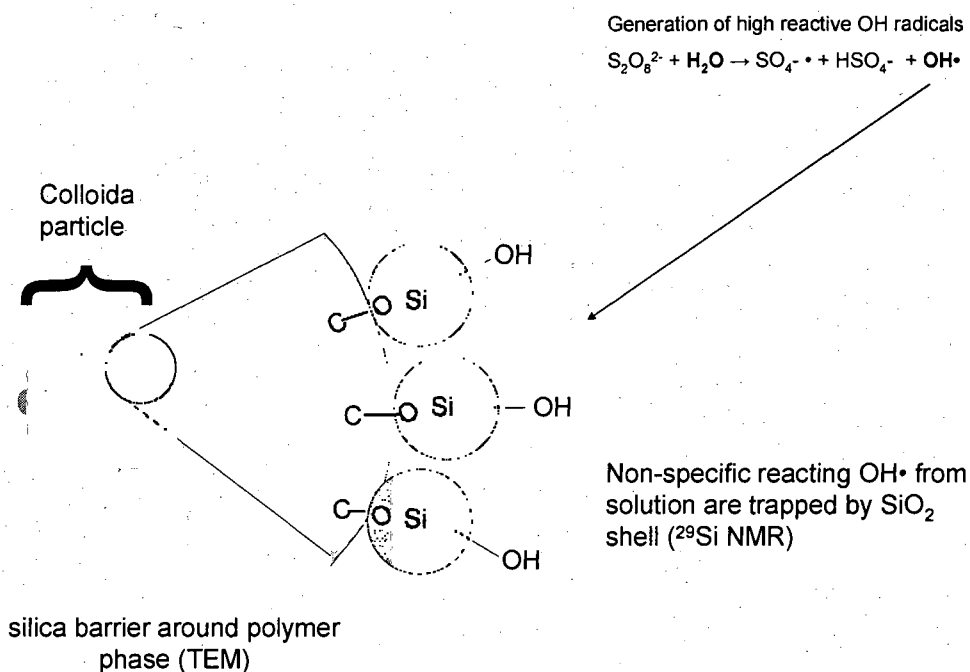


Figure 29: Schematic representation of silica encapsulated micelle illustrating the mechanism for control and entrapment of radicals.

However, the magnitude of PDI is different when AIBN is utilized as the initiator due to the fact that hydroxyl radicals are not produced as a side product. On the other hand, carbon based radicals found in the oil phase are temporarily rendered inactive by the same nano-SiO₂ necklace responsible for trapping hydroxyl radicals in the aqueous phase. Consequently, when nano-SiO₂ are present during polymerization, they act similar to alkoxyamines used in nitroxide mediated polymerizations (NMP) to control PDI.⁴⁰ The general mechanism shown in Figure 30 illustrates that the reversible termination of the growing polymeric chain is the key step for reducing the overall concentration of

propagating radical chain ends. In the absence of other reactions leading to initiation of new polymer chains (i.e., no reaction of the mediating radical with vinylic monomer), the concentration of reactive chain ends is relatively low, minimizing irreversible termination reactions, such as combination or disproportionation.

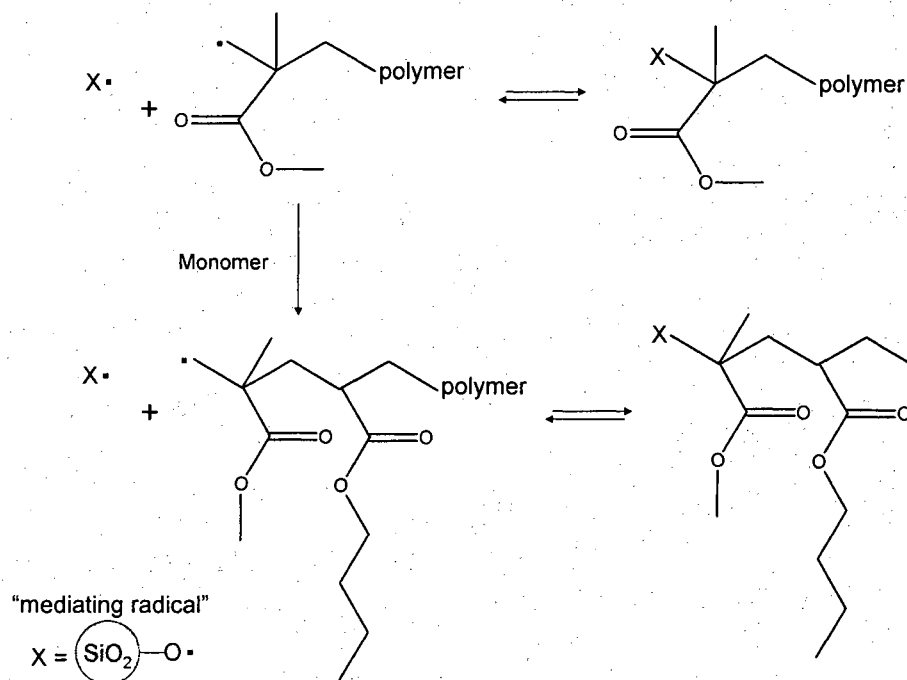


Figure 30: Proposed mechanism of nano-SiO₂ mediated polymerization.

All chains would be initiated only from the desired initiating species and the growth should occur in a pseudo-living fashion. This allows a high degree of control over the entire polymerization process with well-defined molecular weight polymers being produced.

Conclusions

These studies show that the inclusion of nano-SiO₂ during the polymerization of methyl methacrylate and n-butyl acrylate provides control of the PDI. Defects within the nano-SiO₂ lattice can control propagating radicals as well as trap unwanted radicals that

may terminate growing polymer chains. Because nano-SiO₂ particles are located on the exterior of the micelles, they can influence the propagating radicals within the micelles while trapping hydroxyl radicals in the aqueous phase.

References

- (1) Kopecky, K. R. *The Chemistry of Free Radical Polymerization*. By Graeme Moad (CSIRO, Division of Chemicals and Polymers) and David H. Solomon (University of Melbourne), 1997; Vol. 119.
- (2) Szwarc, M. *Carbanions, Living Polymers, and Electron Transfer Processes*; Interscience: New York, 1968.
- (3) Kennedy, J. P. In *Rubber Chemistry and Technology*; Matyjaszewski, K., Ed.; Marcel Dekker: New York, 1996; Vol. 69, p G63.
- (4) Szwarc, M. *Nature (London, United Kingdom)* **1956**, *178*, 1168-1169.
- (5) Solomon, D. H.; Rizzardo, E.; Cacioli, P.: U.S Patent 4,581,429, 1986.
- (6) Wang, J.-S.; Matyjaszewski, K. *Journal of the American Chemical Society* **1995**, *117*, 5614-5615.
- (7) Kato, M.; Kamigaito, M.; Sawamoto, M.; Higashimura, T. *Macromolecules* **1995**, *28*, 1721-1723.
- (8) Matyjaszewski, K.; Gaynor, S.; Wang, J.-S. *Macromolecules* **1995**, *28*, 2093-2095.
- (9) Rizzardo, E.; Chong, Y. K.; Evans, R. A.; Moad, G.; Thang, S. H. *Macromolecular Symposia* **1996**, *111*, 1-11.
- (10) Herk, A. M. V.; Monteiro, M. In *Handbook of Radical Polymerization*; Matyjaszewski, K.; Davis, T., Eds.; The American Chemical Society: New York, 2003; Vol. 125, pp 316-343.
- (11) Bon, S. A. F.; Bosveld, M.; Klumperman, B.; German, A. L. *Macromolecules* **1997**, *30*, 324-326.

- (12) Nicolas, J.; Ruzette, A.-V.; Farcet, C.; Gerard, P.; Magnet, S.; Charleux, B. *Polymer* **2007**, *48*, 7029-7040.
- (13) Marestin, C.; Noel, C.; Guyot, A.; Claverie, J. *Macromolecules* **1998**, *31*, 4041-4044.
- (14) Chambard, G.; De Man, P.; Klumperman, B. *Macromolecular Symposia* **2000**, *150*, 45-51.
- (15) Matyjaszewski, K.; Qiu, J.; Shipp, D. A.; Gaynor, S. G. *Macromolecular Symposia* **2000**, *155*, 15-29.
- (16) Min, K.; Gao, H.; Matyjaszewski, K. *Journal of the American Chemical Society* **2006**, *128*, 10521-10526.
- (17) Lansalot, M.; Farcet, C.; Charleux, B.; Vairon, J.-P.; Pirri, R. *Macromolecules* **1999**, *32*, 7354-7360.
- (18) Butte, A.; Storti, G.; Morbidelli, M. *Macromolecules* **2000**, *33*, 3485-3487.
- (19) Rieger, J.; Stoffelbach, F.; Bui, C.; Alaimo, D.; Jerome, C.; Charleux, B. *Macromolecules (Washington, DC, United States)* **2008**, *41*, 4065-4068.
- (20) Zhou, X.; Ni, P.; Yu, Z. *Polymer* **2007**, *48*, 6262-6271.
- (21) Uzulina, I.; Kanagasabapathy, S.; Claverie, J. *Macromolecular Symposia* **2000**, *150*, 33-38.
- (22) Monteiro, M. J.; Sjoberg, M.; Van der Vlist, J.; Gottgens, C. M. *Journal of Polymer Science, Part A: Polymer Chemistry* **2000**, *38*, 4206-4217.
- (23) Sugimoto, H.; Daimatsu, K.; Nakanishi, E.; Ogasawara, Y.; Yasumura, T.; Inomata, K. *Polymer* **2006**, *47*, 3754-3759.

- (24) Wang, Y.; Li, Y.; Zhang, R.; Huang, L.; He, W. *Polymer Composites* **2006**, *27*, 282-288.
- (25) Luna-Xavier, J.-L.; Guyot, A.; Bourgeat-Lami, E. *J. Coll. Int. Sci.* **2002**, *250*, 82-92.
- (26) Caregnato, P.; Carrillo Le Roux, G.; Martire, D. O.; Gonzalez, M. C. *Langmuir* **2005**, *21*, 8001-8009.
- (27) Caregnato, P.; Mora, V. C.; Le Roux, G. C.; Martire, D. O.; Gonzalez, M. C. *J. Phys. Chem. B* **2003**, *107*, 6131-6138.
- (28) Urban, M. W. *Attenuated Total Reflectance Spectroscopy of Polymers - Theory and Practice*; American Chemical Society: Washington DC, 1989.
- (29) Liu, X.; Zhao, H.; Li, L.; Yan, J.; Zha, L. *Journal of Macromolecular Science, Part A: Pure and Applied Chemistry* **2006**, *43*, 1757-1764.
- (30) Guo, Y.; Wang, M.; Zhang, H.; Liu, G.; Zhang, L.; Qu, X. *Journal of Applied Polymer Science* **2008**, *107*, 2671-2680.
- (31) House, D. A. *Chem. Rev.* **1962**, *62*, 185-203.
- (32) Behrman, E. J.; Edwards, J. O. *Reviews in Inorganic Chemistry* **1980**, *2*, 179-206.
- (33) Awazu, K.; Kawazoe, H. *J. App. Phys.* **2003**, *94*, 6243-6262.
- (34) Nelson, C. M.; Weeks, R. A. *J. Amer. Cer. Soc.* **1960**, *43*, 396-399.
- (35) Pacchioni, G.; Ierano, G. *Physical Review B: Condensed Matter and Materials Physics* **1998**, *57*, 818-832.
- (36) Weeks, R. A. *Physical Review* **1963**, *130*, 570-576.
- (37) Weeks, R. A.; Lell, E. *J. Appl. Phys.* **1964**, *35*, 1932-1938.

- (38) Zhuravlev, L. T. *Colloids and Surfaces, A: Physicochemical and Engineering Aspects* **2000**, *173*, 1-38.
- (39) Heaney, P. J., Prewitt, C.T., and Gibbs, G.V. *Silica: Physical Behavior, Geochemistry, and Materials Applications*; BookCrafters, Inc.: Chelsea, 1994; Vol. 29.
- (40) Chevalier, C.; Guerret, O.; Gnanou, Y. *Living and Controlled Polymerization: Synthesis, Characterization and Properties of the Respective Polymers and Copolymers* **2006**, 51-63.

CHAPTER V

PH-CONTROLLED STRATIFICATION OF AMINO ACIDS IN COLLOIDAL FILMS

Introduction

Protein-protein interactions within the cell membrane are key events in controlling many biological responses. They are thought to be governed by the secondary structure of the trans-membrane domains of the interaction proteins (predominantly α -helices) through the formation of different bonds between their side chains.¹⁻³ These side chain characteristics are a direct result of the type of amino acid building block utilized in the construction of the protein. For example, selected amino acids with neutral, hydrophobic, basic, or acid characteristics were examined in order to understand specificity of binding processes to dendrimers under various environments. The results show that the strongest dendrimer-amino acid interactions are electrostatic and hydrophobic in nature.⁴ Equally as important is the stereoregularity between polymers and amino acids, which is used to detect minute amounts of enantiomeric excess amino acids.⁵ This concept of enantiomer detection was also utilized as chiral discriminating chemical sensitive resistors or even transistors, whereby the modification of polymers with amino acid pendant groups made them capable of detecting organic compounds.⁶

Another appealing opportunity is the creation of polymer surfaces with amino acids to use as bioactive supports in surgery, orthopedics, and tissue engineering. However, limited fundamental knowledge regarding biocompatibility as well as control of interfacial regions currently exists to explore these applications. One approach in polymer surfaces modification is the use of plasma, which have shown to be effective in

creating surfaces with covalently attached species. For example, expanded poly-(tetrafluoroethylene) (ePTFE) was modified by the covalent attachment of ampicillin and penicillin, thus inhibiting microbial growth.^{7-10,11}

While the above examples illustrate new pathways for creating bioactive polymer surfaces, combining amino acid chemistry with colloidal synthesis offers another uncharted opportunity. Colloidal dispersions provide a vehicle for the creation of bioactive surfaces through the specific utilization of bioactive components and through control of the film formation process. One example is the formation of pMMA/nBA colloidal dispersions stabilized by n-dodecyl B-D-maltoside (DDM) capable of recognizing lectin,¹² where upon coalesce, DDM is released to the film-air (F-A) interface, thus providing sites for interaction with lectin. Furthermore, developments of stimuli-responsive systems sensitive to a number of external and internal stimuli, such as mechanical deformation, electromagnetic radiation, temperature, pH, and ionic strength are other examples.¹³ In addition, the mobility of individual components stabilized by a combination phospholipids and other dispersing agents allowed controlled stratification of these species by varying ionic strength and temperature.^{14,15}

As principle building blocks of proteins and enzymes, amino acids are incorporated into proteins by transfer RNA according to the genetic code. These functions, when utilized in colloidal dispersions that coalesce, may result in a variety of recognition processes driven by the ability of amino acids to dictate the spatial and biochemical properties. These unique attributes stimulated interest in incorporating amino acids into colloidal synthesis of methyl methacrylate (MMA) and n-butyl acrylate (nBA) in the presence of aspartic acid (Asp). The choice of Asp was driven by its ability to

control metabolic processes during construction of other amino acids in the citric acid cycle generating such species as asparagine, arginine, lysine, methionine, threonine, isoleucine, and several other nucleotides. Asp functions in RNA, DNA as well as the production of immunoglobulin and antibody synthesis are also significant.

In view of these considerations, the studies focus on incorporating aspartic acid in copolymeration of MMA/nBA to create self-stratifying films. Previous studies¹⁶⁻¹⁸ have shown that the inclusion of components capable of intramolecular hydrogen bonding can create competing interactions capable of releasing individual components to the film-air interface. The unique pH responses of Asp that is illustrated in Figure 31 will allow us to control its behavior during and after coalescence by the pH control of colloidal solutions.

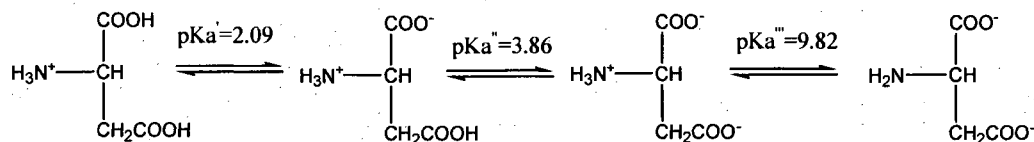


Figure 31: pH dependent structures of aspartic acid.

Experimental

Methyl methacrylate (MMA), n-butyl acrylate (nBA), potassium persulfate (KPS), sodium dodecyl sulfate (SDS), and l-aspartic acid (Asp) were purchased from Aldrich Chemical Co. Aspartic acid and deionized water (DI) were added to a 1 L reaction kettle equipped with a reflux condenser at 75°C in N₂ atmosphere under continuous agitation (300 rpm) using a Caframo BDC3030 digital stirrer. The aspartic acid was allowed to solubilize in DI-water for 30 min, followed by feeding a solution of MMA, nBA, SDS and DI-water were fed using monomer-starved conditions using a semi-continuous

polymerization process.¹⁹ Table 3 lists the concentration levels of individual components. Such prepared colloidal dispersions were cast in silicone rubber molds and allowed to coalesce at 50% relative humidity (RH) for 3 days at 24 °C for the MMA/nBA system. The resulting films formed approximately 0.5 mm thick.

Composition		
	MMA/nBA	MMA/nBA/Asp
DDI (w/w%)	77.5	77.1
MMA (w/w)%	11.3	11.2
nBA (w/w)%	10.4	10.4
KPS (w/w)%	0.2	0.2
SDS (w/w)%	0.6	0.6
Asp (w/w)%	-----	0.5

Table 3: Compositions of colloidal dispersion based on final latex weight.

Attenuated total reflectance Fourier transform infrared (ATR FT-IR) spectra were collected using a Bio-Rad FTS-6000 FT-IR single-beam spectrometer set at a 4 cm⁻¹ resolution. A 45° face angle Ge crystal with 50×20×3 mm dimensions was utilized. This configuration allows the analysis of the film-air (F-A) interface at approximately 0.46 μm from the F-A interface

IR images were obtained using internal reflection IR imaging (IRIRI) with a Ge internal reflection element. This system consist of a Bio-Rad FTS 6000 spectrometer, a UMA 500 microscope, an ImagIR focal plane array detector, and a semispherical Ge crystal which facilitates a spatial resolution of about 1μm.²⁰ IRIRI images were collected using the following spectral acquisition parameters: undersampling ratio = 4, step scan

speed = 2.5 Hz, number of spectrometer steps = 1777, number of images per step = 64, and spectral resolution = 8 cm^{-1} . In a typical experiment, a spectral data acquisition time was approximately 15 min. Image processing was performed using ENVI (The Environmental for Visualizing Images, Research Systems Inc.) version 3.5

Computer simulations were carried out in order to determine structural features of the aspartic acid islands. The choice of theoretical level depends on the accuracy requested and the size of the system. It is well known that DFT-B3LYP method predicts excellent geometries.^{21,22} However, due to the large size of the island systems under consideration, computer simulations at AM1, HF/3-21G, B3LYP²³⁻²⁶/6-31G, and B3LYP/6-31G+(d) levels were employed. It has been proven that the HF/3-21G method well reproduces the geometrical parameters. Thus, only models optimized at the HF/3-21G²⁷ level are discussed in this work unless mentioned otherwise. The characteristics of the local minima were verified by vibrational frequency calculations. The harmonic vibrational wavenumbers and absolute intensities were calculated at the same level using the HF/3-21G optimized structures. The values of the wavenumbers were scaled by a factor of 0.964 for HF/3-21G level of theory.²⁸ All calculations were performed using the Gaussian 03 packageTM.

Results and Discussion

While composition of pMMA/nBA/Asp colloidal dispersions is provided in Table 3, spectroscopic analysis of the film-air (F-A) interface was conducted using ATR FT-IR. The results of the analysis are illustrated in Figure 32, Traces A, B, C, which show a series of spectra recorded from the F-A interface of pMMA/nBA/Asp coalesced at $\text{pH} = 3$

(A), 7 (B), and 10 (C). For reference purposes, Traces D, E, and F represent reference ATR-FTIR spectra of pMMA/nBA, Asp, and SDS, respectively.

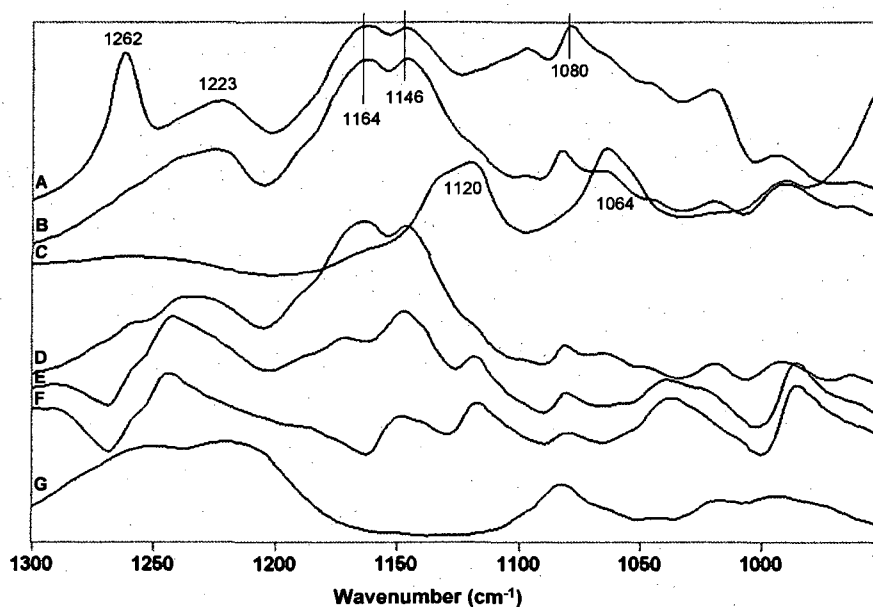


Figure 32: ATR-FTIR spectra recorded from the F-A interface of pMMA/nBA/Asp at pH =: 3 (Trace A), 7 (Trace B), 10 (Trace C), (D) pMMA/nBA reference spectrum, (E) Calculated IR spectrum of 1:1 combination of pMMA/nBA and Asp, (F) Asp reference spectrum, and (G) SDS reference spectrum.

Comparison of Traces A and B (pH 3 \rightarrow 7) show changes of the chemical make-up of the F-A interface when going from a pH of 3 to 7. Analysis of Trace A reveals the presence of a band at 1262 cm^{-1} attributed to $\text{SO}_3^- \text{Na}^+ / \text{COO}^-$ interactions^{17,29} that is not present in Trace B. Also observed in comparison of Trace A to B are decreases in band intensities at 1220 and 1080 cm^{-1} when increasing from pH = 3 to 7 for antisymmetric and symmetric S-O stretching of SDS, respectively. However, when the pH is increased to 10 (Trace C), the antisymmetric and symmetric S-O stretching vibrations of SDS found at approximately 1220 and 1080 cm^{-1} , respectively, as well as, the C-O-C stretching vibrations of the copolymer matrix at 1164 and 1146 cm^{-1} are not observed. Instead, new

bands at 1120 and 1064 cm^{-1} attributed to $-\text{NH}_2$ rocking and C-N stretching vibrations of Asp are detected. The presence of these bands indicates the formation of an Asp rich layer formed at the F-A interface at high pH while SDS is present on the surface at low pH creating the ability to tune interfacial properties by utilizing pH changes of the colloidal solution.

Postponing temporarily the formation of Asp on the surface of pMMA/nBA, we conducted IRIR imaging experiments in order to determine spatial distribution of Asp at the F-A interface. Figure 33A illustrates a series of IRIR images recorded from the F-A interface of pMMA/nBA polymeric films containing Asp coalesced at pH = 3, 7, and 10, while Figure 33B represents IR spectra recorded from the areas labeled 1, 2, and 3. Because IRIRI allows us to tune into a given IR band associated with a specific chemical species, this approach facilitates chemical imaging of the F-A interface in the xy directions. Due to interest in the location of Asp at the F-A interface, the images observed in Figure 33 were generated by tuning into the N-H twisting at 1215 cm^{-1} due to Asp. As shown in Figure 33A, when pH = 3, the surface is homogeneous with no Asp bands in Area 1. However, when the pH is increased to 7 and 10, the band at 1215 cm^{-1} becomes fairly intense, thus implying a heterogeneous distribution of Asp in the form of islands.

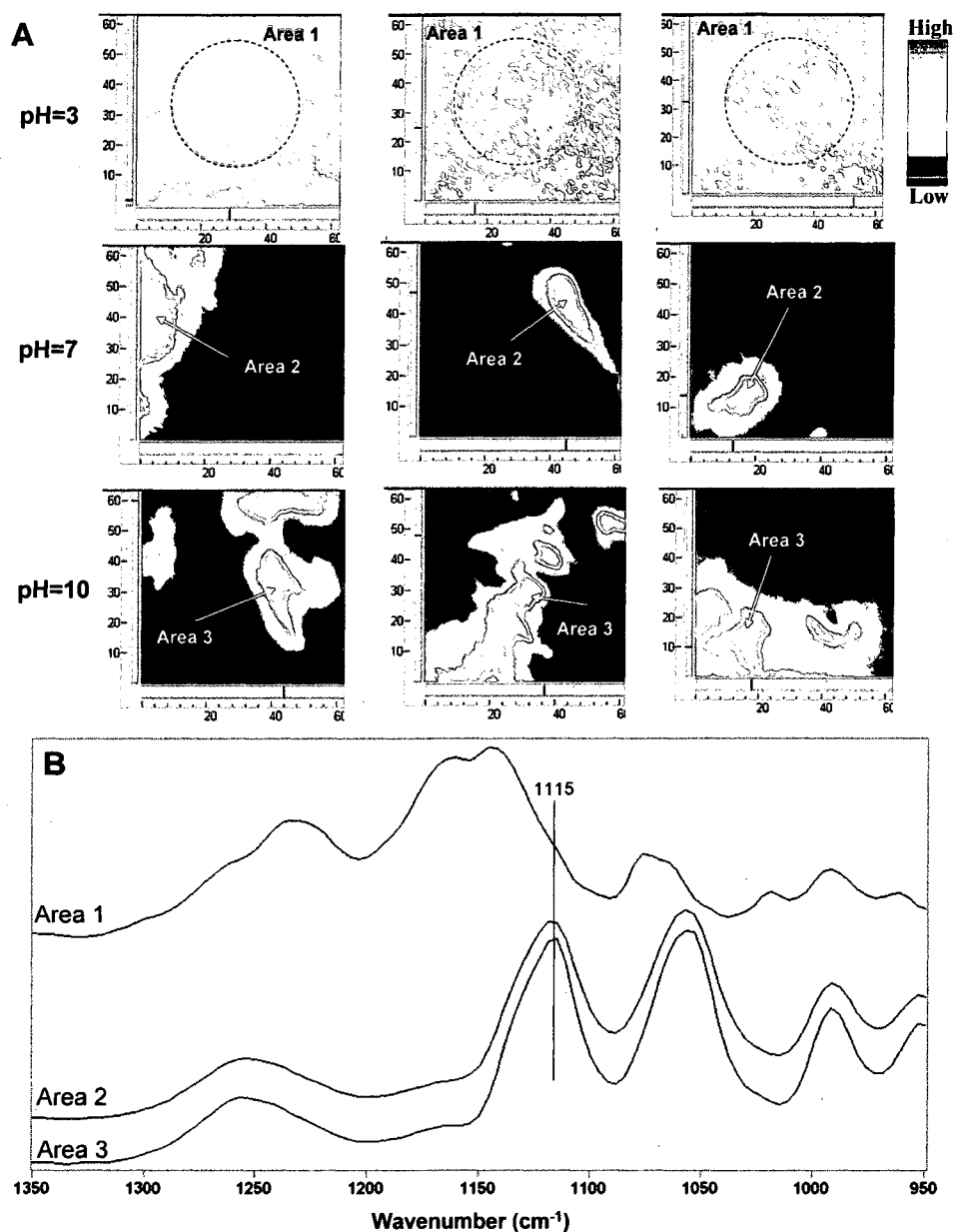


Figure 33: A- IRIR images recorded from the F-A interface of pMMA/nBA/Asp colloidal films coalesced at pH = 3, 7, and 10, B – Generated IR spectra obtained from selected IRIR images.

At this point it is quite apparent that the formation of Asp islands is obtained during coalescence of pMMA/nBA particles and pH changes control its stratification. To aid in the identification of molecular interactions responsible for Asp rich islands, computer simulations were performed. Figure 34 illustrates pMMA/nBA-Asp

interactions at pH = 3, 7, and 10, with Asp allowed to arrange itself with the surrounding copolymer matrix to obtain the most energetically favorable configuration.

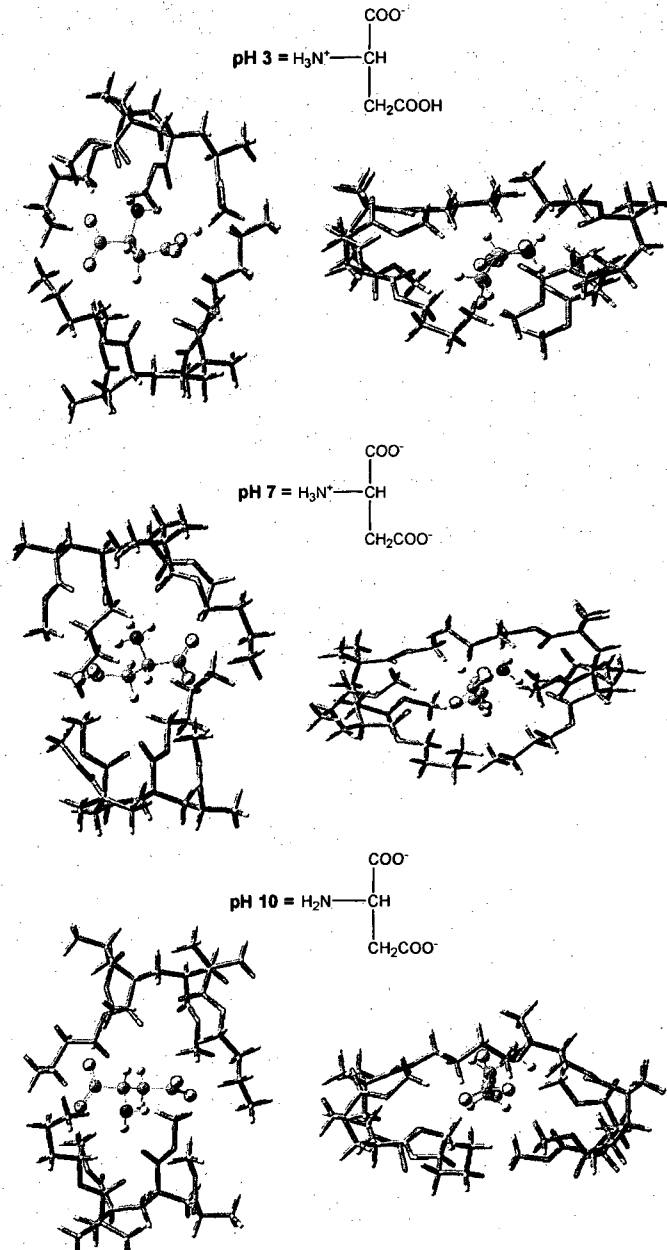


Figure 34: Top view and side view of polymer-aspartic acids at pH 3, 7, and 10.

At pH = 3, the calculated interaction energy is 34.4 kcal/mol, which is somewhat lower than expected. One would assume that the protonated form of Asp would form hydrogen

bonds with the carbonyls in the polymer matrix giving a higher interaction energy, however this is not the case. At pH = 7, the interaction energy is only slightly higher at 36.2 kcal/mol with the only difference being both acid groups are now deprotonated. At pH = 10, the interaction energy increases by almost 200% to 99.8 kcal/mol. Closer examination of the computer models reveals that the interaction between the negatively charged acid groups and the terminal methyl groups of the polymer side chains are critical in to the formation of the Asp rich islands. To test the accuracy and validity of the computer models, calculated IR bands from the computer models were compared to those experimentally observed reported previously in Figure 32, and the results of the comparison are illustrated in Table 4. As one can see, the calculated and experimental IR bands are clearly in good agreement.

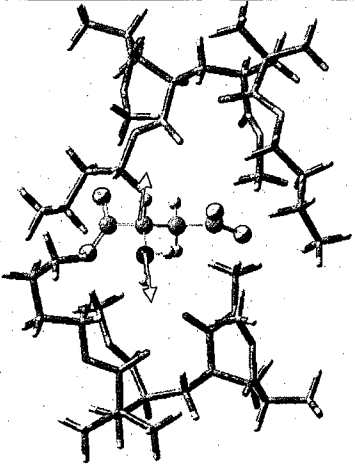
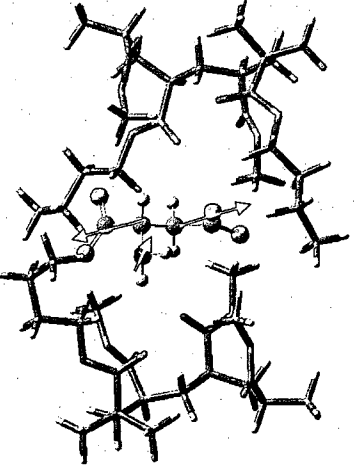
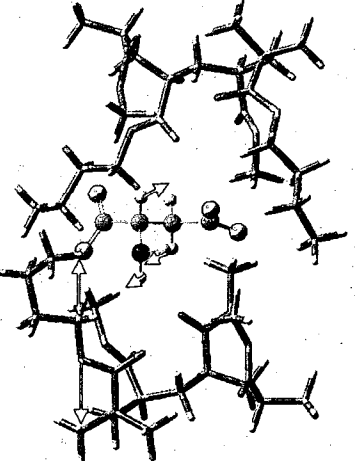
Experimental IR Band (cm^{-1})	Calculated IR Band (cm^{-1})	Vibrational Mode	3D Vibrational Modes
1120	1113	C-N stretching and N-H twisting of Asp.	
1064	1046	C-C stretching N-C-C distortion of Asp	
949	940	O-C stretching of MMA + N-H twisting and CH twisting of Asp (vertical)	

Table 4: Experimental and calculated IR bands obtained from ATR FT-IR measurements and ab initio calculations using model shown in Figure 4 at pH=10.

While it is evident that the combination of computer modeling and experimental data can provide insight into the interactions responsible for the formation of the Asp islands, the data does not answer the question as to how Asp stratifies to the F-A interface during the film formation process in the first place. In fact, the interactions observed from the computer models seem to contradict the original hypothesis. However, the one drawback of the computer models is the fact that they only interactions between the copolymer and Asp are considered. The concept of film formation is much more complex when surfactant and water are included into the equation. Previous studies¹⁶⁻¹⁸ have shown that the inclusion of components that disrupt the interactions between polymer and surfactant allows for the release and ultimate stratification of surfactant to the F-A interface. The question still remains as to why does SDS stratify to the F-A interface at low pH's and Asp at higher pH's? Using the same computer models discussed previously, Asp was replaced with SDS and the interaction energy between the copolymer and SDS was calculated to be 33.3 kcal/mol which is lower than Asp at all three pH's. Also, the solubility of SDS in 100 ml of water is 10g compared to 0.45g of Asp. With all things Since SDS interacts more favorably with water, it is driven to the F-A interface during water evaporation. However, at pH = 10, both acid groups of Asp are deprotonated and thus capable of interacting with surrounding water molecules. In this case, Asp will be driven to the F-A interface. With this in mind, Figure 35 illustrates the proposed mechanism responsible for obtaining Asp rich surfaces.

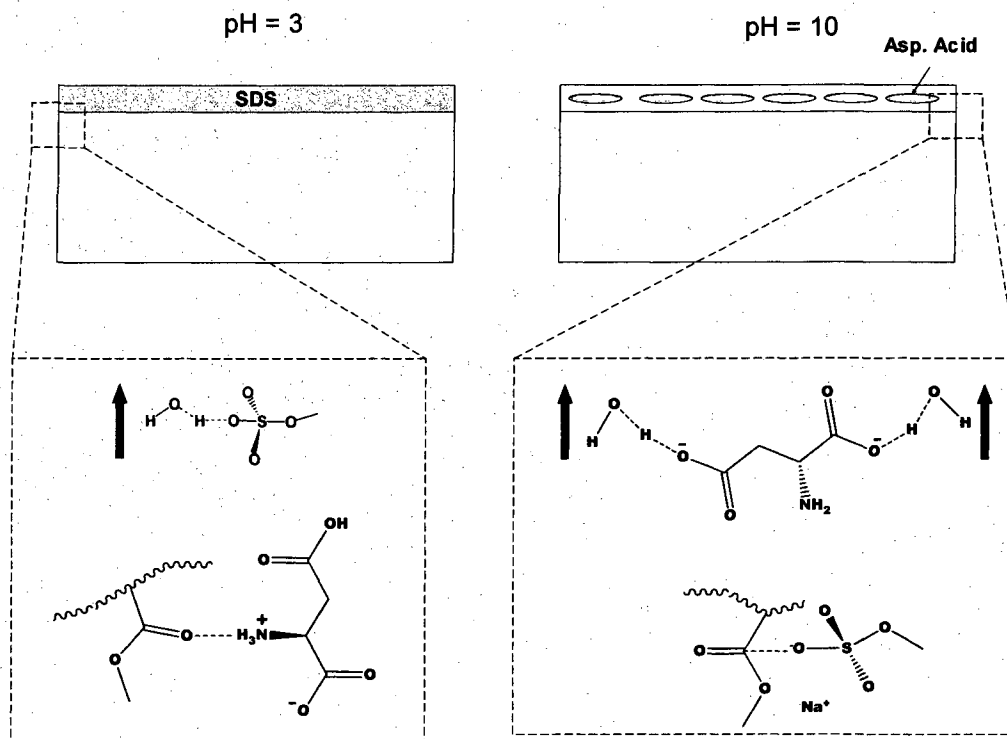


Figure 35: Proposed mechanism of pH dependant stratification of SDS and Asp during the film formation of pMMA/nBA/Asp.

Conclusions

These studies show that by controlling the inter/intramolecular interactions of individual components with pH allows for the creation of stimuli-responsive bioactive surfaces without the need for post-modification techniques. By controlling the ionization of aspartic acid, interactions within the system could be altered. It was shown that at low pH's, the formation of a surfactant rich F-A interface was created. On the other hand, at high pH's aspartic acid islands were observed at the F-A interface. By utilizing computer modeling techniques, it was found that the Asp islands were formed through ionic interactions with the surrounding copolymer matrix.

References

- (1) DeGrado, W. F.; Gratkowski, H.; Lear, J. D. *Protein Science* **2003**, *12*, 647-665.
- (2) Li, E.; Hristova, K. *Biochemistry* **2006**, *45*, 6241-6251.
- (3) Stevens, T. J.; Mizuguchi, K.; Arkin, I. T. *Protein Science* **2004**, *13*, 3028-3037.
- (4) Ottaviani, M. F.; Jockusch, S.; Turro, N. J.; Tomalia, D. A.; Barbon, A. *Langmuir* **2004**, *20*, 10238-10245.
- (5) Nonokawa, R.; Yashima, E. *Journal of the American Chemical Society* **2003**, *125*, 1278-1283.
- (6) Torsi, L.; Tanese, M. C.; Crone, B.; Wang, L.; Dodabalapur, A. *Optical Science and Engineering* **2007**, *128*, 507-528.
- (7) Aumsuwan, N.; Danyus, R. C.; Heinhorst, S.; Urban, M. W. *Biomacromolecules* **2008**, *9*, 1712-1718.
- (8) Aumsuwan, N.; Heinhorst, S.; Urban, M. W. *Biomacromolecules* **2007**, *8*, 3525-3530.
- (9) Aumsuwan, N.; Heinhorst, S.; Urban, M. W. *Biomacromolecules* **2007**, *8*, 713-718.
- (10) Qin, M.; Wang, L.-K.; Feng, X.-Z.; Yang, Y.-L.; Wang, R.; Wang, C.; Yu, L.; Shao, B.; Qiao, M.-Q. *Langmuir* **2007**, *23*, 4465-4471.
- (11) Bae, W.-S.; Urban, M. W. *Langmuir* **2006**, *22*, 10277-10283.
- (12) Bae, W.-S.; Urban, M. W. *Biomacromolecules* **2006**, *7*, 1156-1161.
- (13) Winnik, F. M.; Whitten, D. G.; Urban, M. W.; Lopez, G. *Langmuir* **2007**, *23*, 1-2.
- (14) Lestage, D. J.; Urban, M. W. *Langmuir* **2005**, *21*, 6753-6761.

- (15) Lestage, D. J.; Urban, M. W. In *Responsive Polymer Materials*; Minko, S., Ed.; Blackwell Publishing Professional: Ames, 2006; pp 168-183.
- (16) Zhao, Y.; Urban, M. W. *Macromolecules* **2000**, *33*, 8426-8434.
- (17) Dreher, W. R.; Zhang, P.; Urban, M. W.; Porzio, R. S.; Zhao, C.-L. *Macromolecules* **2003**, *36*, 1228-1234.
- (18) Rhudy, K. L.; Su, S.; Howell, H. R.; Urban, M. W. *Langmuir* **2008**, *24*, 1808-1813.
- (19) Gerrens, H. *Polymer Preprints (American Chemical Society, Division of Polymer Chemistry)* **1966**, *7*, 699-706.
- (20) Otts, D. B.; Zhang, P.; Urban, M. W. *Langmuir* **2002**, *18*, 6473-6477.
- (21) Bauschlicher, C. W., Jr. *Chemical Physics Letters* **1995**, *246*, 40-44.
- (22) El-Azhary, A. A.; Suter, H. U. *Journal of Physical Chemistry* **1996**, *100*, 15056-15063.
- (23) Becke, A. D. *Journal of Chemical Physics* **1993**, *98*, 5648-5652.
- (24) Lee, C.; Yang, W.; Parr, R. G. *Physical Review B: Condensed Matter and Materials Physics* **1988**, *37*, 785-789.
- (25) Miehlisch, B.; Savin, A.; Stoll, H.; Preuss, H. *Chemical Physics Letters* **1989**, *157*, 200-206.
- (26) Stephens, P. J.; Devlin, F. J.; Chabalowski, C. F.; Frisch, M. J. *Journal of Physical Chemistry* **1994**, *98*, 11623-11627.
- (27) Pople, J. A.; Nesbet, R. K. *Journal of Chemical Physics* **1954**, *22*, 571-572.
- (28) Scott, A. P.; Radom, L. *Journal of Physical Chemistry* **1996**, *100*, 16502-16513.
- (29) Zhao, Y.; Urban, M. W. *Langmuir* **2001**, *17*, 6961-6967.

CHAPTER VI

CONCLUSIONS

Although the synthesis and film formation of aqueous colloidal dispersions has been of interest over the past several decades, numerous opportunities still existed for further developments and advancements in these complex colloidal systems. Though recent advancements in molecular-level spectroscopic probes many of the scientific challenges which existed during the development of classical approaches to film formation have been overcome. Emulsions polymers predominantly have end use applications as coatings which entail the addition of functional components to advance the physical properties. In particular, this thesis has explored interactions between low molecular weight entities and high molecular weight colloidal particles. This research has explored numerous scientific issues regarding the development of stable colloidal dispersions and how the presence of functional components within copolymer matrices can affect mechanisms governing their film formation.

Investigations regarding the stratification of SDS as a function of competing interactions with the introduction of polymeric rheological modifiers (PVOH) has introduced many new ideas governing the design and performance of colloidal films. These studies show that during coalescence of pMMA/nBA particles stabilized by SDS, the presence of PVOH causes the displacement of SDS and its stratification near the F-A interface. At the same time, PVOH remains in the bulk of the film. This behavior is attributed to competing interactions between C=O groups of the polymer matrix, SO_3Na^+ polar groups of SDS, and OH of PVOH. As a consequence, stratification of these

compounds can be controlled by changing their concentration levels as well as film formation conditions.

Another functional component of interest is the introduction of crosslinks to polymeric systems to enhance the viscoelastic properties, however little research has been conducted to explore how the film formation process is altered when crosslinks are introduced into colloidal systems. These studies show that when pMMA/nBA colloidal dispersions are crosslinked with chemical crosslinks there is an increase storage modulus at higher temperatures, whereas physical crosslinks are effective at lower temperatures. The overall strength of film is not only dictated by the type of crosslink formed but also the location of individual components. Physical crosslinks facilitate stratification of dispersing agents to the F-A interface which results from lack of ionic interactions between the polar head groups of SDS and the polymer matrix. Chemical crosslinks inhibit stratification of dispersing agents which remain in the bulk of the film and provide plasticization of the matrix. A combination of chemical and physical crosslinks permit stratification of dispersing agents to the F-A interface, thus eliminating the plasticization effect observed for chemically crosslinked networks, and maintains storage modulus at higher temperatures.

Over the past decade, great interest in nano-sized fillers has been garnered due to the unique physical property changes observed compared to traditional micro-sized fillers when introduced into polymeric matrices. These studies show that the inclusion of nano-SiO₂ during the polymerization of methyl methacrylate and n-butyl acrylate provides control of the PDI. Defects within the nano-SiO₂ lattice provide the opportunity to control propagating radicals as well as trap unwanted radicals that may terminate

growing polymer chains. Due to the location of the nano-SiO₂ particles being on the exterior of the micelles, the nanoparticles influence the propagating radicals within the micelles while trapping hydroxyl radicals in the aqueous phase.

Finally, the idea of creating bioactive surfaces with possible sensing applications within the body prompted research into idea of using amino acids within colloidal dispersions. These studies show that by controlling the inter/intramolecular interactions of individual components with pH allows for the creation of stimuli-responsive bioactive surfaces without the need for post-modification techniques. By controlling the ionization of aspartic acid, interactions within the system could be altered. It was shown that at low pH's, the formation of a surfactant rich F-A interface was created. On the other hand, at high pH's aspartic acid islands were observed at the F-A interface. By utilizing computer modeling techniques, it was found that the Asp islands were formed through ionic interactions with the surrounding copolymer matrix.